RPU-203

TECHNICAL REPORT NO. 9

ANALYSIS AND PREDICTION OF SKY-WAVE FIELD INTENSITIES IN THE HIGH FREQUENCY BAND

BY

PAUL O. LAITINEN and GEORGE W. HAYDON

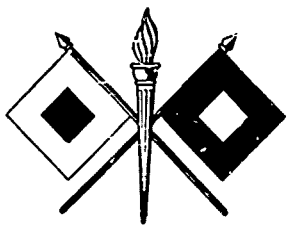

REVISED OCTOBER 1962

U. S. ARMY SIGNAL RADIO PROPAGATION AGENCY

FORT MONMOUTH, NEW JERSEY

U. S. ARMY SIGNAL RADIO PROPAGATION AGENCY
FORT MONMOUTH, NEW JERSEY

15 October 1962

Analysis and Prediction of Sky-Wave Field Intensities in the High Frequency Band was revised by the Radio Propagation Agency and is published for the information and guidance of all concerned. Suggestions or criticisms relative to the form, contents, purpose, or use of this publication should be referred to the Commanding Officer, U. S. Army Signal Radio Propagation Agency, Fort Monmouth, New Jersey.

FRANCIS E. WALDORF
Lt Col SigC
Commanding

OFFICIAL:
FREDERIC H. DICKSON
Scientific Director
U. S. Army Signal
Radio Propagation Agency

TABLE OF CONTENTS

TABLE INDEX

FIGURE INDEX

1. Introduction

a. SCOPE. The purpose of this report is to present an engineering method of evaluating sky-wave field intensities in the high frequency band for any transmission distance up to about 15,000 kilometers. Field intensity recordings were statistically analyzed in order to study daytime absorption, day-to-day variations, and absolute magnitudes. Based upon the analysis, a proposed prediction method was obtained which should give relatively accurate sky-wave field intensities for the frequencies and distances considered. Succeeding sections show the method of analysis of absorption, the method of analysis of absolute magnitudes, the method of analysis of day-to-day variations, the proposed field intensity prediction method, and summarizing conclusions. All necessary equations used in the prediction method are represented in nomograms.

b. DATA. The data analyzed consists of monthly median receiver input voltages at one hour time intervals throughout the day and mass plots showing hourly median receiver input voltages in 2 decibel class intervals for the days of the month. The circuits analyzed are listed in Table I. This table shows the period for which the data was available, the distance between the transmitting and receiving station, the wave frequency, and type of data. These records were continuous over a period of at least as long as one year. The circuit distances range from 55 to 15,000 kilometers and the frequencies from 0.7 to 20 megacycles per second. Eighty-three circuit years of monthly median hourly median receiver input voltages were used in the daytime absorption analysis. Data for 36 circuits, including information about transmitter output powers, transmitting antenna gains, and receiving system input characteristics were used in the analysis of absolute magnitudes. The receiving system installations were so designed as to make estimations of absolute magnitudes possible. Forty-three years of massplot data was used in the analysis of day-to-day variations of hourly median field intensities. Other data not shown in the table covering a period from 1937 to 1944 was used in studying the relationship between daytime absorption and 12 month running average sunspot number.

c. THE METHOD OF ANALYSIS. This analysis is based upon the assumption that at high frequencies sky-wave field intensities can be computed by geometric optical methods. Various authors show the applicability of ray theory at these frequencies.[1] Sky wave propagation is a geometric rather than a diffraction problem since each place on earth at distances greater than the skip distance is accessable by geometric trajectories. A method such as a residue series would be more applicable if a large number of geometric rays existed all having the same order of intensity. It has been shown by L. E. Beghian that, for high frequencies, only a few rays are required and that under conditions of absorption the first ray approximates the field strength obtained by assuming all possible rays.[2] When several raypaths exist having the same order of magnitudes, it is necessary to evaluate the field by summing the contribution of all the rays. Occasionally for long distances, the error in assuming that

the field intensity can be represented by one ray alone can be relatively large since ray intensities of equal magnitudes are possible along several ray paths.

2. The Analysis of Sky-wave Absorption

a. GENERAL. (1) In the ionosphere, gas molecules are ionized into electrons and positive ions principally by the action of ultra-violet solar light. A passing radio wave sets electrons in vibratory motion. The electrons randomaly collide with gas molecules and lose part of the energy of vibration during collisions. The absorption of a radio wave per unit path length depends on the collision frequency and the number of electrons per unit volume, both of which vary with height above earth.

(2) During daylight hours, the majority of sky-wave absorption at high frequencies occurs in the lower E region. This region is known as the D region although it is not certain that it is physically distinct from the E. The collision frequency is high while the ion density is low so that a radio wave is absorbed but not greatly refracted. This type of absorption is called *non-deviative* absorption. The geometric ray theory approximation is applicable for frequencies not too close to the collision frequency, the ionosphere approximating a partially reflecting dielectric.

(3) During the night hours, the ionosphere acts as an almost totally reflecting dielectric at high frequencies. The effects of the passage of radio-waves through the D and E layers are negligible, since the ionization of these layers is very small. A small but not negligible absorption occurs upon reflection at the F2 layer particularly near the maximum usable frequency. This absorption occurring at the same time as wave refraction is known as *deviative* absorption. The F2 layer collision frequency is low due to low molecular density so that non-deviative absorption within the layer is negligible.

(4) For long wave lengths, the geometric optics approximation is not valid particularly during daylight. The ionosphere can be considered as a conductor at these frequencies. A large number of modes are possible which have the same order of intensity.

b. THEORY. Equations for sky-wave absorption have been derived by many theoretical investigators. One method of deriving absorption equations, shown by Bremmer in "Terrestrial Radio Waves," is indicated below.[3] The geometric-optics approximation for sky-wave field intensities is applicable to an absorbing region if [illegible] too great. In an absorbing region the index of refraction is complex and [illegible] generalized form of Snell's Law. In the mathematical expression [illegible] intensity of the electro-magnetic

wave, an exponential term appears accounting for the attenuation per unit length along the path trajectory. This attenuation factor can be written as:

$$\text{Attenuation Factor} \quad = e^{-k\int_{l_1}^{l_2} I_m(\mu)\, dl} \qquad \text{Equation}$$

where k is the wave number, $2\pi/\lambda$; λ being the wave length
$I_m(\mu)$ is the imaginary part of the refraction index
dl is a differential distance along the path trajectory

When the value for the refraction index is substituted in the equation above and the differential distance along the ray path is replaced by the differential distance perpendicular to the earth, this attenuation factor can be written in the following form: (See Bremmer, pages 176 and 177).

$$A\,F \quad = e^{\frac{-n \sec \phi}{c\omega^2} \int_{r_1}^{r_2} \nu(r)\, \omega_{cr}^2 dr} \qquad \text{Equation 2}$$

where c is the velocity of light
r is the distance from the center of the earth
n is the number of hops
ω is the wave angular frequency
ϕ is the angle of incidence at the ionosphere
ω_{cr} is the critical angular frequency
$\nu(r)$ is the collisional frequency

The expression within the integral sign is independent of wave frequency for frequencies exceeding the collision frequency. This approximation is valid for waves reflected by the E or F2 layer after passing through the D or E layer. The integral expression represents the number of collisions between molecules and electrons situated in a vertical column extending through the entire lower layer. It corresponds to non-deviative absorption. The expression, $n \sec \phi$, can be approximated by a constant multiplied by the distance between the receiver and the transmitter. When this is done and noting that all the other terms in the exponential expression can be considered constant, the attenuation factor can be written in Eckersley's form:

$$A\,F \quad = e^{\frac{-ad}{f^2}} \qquad \text{Equation 3}$$

where a is a constant for particular ionization conditions
f is the wave frequency
d is the transmission distance between the receiver and transmitter

This form of absorption factor has been used in the absorption calculat-

tion methods for long distance circuits. It should be noted that the effects of the earth's magnetic field are not included in the formula.

c. APPLETON'S EQUATION. Sir E. V. Appleton derived an expression for the total non-deviative F layer absorption under the condition that the frequency of the transmitted wave was much greater than the collision frequency.[11] This equation written in terms of an ionosphere reflection coefficient for vertical incidence follows:

$$-\log \rho = 4.13 H \frac{\pi e^2 N_0 \nu_0 \cos^{1.5}\psi}{mc(\omega + \omega_L)^2} \qquad \text{Equation 4}$$

where ρ is the reflection coefficient
e is the electronic charge
m is the mass of the electron
c is the velocity of light
N_0 is the electron density at the maximum ionization of the layer when the sun's zenith angle is zero
ν_0 is the collisional frequency at the height of maximum ionization
H is the scale height
ψ is the zenith angle of the sun
ω is the angular frequency of the propagated radio wave
ω_L is the angular gyro-magnetic frequency due to the longitudinal component of the earth's magnetic field

This equation, based on a Chapman distribution of ionization, shows the vertical incidence absorption for the ordinary component of the electromagnetic wave. The absorption varies directly with ν_0 and inversely with the square of the sum of the wave frequency and the longitudinal component of the gyro-frequency.

d. EFFECT OF THE EARTH'S FIELD UPON ABSORPTION. Theoretical equations show the effect of the earth's field upon absorption. The ratio of absorption in the presence of the earth's magnetic field to absorption in absence of the earth's magnetic field is equal to the ratio of the imaginary components of the respective indices of retraction. This theoretical ratio, plotted in Figures 46 and 47, is given by the following equation:

$$\frac{I_m(\mu)}{|I_m(\mu)|_{H=0}} = 2 \frac{\left(1 + \frac{\omega_H^2}{\omega^2}\sin^2\theta\right)\sqrt{1 - \frac{\omega_H^4}{\omega^4}\sin^4\theta}}{\sqrt{1}\left(\sqrt{1 + \frac{\omega_H^2}{\omega^2}\sin^2\theta} + \cos\theta\right)^2} \qquad \text{Equation 5}$$

where ω is the angular frequency of the radio wave
ω_H is the angular gyro-frequency

θ is the angle between the earth's magnetic field and the radio wave

$$A = \frac{4\omega_H^2}{\omega^2}\cos^2\theta + \frac{\omega_H^4}{\omega^4}\sin^4\theta$$

The upper sign refers to the ordinary ray and the lower sign to the extraordinary ray. This ratio for the longitudinal case (direction of the earth's field parallel to wave normal) can be written as follows:

$$\frac{I_m(\mu)}{|I_m(\mu)|_{H=0}} \cong \frac{1}{\left(1 \pm \frac{\omega_H}{\omega}\right)^2}$$

When the earth's field is perpendicular to the wave normal, the ratios for the ordinary and the extraordinary ray are given by the following expressions:

$$\cong 1 \text{ (ordinary ray)} \; ; \quad \cong \frac{1 + \frac{\omega_H^2}{\omega^2}}{\left(1 - \frac{\omega_H^2}{\omega^2}\right)^2} \text{ (extraordinary ray)}$$

e. ABSORPTION ANALYSIS INTRODUCED. For the absorption analysis, the effects on the daytime monthly median receiver input voltages of variations in ray angle, running average sunspot numbers, gyro-frequency, wave frequency, and the zenith angle of the sun were studied in a manner separating the individual variables. Initially, the receiver input voltages for each circuit and for each month were plotted against hour of the day, as shown in Figure 1. The daytime minimum of receiver input voltage occurs at an hour corresponding to local noon at the midpoint of the path between the transmitter and receiver for all circuits.

f. SOLAR ZENITH ANGLE RELATIONSHIPS. (1) The study of the variation of receiver input voltages with the sun's zenith angle consisted of determining the angle at which the daytime absorption starts and ceases, and the functional relationship between absorption and the sun's zenith angle. The sun's zenith angle is the angle between the perpendicular to the earth at the ionosphere reflection point and the direction to the sun. The cosine of this angle is given by the general formula of spherical trigonometry:

$$\cos\psi = \sin L_1 \sin L_2 + \cos L_1 \cos L_2 \cos\Omega \qquad \text{Equation 6}$$

where L_1 is latitude of the ionosphere reflection point

L_2 is latitude of the sun's sub-solar point

Ω is the hour angle of the sun referred to the ionosphere reflection
ψ is the solar zenith angle

In this analysis, solar zenith angles were obtained graphically from contours of equal zenith angles. These contours, drawn on the same rectangular grid system used in the Central Radio Propagation Laboratory "D" series predictions were computed by the equation above with respect to the sub-solar points for the fifteenth day of the month from the declination of the sun and the equation of time given in Nautical almanac of 1948. Since the position of the sub-solar points do not change much from year-to-year; the contours, Figures 2 through 13, can be used for any year.

(2) A study was made of the starting and stopping times of daytime absorption using the curves showing monthly median receiver input voltage plotted against the hour of the day. These times occur when the receiver input voltage curves begin to decrease at dawn and begin to reach their nighttime value at sunset. The analysis for all the circuits for each month indicates that daytime absorption begins and ceases at about the same solar zenith angle. This angle is independent of month, circuit length, and wave frequency. Figure 14 shows the solar zenith angle where absorption begins and where it ceases plotted against wave frequency. Figure 16 is a mass plot showing the 602 available cases plotted over a five year period. Figure 17 is the cumulative distribution of this mass plot data. The arithmetic mean for the starting or stopping of daytime absorption is 102.2 degrees. Figure 15 shows the dawn and sunset time at various heights above the earth. The angle of 102.2 degrees indicates that daytime absorption occurs between dawn and sunset at an E layer ionosphere height of approximately 115 kilometers.

(3) The functional relationship with the solar zenith angle in Appleton's absorption equation would give zero absorption for an angle of 90 degrees. Absorption is indicated by this analysis to start or cease at a zenith angle of 102.2 degrees and to be maximum at a zenith angle of zero degrees. It is possible to set the cosine solar angle relationship equal to zero at 102.2 degrees by multiplying the solar zenith angle by a constant such that the product of the constant and 102.2 would give a value of 90 degrees. Thus, absorption would start or cease at the observed angle and would be maximum when the sun is overhead. Based on the above, the functional relationship of absorption with the angle was assumed to be of the following form in this report:

$$(\cos \alpha\psi)^m = (\cos .881\psi)^m \qquad \text{Equation 7}$$

where α is a constant equal to $90°/102.2° = .881$
m is a constant to be obtained from the data
ψ is the solar zenith angle

(4) The monthly median receiver input voltages were plotted for all circuits for each month against the cosine of .881 ψ as shown in Figure

18. In many cases the morning curve is not as symmetrical as the afternoon curve due to lack of ionospheric support during the morning hours. A composite curve, Figure 19, is drawn between the values for morning and the values for afternoon. From this composite curve, the voltage value at $\cos .881\ \psi$ equal to zero was taken as a reference. In cases where this value was not obtainable from the data, the reference voltages were obtained by extrapolating the curves to $\cos .881\ \psi$ equal to zero. Absorption values were obtained as the decibel difference between the reference and voltage values at particular solar angles. These absorption values were then plotted against $\cos .881\ \psi$ on log paper as shown in Figure 20. These curves are nearly straight lines. The absorption curves described above are not exactly useful since absorption is also a function of running average sunspot number and the angle of incidence at the ionosphere. In order to separate these variables, it is desirable to convert oblique absorption values to vertical incidence at a particular sunspot number. The following paragraphs indicate how the oblique incident absorption values were converted to vertical incidence values for sunspot number zero.

g. SOLAR ACTIVITY EFFECTS. In order to study the variation of daytime absorption with average sunspot number, it was necessary to analyze data covering a period of several years. Figure 21 shows absorption and 12 month running average sunspot number plotted against time for four routes. There was an initial attempt to analyze the absorption for a particular value of the sun's zenith angle. A higher correlation coefficient was obtained for the analysis of the absorption at midday. Twelve month running average midday absorption was plotted against 12 month running average sunspot number for the eight routes that had data over a sufficiently long time period. The circuits analyzed cover various transmission distances from 55 kilometers to 3636 kilometers and frequencies from about 2 megacycles to 10 megacycles. By plotting 12 month running averages, the seasonal trends of absorption were removed. The data shows that absorption varies linearly with sunspot number as shown in the following equation:

$$A_X = A_0(1 + bs) \qquad \text{Equation 8}$$

where s is the running average sunspot number
b is a constant obtained from the experimental data equal to .0037
A_0 is the absorption at Sunspot Number 0
A_X is the absorption at Sunspot Number X

The slope of the linear relation between absorption and sunspot number is .0037 as an average for the eight circuits. Table 2 lists the values of the slope and the linear correlation coefficient obtained from the least squares analysis.

h. LAYER HEIGHT VARIATIONS. [1] F. W. G. White mentions that the variation of absorption between winter and summer is less than that expected by theory based on the solar zenith angle.[4] Figure 22 shows the midday

absorption extrapolated to a zero degree zenith angle for the radio circuit between Mexico City and Boston. This figure shows the minimum F2 layer virtual heights observed at Louisiana State University for the same period of time covered by the absorption curves. This minimum virtual height curve is plotted with increasing height in a downward direction. By comparing the month-to-month variations of midday absorption with the monthly average F2 layer midday virtual height, it is seen that the absorption appears to follow F2 layer heights inversely. During the summer season, the F2 layer heights are higher and, thus, the ray angles at the ionosphere are steeper than during the winter season. *This tends to decrease absorption during the summer months relative the values during the winter months, explaining the difference between winter and summer absorption not accountable by the zenith angle alone.*

(2) The diurnal variation of minimum monthly median F2 layer virtual heights for each month are shown in Figures 23 through 34. These figures represent the average F2 layer virtual height at all ionosphere stations as reported by the National Bureau of Standards in the Central Radio Propagation Laboratory F Series reports for 1945 through 1948. Based on this analysis, F2 layer virtual heights do not appear to have a regular variation pattern throughout the solar cycle or between geomagnetic zones. Figures 23 through 34 may therefore be used to approximate the minimum F2 layer virtual height at any geographic location at any time. Figure 35 shows that, in some locations the minimum F2 layer virtual height increases while in others it decreases or remains constant as the moving average sunspot number increases. Figure 36 shows the average heights obtained from the contours and the observed noon F2 layer heights at Washington, D. C. for five years. The monthly median F layer virtual heights do not vary greatly from month-to-month. Figure 37 shows the minimum virtual E layer heights as observed in Washington, D. C. in June and December of 1946 plotted against hour of the day.

(3) Only F2 layer and E layer transmission modes are considered in this report. E layer transmission modes are assumed to be reflected from a 110 kilometer virtual height. F1 layer transmission modes for equal antenna radiations probably fall between the F2 and the E modes in intensity. Generally, rays that penetrate the E layer will be reflected by the F2 layer and F1 layer modes probably are smaller in magnitude than the F2 layer modes.

1. CONVERSION TO VERTICAL INCIDENCE — Absorption was assumed to be directly proportional to the angle of incidence at a 100 kilometer height. These angles were based on great circle reflected rays between a curved earth and a curved ionosphere. For convenience in analysis, the secant of the angle at 100 kilometers was related to the angle between the ray and ground. Figure 38 shows the secant of the angle of incidence for the various layer heights as a function of great circle distance and angle between the ray and the ground. The secant factors for multihop modes are equal to the secant factors for single hop modes of the same radiation angle multiplied by the number of ionosphere reflections.

For the various possible propagation modes reflected from the E and F2 layers, the secant factors at a 100 kilometer height were obtained at the radiation angles determined by the number of ionospheric reflections, the virtual layer height, and transmission distance. Maximum usable frequency curves were plotted for the transmission path for the period of the data from the observed critical frequencies shown in the Central Radio Propagation Laboratory F Series. These curves, see Figure 39, show which sky-wave modes were possible at certain hours and frequencies.

(2) The oblique incidence absorptions were converted into vertical incidence absorptions by dividing by the secant factors. The layer heights corresponding to the particular local time at the ionosphere reflection point were determined from Figure 23 through 34, which give the average layer heights for each month of the year. Since both the solar zenith angles and the layer heights were obtained from charts in terms of latitude and local time, the secant factors for F2 layer modes were obtained at corresponding solar zenith angles. In addition to dividing the oblique incidence absorptions by the secant factors, they were divided by the solar activity factor given in Equation 8 to convert the vertical incidence values to sunspot number zero.

(3) The vertical incidence absorption at sunspot number zero for each month and for all the circuits was then plotted against the cosine of $.881\psi$. Figure 40 shows a typical plot of this kind and indicates the mathematics used in obtaining the vertical incidence absorption for sunspot number zero from the oblique incidence absorption at a known sunspot number. These curves are more linear than the plots of oblique incidence absorption against the same function of solar zenith angle. Secant factor variations due to ionospheric layer height variations are accounted for. In this analysis, no account is made of the change in antenna radiation due to hourly changes in layer heights. It is felt that apparent absorption variations due to differences in antenna radiations that occur from hour-to-hour do not cause large errors when all the routes are considered as a group. Some of the circuits have higher total antenna gains at lower angles than at higher angles, while other circuits have opposite characteristics.

(4) The plots of vertical incidence absorption against the cosine of $.881\psi$ were extrapolated to the value of cosine $.881\psi$ equal to 1, the sub-solar absorption for vertical incidence at sunspot number zero. These values should not vary with season since the effect of height variations have been accounted for. Table 3 shows that residual seasonal fluctuations are negligible. The effect of transmission distance upon these vertically incident values should also have been removed. Figure 41 shows the vertical incidence absorption plotted against transmission distance for those values of frequency for which data is available at several distances. No appreciable variations were noted with transmission dis-

tance. The exponent of the relationship between vertical incidence absorption and cos .881 ψ varied somewhat between circuits. These exponents are plotted as a mass plot against the months of the year in Figure 42. Figure 43 shows the cumulative distribution of the exponents for all the observations from the data, plotted on normal probability paper. Figure 44 shows the exponents plotted against wave frequency. Table 3 is a summary of the seasonal variations of the exponents. It is noted that the seasonal average values are very nearly alike and that the composite median for all available observations is 1.30, (Figure 43).

(5) For distances greater than 4000 kilometers, the conversion of oblique incidence absorption to vertical incidence was performed in a slightly different manner. The average of the layer heights between 2000 kilometer points from the transmitting and receiving locations was used in determining the radiation angles above the ground plane for various probable transmission modes. For these modes, the solar zenith angles were determined at points corresponding to the positions of ionosphere reflections. The average of the cos .881 ψ for these reflection points was taken as the value for the circuit. The oblique incidence absorptions were divided by secant factors for the most probable modes and by the solar activity factor to transform the values to vertical incidence and sunspot number zero. Figure 45 shows the secant factors at a 100 kilometer height plotted against distance for various number of hops for a reflecting layer height of 300 kilometers. Figure 38 was used to obtain the secant factors in this report, the secant factors for multi-hop modes being equal to that for single hop modes of the same radiation angle multiplied by the number of hops. The vertical incidence absorption values at sunspot number zero were then plotted against the average cosine of .881 ψ as in the case of shorter routes. The subsolar absorption values at sunspot zero and slopes are included with the values for shorter routes in Figures 41, 42, 43, and 44.

j. Observed Effects of the Earth's Magnetic Field. (1) Since absorption is a function of both wave frequency and gyro-frequency, it is desirable to analyze the relationship between absorption and wave frequency in a manner eliminating the effects of the magnetic field. The Appleton equation for the ordinary ray indicates that absorption varies inversely with the square of the sum of the wave frequency and the longitudinal component of the gyro-frequency. Theoretical equation 5 shows how absorption values can be obtained in absence of the earth's magnetic field. These absorption values should show a consistent relationship with wave frequency since the magnetic field effect has been removed. In this report, the relationship between absorption and wave frequency was studied in absence of the magnetic field and by a more approximate method.

(2) Figures 46 and 47 can be used to convert absorption to values in absence of the earth's field. These curves show the relationship between absorption with and without the presence of the earth's field for both the ordinary and the extraordinary rays. In order to use these

curves, the angle between the earth's magnetic field and the ray direction must be known in addition to the gyro-frequency.

(3) Two space angles in a spherical coordinate system determine the direction of any line. The variation and the dip determine the direction of the earth's field. Figure 48 shows the variation of the earth's field while Figure 49 shows its dip. The angle of incidence at a 100 kilometer height and the bearing of the great circle path between the transmitter and receiver at the ionosphere reflection point determine the direction of a ray at the absorption height. The variation and dip of the earth's field and the bearing of the great circle path are determined graphically by using an overlay and charts drawn on the National Bureau of Standards rectangular grid system. Figure 50 is a bearing chart which has been devised at the Radio Propagation Unit to determine the bearing from north for any point along the great circle path between any two points on the earth's surface.

(4) A transparent piece of paper is placed on a world map, Figure 83, and the positions of the transmitting and receiving stations are marked in addition to drawing a line over the equator. This overlay is then placed on the great circle chart, Figure 84, and moved horizontally with the equatorial lines coinciding until the transmitting and receiving locations lie on the same great circle or proportional distance between adjacent great circles. The great circle is sketched on the transparency to the point where the great circle path crosses the equator. The transparency is then placed on the Radio Propagation Unit Bearing Chart with the equatorial lines coinciding and the point where the great circle path crosses the equator is placed on one of the two equatorial polar points. The bearings are found in either direction at any point along the great circle path. If a point on the great circle lies over a section of the bearing chart marked E (or W) the bearing is found for an easterly (westerly) direction. The overlay is then placed over the dip and variation charts to find these values at the path midpoint. The overlay is also used to find the gyro-frequency at the ionosphere reflection point. Figure 51 shows the gyro-frequency chart drawn on the same rectangular grid. The values are obtained from the measured total earth's magnetic field at the surface from the Hydrographic Office Charts of 1945 extrapolated to a 100 kilometer height by Schmidt's equation.[5]

(5) Since the directions of the earth's field and the ray path are known, the angle between the two can be determined by the general formula of spherical trigonometry or from the D'Ocagne Nomogram, Figure 52. All the variables required for the determination of the factor relating absorption in presence of the earth's field with absorption in the absence of the earth's field are known since the angle between the ray direction and the earth's field is known in addition to the gyro-frequency and the wave frequency. In this analysis, separate factors are determined for both entry and exit since the angle between the earth's field and ray differs for the upgoing and downcoming parts of the ray paths. The average of the factors for entry and exit were used to convert

absorption to that expected when the earth's field is not present. Figure 53 shows this absorption in absence of the earth's magnetic field at vertical incidence plotted against the wave frequency for ordinary ray transmission. The curve includes absorption values for all four seasons. Monthly median values for each individual circuit are shown by dots.

(6) Due to the complexity required in determining the angle between the earth's field and the geometric rays, it is desirable to use a method which closely approximates the effect of the earth's field but does not require the determination of the angle. Various approximations were investigated. The data indicates that when absorption is plotted against the sum of the wave frequency and the total gyro-frequency that a consistent relationship is obtained. Figure 54 shows the equivalent vertical absorption for sunspot number zero and solar zenith angle zero plotted against the sum of the wave frequency and the gyro-frequency for all four seasons of the year. The individual dots represent monthly median values for each circuit. Figure 55 shows the same curve when the yearly average values are used. Least squares straight lines based on the yearly average values are drawn on all these plots. The slope of these lines shows that absorption varies closely in an inverse squared relationship with the sum of the wave frequency and the total gyro-frequency. It is noted that few experimental points were available below about 5 megacyles and , thus, the reliability of the curve is less at these lower frequencies. Thus, the data shows that vertical incidence absorption for a solar zenith angle of zero degrees and a sunspot number of zero can be related to the sum of the wave frequency and the gyro-frequency by the following equation:

$$\text{Frequency Function} = \frac{\text{Constant}}{(f + f_H)^d} \qquad \text{Equation 9}$$

where f_H is the gyro-frequency
f is the wave frequency
d is a constant

k. RADIO PROPAGATION UNIT EQUATION. The statistical analysis of the monthly median receiver input voltages indicates that absorption fits a formula similar to Appleton's converted to oblique incidence.

$$A \text{ in decibels} = \frac{Cn \sec \varphi \, (\cos \alpha\chi)^n (1 + bs)}{(f + f_H)^d} \qquad \text{Equation 10}$$

where φ is the sun's zenith angle
a is a constant = .881
b is a constant = .0037
C is a constant = 615.5
n is a constant = 1.3

d is a constant = 1.98
f is the wave frequency
f_H is the gyro-frequency at a 100 kilometer height
n is the number of ionospheric reflections
ϕ is the angle at a 100 kilometer height between a perpendicular to the earth and the ray path
S is the 12 month running average sunspot number

It should be noted in the above equation that the total gyro-frequency is used instead of the longitudinal component and that this gyro-frequency is the value at a 100 kilometer height.

3. Analysis of Statistical Variation of Hourly Median Sky-wave Field Intensities.

a. GENERAL. The mass plots of the hourly median receiver input voltages were used in studying the day-to-day variations over monthly and yearly time periods. Figure 64 shows a typical mass plot. The dots show the number of days that the hourly median voltages lie within 2 decibel class intervals over the month. Separate studies were performed for day and night hours. These studies indicated that when a sufficiently long time period was used both the nighttime and the daytime day-to-day variations were similar for each circuit and are practically independent of wave frequency, transmission distance, and hour of the day.

b. NIGHTTIME DAY-TO-DAY VARIATIONS. In the analysis of nighttime voltages, the statistical study was made at the night hour at which the monthly median value was the highest. The data was plotted in histograms, indicating the number of cases where the voltage fell between 4 decibel intervals, as shown in Figure 65. Cumulative distribution plots were made for each month for all the circuits. These distributions were plotted both on normal probability paper and on Rayleigh coordinate paper, as shown in Figures 66 and 67. The number of cases within 4 decibel class intervals were also plotted against the months of the year. Figure 68 shows one of these plots which were used in analyzing the yearly trend of the monthly median values. For each circuit, the cumulative sums of all the cases within 4 decibel class intervals for the entire year were plotted on Rayleigh coordinate graph paper. These curves are shown for each route of this report, Figures 69 through 72. Comparing the various figures, it can be noted that they are nearly linear between percentages exceeded 90 percent of time and 10 percent of time. Receiver input voltage in decibels referred to the yearly median were plotted against percentage of the time the voltage is exceeded. Figure 73 is a cumulative distribution that includes all the circuits. The decibel values referred to the median for each circuit were read from the cumulative distribution plots at particular percentage values and these were plotted as a composite. The composite is nearly a straight line with a slope approximating that obtained by plotting a Rayleigh distribution on this paper. There are approximately 15

decibels between the exceeded 10 percent of the time and the exceeded 90 percent of the time values. Figure 74 shows the cumulative distribution of the decibel differences between the exceeded 10 percent of the time and the exceeded 90 percent of the time values for each circuit when these are taken on a yearly basis. This figure is useful in showing the percentage of circuits having particular decibel differences between the 10 percent exceeded and the 90 percent exceeded values.

c. DAYTIME DAY-TO-DAY VARIATIONS. (1) The daytime voltages were analyzed in a similar manner. These again show considerable differences if individual routes are examined on a monthly basis. But, again, if the data for a period as long as a year is used in analyzing the day-to-day variations, the routes appear similar. For the daytime voltages, there were two separate analyses. In one, the data was analyzed at four six hour intervals; 6 a. m., noon, 6 p. m., and midnight. For each circuit at these hours, the decibel differences between the monthly median and percentages exceeded 10, 30, 70, and 90 percent of the time were obtained from the mass plots by counting the number of cases above and below the monthly median values. The average differences between these percentages for all the circuits at the four hours of the day were combined into composite plots at approximately the same wave frequencies. Figure 75 shows this composite cumulative distribution for particular wave frequency values.

(2) In the other analysis, the variations were obtained at a solar zenith angle of 60 degrees. The zenith angle of 60 degrees was chosen to have data throughout the year for a large number of circuits. Large zenith angles are not possible at all locations for the entire year. The receiver input voltages were grouped into 2 decibel class intervals for for both morning and afternoon for each month for all the circuits. Figure 76 is a typical histogram showing the number of instances at 2 decibel class intervals referred to the monthly median for both morning and afternoon at a solar zenith angle of 60 degrees for a circuit for one month. The cumulative distributions were calculated and plotted. From the plotted cumulative distribution curves for each circuit and each month for morning and afternoon, the decibel differences between the median value were read at percentages exceeded 1, 5, 10, 30, 70, 90, 95, and 99 percent of the time. These were averaged for all the months of the year with both morning and afternoon values included. Figures 77 and 78 are cumulative distributions for each circuit on this yearly basis. Figure 79 is a composite for all the circuits. The composite curve for all the circuits during daylight hours again plots nearly linearly on Rayleigh coordinate paper. The decibel difference between the exceeded 10 and 90 percent of the time values is 14 decibels, nearly that expected for a Rayleigh distribution. The decibel differences between the 10 and 90 percent values were plotted for all the routes for the solar zenith angle for 60 degrees as a cumulative distribution on Figure 80.

d. SUMMARY. (1) Smith and Harrington in Central Radio Propagation Laboratory Report 1 - 6 show that the distribution of day-to-day hourly

median field intensities over long time periods is roughly normal in decibels, between exceeded 10 to 90 percent of the time values. They show a 12 decibel difference between the exceeded 10 and the exceeded 90 percent of the time values as a median for the circuits analyzed. The standard deviation of the approximate normal distribution was shown to be about 5 decibels. Figure 81 shows a normal distribution with a 5 decibel standard deviation plotted on Rayleigh coordinate paper. Short term variations in sky-wave field intensities, appear to follow the Rayleigh distribution, given by the following equation:

$$P = 100\, e^{-.6931\left(\frac{E}{E_m}\right)^2} \qquad \text{Equation 11}$$

where E is the instantaneous field intensity
E_m is the median field intensity
P is the percentage of the time the instantaneous value is exceeded

(2) As indicated in the preceding paragraphs, both daytime and nighttime hourly median receiver input voltages plot nearly linearly on Rayleigh coordinate paper with about the same slope as expected from a Rayleigh distribution. Thus, the day-to-day variations over a period as long as a year have approximate Rayleigh distributions. A Rayleigh distribution is the same as the distribution for the magnitudes of a complex variate with equal standard deviations along two rectangular axes. The work of Ray S. Hoyt of the Bell System on probability theory for two dimensional normal distributions can be cited.[8] In his 1933 paper, he shows cumulative distributions for the magnitudes for various values of a function, b.

$$b = \frac{1 - \left(S_V / S_U\right)^2}{1 + \left(S_V / S_U\right)^2} \qquad \text{Equation 12}$$

where S_U is the standard deviation along the U axis
S_V is the standard deviation along the V axis

When the standard deviations along two rectangular axes are equal, the value of the function is equal to zero. When one standard deviation greatly exceeds the other, the function is equal to 1. Cumulative distributions for b values of 0 and 1 are also shown on Figure 81.

(3) The day-to-day variations over as short a period as a month vary from month-to-month and between circuits. Many of these variations can be accounted for by variations in ionospheric support. Figures showing the critical frequencies for transmission by various sky-wave modes are usable in analyzing reasons for many of these variations. The extent of ionization of the layers of the ionosphere determines which modes are possible. Many of the variations can be traced to solar

activity. Figure 82 shows the nighttime monthly median receiver input voltages for MIT receiving XEWW at two night hours. Night values remain high between early 1946 and midyear 1948, the peak of the present solar cycle. This is probably due to the fact that the ionosphere is sufficiently ionized to consistently support the F2 two hop transmission mode, the predominate sky-wave mode for that circuit.

4. The Analysis of the Absolute Magnitude of Field Intensities

a. GENERAL. The absolute magnitudes of the sky-wave field intensities were analyzed by using the measured data and circuit information. Theoretical receiver input voltages were compared with observed data values in microvolts receiver input. Measured instantaneous output voltages, recorded on continuous Esterline-Angus type recorders, were calibrated in terms of receiver input voltage at the receiving stations. Hourly median values were computed at the receiving locations from the instantaneous recordings. Information about the transmitting and receiving antenna gains, the transmitting antenna radiated powers, and the receiving circuit input characteristics was obtained directly from the various transmitting and receiving stations. Measured antenna gains were available for a few of the circuits. The antenna gains were calculated in this analysis from standard equations such as shown in Radio Propagation Unit Report No. 7 for linear thin wire antennas, accounting for imperfect earth conditions and assumed antenna losses.[6] Table 4 shows the transmitting antenna gains and the receiving antenna effective heights for various radiation angles above the ground plane. Mismatch losses based on the input circuit characteristics were included in the receiving antenna effective heights.

b. THE CALCULATED RECEIVER INPUT VOLTAGES. (1) The measured and calculated receiver input voltages were compared for night hours. For daytime hours, the absolute magnitude can be obtained from the night values by accounting for the daytime absorption losses. The receiver input voltages were calculated for various possible ray paths for assumed lossless reflections at the ionosphere. These values show what the receiver input voltage would be if the only losses are those due to free space distance attenuation and ground reflections.

(2) The free space loss along a ray path is dependent upon distance between the transmitter and receiver, the virtual layer height, and the number of hops. These were calculated for various assumed layer heights. The analysis indicates that within a very close approximation that the ratio between the distance along a ray path and the distance along the curved earth between the transmitter and receiver is independent of layer height for equal radiation angles. Thus, the free space field intensity of any ray can be given as a function of the radiation angle and the transmission distance alone. The incident field intensity in free space for a reference inverse distance field intensity can be given by the following equation:

$$E = \frac{E_0}{T} \cdot \frac{T}{D} = \frac{E_0}{T} f(\Delta) \qquad \text{Equation 13}$$

where E is the incident field intensity in free space
E_0 is the reference inverse distance field intensity
T is the transmission distance
D is the distance along ray path
$f(\Delta)$ is the functional relationship between the transmitter distance, the ray distance, and the radiation angle
Δ is the angle between ray and ground plane for an inverse distance field intensity of 300 millivolts per meter at one kilometer

Figure 56 is a nomographic solution for this equation.

(3) Ground reflection losses were calculated for randomly polarized sky-waves for various angles with the ground for three types of earth, good earth ($\epsilon = 10$, $\sigma = 10^{-2}$ mhos/m), poor earth ($\epsilon = 4$, $\sigma = 10^{-3}$ mhos/m), and seawater ($\epsilon = 80$, $\sigma = 5$ mhos/m), as shown in Figures 57, 58, and 59. Equal amounts of energy are assumed in the horizontally and vertically polarized fields. These reflection losses are given by the following equation:

$$L = 10 \log_{10} \frac{R_V^2 + R_H^2}{2} \qquad \text{Equation 14}$$

where L is the earth's reflection loss in decibels
R_V is the magnitude of the vertical polarization reflection coefficient
R_H is the magnitude of the horizontal polarization reflection coefficient

c. COMPARISON BETWEEN MEASURED AND CALCULATED VALUES. The theoretical receiver input voltages based on free space and ground reflection losses alone were calculated for the various probable ray angles for all the circuits with sufficient circuit information. These theoretical values and observed yearly peak nighttime receiver input voltages agreed closely for most of the circuits. The yearly peak receiver input voltage is the nighttime value exceeded 10 times during the month that the highest values were observed. Table 5 shows the comparison between calculated values and values observed for various percentages of the time. The statistical analysis indicates that the calculated voltage based on free space and ground reflection losses alone is 8.4 decibels above the yearly median value of the composite of all circuits during the night hours. This 8.4 decibels value can be assumed to be a factor to obtain median field intensities from calculated values during the night hours. During the day hours, the additional daytime absorption loss must be subtracted. The 8.4 decibels value may contain additional losses due to magneto-ionic splitting and layer reflections. For many circuits, this value

may be too large. These circuits have a single predominate sky-wave mode throughout the entire year. Table 6 shows comparisons between calculated and measured receiver input voltages.

d. CONVERGENCE GAINS. In comparing theoretical and observed values, theoretical ionosphere convergence gains were considered. Figures 60 through 63 show convergence gains computed for reflection of electromagnetic waves from a smooth ionosphere as indicated by K. A. Norton.[7] The observed differences between the calculated and measured values indicated that the convergence gains would generally give too high received voltages and, thus, the effects of convergence gains were not included. If the magnitudes along any ray path are determined by areas only a few Fresnel zones in diameter, convergence gains which are based on reflections over a wide smooth reflecting area are probably not applicable. Scattering and wave divergence at the ionosphere were not computed.

5. Proposed Prediction Method for Monthly Median Sky-wave Field Intensities.

a. GENERAL. The proposed prediction method is designed for distances up to about 15,000 kilometers for short wave frequencies. The field intensity values obtained are for the incident waves from the ionosphere and do not include ground reflected components at the receiving location and are median unabsorbed field intensities less ionospheric absorption. An unabsorbed field intensity is that expected during hours of darkness. These values given in this report are for a reference antenna which radiates a signal of 300 millivolts per meter at 1 kilometer. Unabsorbed field intensities for any antenna can be obtained from those based on the reference antenna by accounting for the difference in radiation between the actual transmitting antenna and the reference antenna. If the antenna gains are calculated with reference to the gain of a short dipole with one kilowatt of input power (300 millivolts per meter at one kilometer), and the antenna radiated powers are given referred to one kilowatt, the unabsorbed field intensity for any antenna in decibels is the transmitting antenna gain plus the transmitter power added to the median unabsorbed field intensity of the reference antenna. Unabsorbed field intensities for the reference antenna are obtained from the free space distance attenuation along the ray paths, ground reflection losses, and an experimental factor which converts these theoretical values to median values. These values are calculated for angles above the ground plane which are determined by the minimum virtual layer heights, the transmission distance along the earth's surface between the transmitter and receiver, and the number of reflections between the ionosphere and the ground. Sky-wave field intensities must be computed in slightly different manner for short and long distances. The method for distances short enough that the ionospheric characteristics at the path mid-point determine propagation conditions is shown first and then the method for longer distances is described.

b. UNABSORBED FIELD INTENSITIES. (1) The unabsorbed or nighttime

incident down-coming sky-wave field intensities can be calculated if the transmitting antenna output power and gain, the ray angle above the ground plane, and the distance between the receiver and transmitter are known. The ray angle determines the antenna radiation, the inverse distance losses, and the ground reflection losses (for routes with more than one ionosphere reflection point).

(2) A graphical procedure is followed requiring various charts drawn on the same rectangular grids as the Central Radio Propagation Laboratory monthly predictions. The layer height is found first and then using the layer height, the transmission distance, and the number of hops; the radiation angle is determined from a nomogram. Average F2 layer minimum virtual heights can be found for the required time and geographic location for any month from Figures 23 through 34. Figure 83 is a world map and Figure 84 is a great circle chart used in determining the position of the great circle path between any two points on the earth.

(3) An overlay is required in addition to these charts in order to determine F2 layer heights for any hour referred to any reference longitude. A transparency is placed on the world map and marks are placed over the position of the transmitting and receiving stations. A horizontal line is drawn over the equator line on the world map and a vertical is drawn at the longitude for which the hours of time are desired to be based. If it is desired to have the hours in Eastern Standard Time, the vertical line is drawn at a longitude of 75 degrees west. This overlay is now placed on the great circle chart with the equatorial lines coinciding. The overlay is moved horizontally until the transmitting and receiving locations lie on the same great circle contour or at proportional distances between adjacent great circles. The great circle is sketched in and the path midpoint is marked, using the dash-dotted scale of the great circle chart as the distance scale. The overlay is now ready for use in determining the layer heights for any month for any hour referred to the time reference for the particular circuit. This overlay is placed on the F2 layer minimum virtual height chart for the required month. The equatorial line on the overlay is aligned with the equatorial line of the height chart and the vertical reference line is placed over the desired hour of the day. The F2 minimum virtual layer height is read at the path midpoint.

(4) The radiation angle for any assumed number of hops can now be determined since the layer heights and transmission distances are known. Nomogram, Figure 85, is used in this determination. Figure 86 is a nomogram that can be used for single hop modes. These nomograms are based upon sharp reflections and a curved earth. The slider of Figure 85 is placed in a horizontal position at the layer height with the transmission distance scale of the slider set at the left vertical reference line of the nomogram at the transmission distance. Thus, the radiation angle can be read directly corresponding to any number of hops for any height. In this method, all E layer reflections are assumed to occur at 110 kilometers while the F2 layer reflections occur at heights based

on the average of four years' observations.

(5) Knowing the radiation angle for the probable mode, it is now possible to find the unabsorbed field intensity. Nomogram, Figure 56, shows the free space field for the reference antenna. This nomogram is entered with the radiation angle and the transmission distance to obtain the free space field for any ray path. The unabsorbed field intensity for the reference antenna includes additional losses due to intermediate ground reflections and an experimental factor converting the calculated values to median values. Nomogram, Figures 57 through 59, are used to determine the ground reflection losses over three types of terrain, good earth ($\epsilon = 10$, $\sigma = 10^{-2}$ mhos/m, poor earth ($\epsilon = 4$, $\sigma = 10^{-3}$ mhos/m), and seawater ($\epsilon = 80$, $\sigma = 5$ mhos/m), for any number of ground reflections for any radiation angle. The conversion factor between calculated and median values was shown to be . decibe. Thus, in summary, the unabsorbed field intensities for the reference antenna are obtained by finding the minimum virtual layer heights from a nomogram, finding the radiation angle corresponding to any number of hops from a nomogram, and then finding the free space field intensity from another nomogram. The unabsorbed field intensity, or night time field intensity, for the reference antenna is equal to the free space value for the particular transmission distance and angle above the ground, less the ground losses at the intermediate ground reflections for that radiation angle and less the factor of .. decibels. Generally, one ray path alone determines the sky-wave field intensity for most distances since the ionospheric conditions limit the number of possible ray paths and the antenna radiation is generally stronger along one ray path in addition to the ground reflection losses effecting the strength of multiple hop rays.

c. DAYTIME FIELD INTENSITIES (1) The daytime incident sky-wave field intensities are obtained from unabsorbed field intensities by subtracting the daytime absorption. A graphical method, based on the semi-empirical formula of the statistical analysis is used to calculate the absorption. It is required to know the solar zenith angle at the path midpoint, the running average sunspot number, the angle of incidence at a 100 kilometer height, the number of reflections between the ground and the ionosphere, and the gyro-frequency. These are obtained graphically from the standard rectangular grids mentioned previously. The angle of incidence is expressed in a relationship with the radiation angle determined by the transmission distance, the layer height, and the number of ionospheric hops. The running average sunspot number is predicted while the wave frequency is usually known.

(2) The solar zenith angle and gyro-frequency are obtained by using an overlay; the solar zenith angle charts, Figures 2 through 13; and the gyro-frequency chart, Figure 51. The overlay, which was discussed in preceeding paragraphs, is placed on the solar zenith angle chart for the required month with the equatorial line coinciding and the vertical reference line set at the desired hour. The solar zenith angle is read at the path midpoint.

(3) In order to simplify the graphical method, a new function is defined. This function, called the absorption index, I, is given by the following formula.

$$I = (\cos .881\,\psi)^{1.30}\ (1 + .0037\,S) \qquad \text{Equation 15}$$

where S is the running average sunspot number
ψ is the solar zenith angle
I is the absorption index

With the value of solar zenith angle obtained in the preceding paragraph and the predicted running average sunspot number, the index I can be obtained from the nomogram Figure 87. The index is read at the intersection of the absorption index scale with a straightedge placed between the solar zenith angle and the running average sunspot number.

(4) The sky-wave absorption is a function of the absorption index, sum of the wave frequency and the gyro-frequency, and the radiation angle. The distance factor, sec ϕ, is uniquely determined by the radiation angle and can be implicitly given in a relationship with this angle above ground. The absorption can be found for any single hop transmission mode from the absorption index value, the radiation angle, sum of wave frequency, and the gyro-frequency from nomogram, Figure 88. This proportional nomogram requires two settings of a straightedge. A straightedge is placed between the absorption index value and the radiation angle value and a mark is placed on the central index line. The straightedge is then placed between this point and sum of the wave frequency and the gyro-frequency and the absorption is read on the absorption scale. The absorption for multi-hop routes is equal to the absorption for one hop routes multiplied by the number of hops.

d. MODE DETERMINATION. The extent of ionization can be used to eliminate improbable modes. It has been shown that the maximum frequency usable over routes of various lengths is proportional to the secant of the angle of incidence at the ionized layers. This relationship has been incorporated into Nomogram, Figure 89, which can be used to show whether or not a layer will support a radio wave at various angles referred to the ground plane. The monthly predictions issued by the Central Radio Propagation Laboratory for the F2 4000 MUF and the E 2000 MUF are used with this nomogram. The slider of the nomogram is set in a horizontal position at the layer height with either the F2 4000 MUF value or the E 2000 MUF value (read from the predictions at the path midpoint) on the slider being set at the left vertical index line. The maximum possible radiation angle is read from the angle curves at the wave frequency on the frequency scale of the slider. The value of minimum F2 layer virtual height used is that found in the preceding paragraphs, while the E layer height is assumed to be 110 kilometers. Thus, the greatest angles for E layer and F2 layer transmission can be simply

determined. In order for a F2 layer transmission mode to be possible during the daylight hours, the waves at that radiation angle must be able to penetrate the E layer. This nomogram can also be used to find these E layer penetration frequencies. The slider is set at a 110 kilometer height and it is slid horizontally until the E 2000 MUF is at the left vertical index line. The E layer penetration frequency for a F2 layer transmission mode is read on slider at the angle for the F2 layer transmission mode. A F2 layer mode must penetrate the E layer and not exceed the F2 layer maximum usable frequency. During the night hours, it is only necessary to find the maximum radiation angle for F2 layer modes.

e. LONG DISTANCES. For path lengths exceeding 4000 kilometers, there are certain modifications necessary in the field intensity method. The absorption index cannot be read at the path midpoint. An average absorption index must be used. The solar zenith angle is read at uniform intervals along the great circle path between points 2000 kilometers from each end of the path. The absorption index is found corresponding to these solar zenith angles and averaged. For long distances, the obliquity factors appear to be nearly independent of the number of hops. Thus, the absorption can be solved for any angle which is probable. These angles are again determined from Nomogram, Figure 89, which shows radiation angle corresponding to any transmission distance, layer height, and number of hops. The layer height chosen is taken to be the average of the heights along the great circle path between 2000 kilometer points from the ends of the paths. Paths with a lower number of hops (lower radiation angle) are favored, due to ground reflection losses, particularly over poor ground. Nomogram, Figure 89, can again be used to determine the maximum radiation angle and to determine the E layer penetration angle for the wave frequency. There are occasions when F2 layer propagation is improbable at any angle for a given wave frequency. The critical frequencies are read from the central radio Propagation Laboratory predictions for the required month at 2000 kilometer points from the ends of the path for the F2 layer and 1000 kilometer points from the ends of the path for the E layer. The lower value at the two path ends determines the maximum usable frequencies.

f. EXAMPLES. Several circuits of this report were used to show comparisons between observed monthly median receiver input voltages and calculated values obtained by the proposed prediction method. The results are given on Figures 90 through 93. A sample of the required calculations for the proposed prediction method is given in Table 7. A flow chart of the required calculations is shown in Figure 94.

6. Conclusions

a. ABSORPTION. It is believed that more experimental data was available than in preceding analyses of the same type. In this report, the method differs from others in that an attempt is made to account for variations in ionospheric layer heights. The anomalous absorption variation between seasons is accounted for by layer height variations.

The secant distance factors are computed for ionosphere angles of incidence at a 100 kilometer height, roughly corresponding with the theoretical absorption height. The gyro-frequencies are also computed for this 100 kilometer height. The analysis of the measured data shows that the following semi-empirical equation, similar in form to Appleton's, can be used to account for daytime absorption at frequencies greater than about 3 megacycles per second.

$$A = \frac{615.5\, n \sec \phi\, [1 + .0037\, s]\quad [\cos .881\psi]^{1.30}}{[f + f_g]^{1.98}}$$

The effect of solar activity on absorption is based on the calculations for eight circuits, the correlation coefficients ranging from .603 to .949. The correlation coefficient of the relationship between wave frequency and absorption is .9424, based on the 83 circuit years of data.

b. DAY-TO-DAY VARIATIONS. Forty-three circuit years of mass plots were available for the study of the long statistical variations of hourly median field intensities. The difference in the day-to-day distributions for a period of a month is quite large between different months and circuits. When the day-to-day analysis is made for a year, the distributions become more nearly alike. The variations that occur from month-to-month are usually explainable by some physical cause, such as variation of ionospheric support. *When the data is analyzed over a long time period, both the day and night voltages have distributions that agree at least roughly to the Rayleigh distribution.*

c. ABSOLUTE MAGNITUDES. Theoretical nighttime receiver input voltages based on distance and ground reflection losses alone agree closely with yearly peak nighttime observed voltages for most of the circuits. Monthly median hourly median nighttime voltages were obtained from the theoretical peak voltages by accounting for the difference between peak and median hourly median values based upon the statistical analysis of the day-to-day variations. Although the antenna gains could not be calculated with great accuracy for some of the circuits due to non-standard antenna installations, it is believed that some of the discrepancies are averaged out since many circuits are used in this analysis. No arbitrary theoretical factors are required in computing monthly median nighttime voltages.

d. FIELD INTENSITY METHOD. As indicated by the examples, this field intensity calculation method is reasonably accurate for both relative and absolute values. Absorption variations, which cannot be accounted for by variations of the solar zenith angle alone, are accounted for by variations in ionospheric layer heights instead of presently used arbitrary seasonal factors. *There are no arbitrary theoretical factors in this method.* It is easy and fast to perform since all operations are graphical.

e. ACKNOWLEDGEMENTS. (1) The National Bureau of Standards furnished the majority of the data used. Personnel at the Bureau and contributing organizations performed the great amount of work necessary in converting continuous instantaneous recordings to hourly median values. Thanks are given to Dr. Newbern Smith, Mr. A. G. McNish, and Mr. K. A. Norton of Central Radio Propagation Laboratory for their cooperation and interest in this work.

(2) The authors of this report wish to acknowledge the assistance of the other members of the Radio Propagation Unit. In particular Mr. Louis C. Hayden, Jr. who assisted in the design of the nomograms and contributed generally in other phases and Mr. Frederick A. Jones who calculated the antenna characteristics and constructed most of the figures and nomograms. Mr. James F. Roche (formerly with the Radio Propagation Unit), Mr. William H. Winston, Mr. Edgar C. Sell, and Mr. S. Edward Probst also made substantial contributions to the analysis. The many helpful suggestions and criticisms of Mr. A. R. Beach, the former Chief of the Radio Propagation Section, OCSigO. are also acknowledged.

Paul O. Laitinen
PAUL O. LAITINEN
Radio Engineer
Chief, Radio Propagation Unit

George W. Haydon
GEORGE W. HAYDON
Radio Engineer
Radio Propagation Unit

7. Bibliography

1. H. T. Friis, C. B. Feldman and W. M. Sharpless, "Determination of the Direction of Arrival of Short Radio Waves", Proc. I. R. E. Vol. 22, pp. 47-78, January 1934.

2. L. E. Beghian, "The Estimation and Forecasting of Short Wave Propagation Conditions, With Special Reference to Naval Communications", Radio Section, Admiralty Signal Establishment, February 1948.

3. H. Bremmer, "Terrestrial Radio Waves", Elesvier Publishing Company, Inc., New York, 1949.

4. F. W. G. White, "The Absorption of Radio Waves at Vertical Incidence", Council for Scientific and Industrial Research, Radiophysics Laboratory, Chippendale, N. S. W., May 1943.

5. S. K. Mitra, "Report on the Present State of Our Knowledge of the Ionosphere", Proceedings of the National Institute of Sciences of India, Vol. I, No. 3, Calcutta, 1935.

6. P. O. Laitinen, "Linear Communication Antennas", Radio Propagation Unit Report No. 7, Baltimore, Maryland, May 1949.

7. K. A. Norton, "The Nature of Very High Frequency Ionospheric Wave Propagation", FCC Docket No. 6651, September 1944.

8. R. S. Hoyt, "Probability Theory and Telephone Transmission Engineering", Bell System Technical Journal, Vol. XII, No. 1, January 1933.

9. N. Smith and M. B. Harrington, "The Variability of Sky-Wave Field Intensities at Medium and High Frequencies", Central Radio Propagation Laboratory Report CRPL-1-6, April 1948.

10. R. S. Hoyt, "Probability Functions for the Modulus and Angle of the Normal Complex Variate", Bell System Technical Journal, Vol. XXVI, No. 2, April 1947.

11. L. G. McCracken, "A Note on the Ionospheric Absorption Problem", Journal of Applied Physics, Vol. 20, No. 2, pp 220-230, February 1949.

12. "Ionospheric Radio Propagation", National Bureau of Standards Circular 462, June 1948.

13. S. Chapman and J. Bartels, "Geomagnetism", Vol. I and Vol. 2, Oxford Press, 1940.

14. H. J. Allcock and J. R. Jones, "The Nomogram", Sir Isaac Pitman & Sons, Ltd., London, 1939.

15. J. A. Stratton, "Electromagnetic Theory", McGraw-Hill Book Co., Inc. New York, 1941.

16. W. T. Skilling and R. S. Richardson, "Astronomy", Henry Holt and Company, New York, Second Edition, July 1947.

CIRCUITS AND TYPE OF DATA ANALYZED

TRANSMITTING STATION	RECEIVING STATION	DISTANCE Km	FREQUENCY Mc/s	YEAR	MONTHLY MEDIAN HOURLY MEDIAN RECEIVER INPUT VOLTAGE	MASS PLOTS OF HOURLY MEDIAN RECEIVER INPUT VOLTAGE
WWI	NBS	55	2.06	1946	x	
WWI	NBS	55	2.06	1947	x	
WWI	NBS	55	2.06	1948	x	
WWI	NBS	55	2.06	1949	x	
WWI	NBS	55	4.27	1946	x	x
WWI	NBS	55	4.27	1947	x	
WWI	NBS	55	4.27	1948	x	
WWI	NBS	55	4.27	1949	x	
WWI	NBS	55	5.89	1944	x	
WWI	NBS	55	5.89	1945	x	
WWI	NBS	55	5.89	1946	x	
WWI	NBS	55	5.89	1947	x	
WWI	NBS	55	5.89	1948	x	
WWI	NBS	55	5.89	1949	x	
KHDG	College	150	3.02	1947		x
KHDG	College	150	3.02	1948		x
KHDG	College	150	3.02	1949		x
WQXR	NBS	360	1.56	1946	x	x
CFRX	NBS	552	6.07	1946	x	x
CFRX	NBS	552	6.07	1947	x	x
WWV	MIT	581	5.00	1946	x	x
WWV	MIT	581	5.00	1947	x	x
WWV	MIT	581	5.00	1948	x	
WWV	MIT	581	5.00	1949	x	
WWV	MIT	581	10.00	1946	x	
WWV	MIT	581	10.00	1947	x	x
WLW	NBS	591	0.70	1946	x	x
W8XAL	NBS	691	6.08	1946	x	x
W8XAL	LSU	1176	6.08	1946	x	x
WWV	LSU	1617	5.00	1946	x	x
WWV	LSU	1617	5.00	1947	x	x
WWV	LSU	1617	5.00	1948	x	x
WWV	LSU	1617	5.00	1949	x	x
WWV	LSU	1617	10.00	1946	x	x

(Continued on next page)

TABLE 1

CIRCUITS AND TYPE OF DATA ANALYZED (CONTINUED)

TRANSMITTING STATION	RECEIVING STATION	DISTANCE Km	FREQUENCY Mc/s	YEAR	MONTHLY MEDIAN HOURLY MEDIAN RECEIVER INPUT VOLTAGE	MASS PLOTS OF HOURLY MEDIAN RECEIVER INPUT VOLTAGE
WWV	LSU	1617	10.00	1947	x	x
WWV	LSU	1617	10.00	1948	x	
WWV	LSU	1617	10.00	1949	x	
WWV	LSU	1617	15.00	1946	x	x
WWV	LSU	1617	15.00	1947	x	x
WWV	LSU	1617	15.00	1948	x	x
WWV	LSU	1617	15.00	1949	x	
WWV	LSU	1617	20.00	1947	x	x
WWV	U of PR	2494	5.00	1946	x	x
WWV	U of PR	2494	5.00	1947	x	x
WWV	U of PR	2494	5.00	1948	x	
WWV	U of PR	2494	5.00	1949	x	
WWV	U of PR	2494	10.00	1944	x	
WWV	U of PR	2494	10.00	1945	x	
WWV	U of PR	2494	10.00	1946	x	x
WWV	U of PR	2494	10.00	1947	x	x
WWV	U of PR	2494	10.00	1948	x	
WWV	U of PR	2494	10.00	1949	x	
WWV	U of PR	2494	15.00	1946	x	x
WWV	U of PR	2494	15.00	1947	x	x
WWV	U of PR	2494	15.00	1948	x	
WWV	U of PR	2494	15.00	1949	x	
WWV	U of PR	2494	20.00	1947	x	x
WWV	Churchill	2523	10.00	1946	x	
WWV	Churchill	2523	10.00	1947	x	
WWV	Churchill	2523	15.00	1946	x	
WWV	Churchill	2523	15.00	1947	x	
XEWW	NBS	3000	9.50	1945	x	x
XEWW	NBS	3000	9.50	1946	x	x
CXA19	Huancayo	3194	11.83	1946	x	x
CXA19	Huancayo	3194	11.83	1947	x	x
CXA19	Huancayo	3194	11.83	1948	x	
CXA19	Huancayo	3194	11.83	1949	x	
WWV	Ft Read	3558	10.00	1946	x	x

(Continued on next page)

TABLE 1

CIRCUITS AND TYPE OF DATA ANALYZED (CONCLUDED)

TRANSMITTING STATION	RECEIVING STATION	DISTANCE Km	FREQUENCY Mc/s	YEAR	MONTHLY MEDIAN HOURLY MEDIAN RECEIVER INPUT VOLTAGE	MASS PLOTS OF HOURLY MEDIAN RECEIVER INPUT VOLTAGE
WWV	Ft Read	3558	15.00	1946	x	x
XEWW	MIT	3636	9.50	1944	x	x
XEWW	MIT	3636	9.50	1945	x	x
XEWW	MIT	3636	9.50	1946	x	x
XEWW	MIT	3636	9.50	1947	x	
XEWW	MIT	3636	9.50	1948	x	
XEWW	MIT	3636	9.50	1949	x	
WWV	Stanford	3980	5.00	1946	x	x
WWV	Stanford	3980	10.00	1946	x	x
WWV	Stanford	3980	15.00	1946	x	x
WWV	College	5269	10.00	1946		x
WWV	College	5269	10.00	1947		x
WWV	College	5269	10.00	1948		x
GLH	Riverhead	5337	13.52	1946	x	x
WWV	Huancayo	5670	10.00	1946	x	x
WWV	Huancayo	5670	15.00	1946	x	x
GSD	College	6707	11.75	1946		x
GLH	U of PR	6750	13.52	1946	x	x
WWV	Maui, TH	7684	10.00	1947	x	x
WWV	Maui, TH	7684	15.00	1947	x	x
KWE	Komuro	8228	15.43	1947	x	
VIY	Stanford	12,630	12.02	1946	x	x
N>N	Huancayo	15,689	12.80	1946	x	x
WWVH	Hiraiso	6099	5.00	1949		
WWVH	Hiraiso	6099	10.00	1949		
WWVH	Hiraiso	6099	15.00	1949		
WWV	Hiraiso	10,765	5.00	1949		
WWV	Hiraiso	10,765	10.00	1949	Median Field intensities available for parts of some months	
WWV	Hiraiso	10,765	15.00	1949		
WWV	Hiraiso	10,765	20.00	1949		
WWVH	Fukuoka	7042	10.00	1949		
WWVH	Fukuoka	7042	15.00	1949		
WWVH	Sapporo	6047	10.00	1949		
WWVH	Sapporo	6047	15.00	1949		

TABLE I

SOLAR ACTIVITY

EVALUATION OF b WHEN $A_x = A_o(1+bS)$

WAVE FREQUENCY Mc/s	TRANSMISSION DISTANCE Km	b	CORRELATION COEFFICIENT
2.061	55	.00225	.837
4.270	55	.00385	.603
5.89	55	.00348	.949
5.00	581	.00617	.924
6.08	591	.00305	.848
10.00	1617	.00360	.613
10.00	2494	.00500	.936
9.50	3636	.00209	.875
	Σb	.02949	
	average b	.00369	

TABLE 2

SEASONAL VARIATIONS IN, m, THE EXPONENT OF THE SOLAR ZENITH ANGLE FUNCTION AND RESIDUAL ABSORPTION

$$A_x = A_o (\cos .881\psi)^m$$

SEASON	NUMBER OF YEARS DATA	AVERAGE m	SEASONAL ABSORPTION EXPRESSED AS A PERCENTAGE OF THE YEARLY AVERAGE
Spring	81	1.33	100.0
Summer	78	1.34	100.8
Fall	69	1.33	99.5
Winter	81	1.31	99.5

TABLE 3

CALCULATION OF THEORETICAL RECEIVER INPUT VOLTAGES

Transmitting Station	Receiving Station	Transmission Distance Km	Frequency Mc/s	Transmission Mode	Radiation Angle	Transmitter Power DB>1Kw	Transmitter Antenna Gain DB	Inverse Distance Field DB	Type of Terrain	Ground Loss DB	Receiver Effective Height DB	Receiver Input Voltage DB>1mv
WWI	NBS	55	2.06	1F	84.0	-6.1	1.7	54.3	-	-	32.1	82.0
WWI	NBS	55	4.27	1F	84.0	-6.1	2.0	54.3	-	-	27.8	78.0
WQXR	NBS	360	1.56	1F	55.0	10.0	-18.2	53.2	-	-	18.7	63.7
WWV	MIT	581	5.00	1F	41.0	10.0	-10.5	51.5	-	-	8.1	59.4
WLW	NBS	591	0.70	1F	41.0	17.0	-9.3	51.4	-	-	21.7	80.8
WLW-K	NBS	591	6.08	1F	41.0	0.0	-10.5	51.4	-	-	23.8	64.7
WLW-K	LSU	1176	6.08	1F	21.9	0.0	-4.5	47.3	-	-	18.9	61.7
WWV	LSU	1617	5.00	2F	31.1	9.0	-6.5	43.6	GG	2.5	22.8	66.4
WWV	LSU	1617	10.00	1F	15.9	9.5	-5.0	44.6	-	-	14.1	63.2
WWV	LSU	1617	15.00	1F	15.9	9.5	-5.3	44.6	-	-	14.5	63.3
WWV	U of P R	2494	15.00	1F	6.2	9.5	-9.2	41.3	-	-	5.2	46.8
WWV	U of P R	2494	20.00	1F	6.2	9.3	-9.2	41.3	-	-	9.0	50.4
WWV	Churchill	2593	10.00	1F	6.1	9.5	-8.6	41.3	-	-	-1.2	41.0
XEWW	Stanford	3000	9.50	2F	16.6	9.5	-5.1	39.3	GG	3.3	14.1	56.5
XEWW	NBS	3000	9.50	2F	16.6	9.5	-5.1	39.3	GG	3.3	18.7	61.1
CXA19	Huancayo	5194	11.72	2F	15.5	7.0	-5.2	38.8	GG	3.4	17.0	54.2
WWV	Ft. Read	3958	10.00	2F	14.1	9.5	-5.2	37.8	SW	.4	17.8	59.5
WWV	Ft. Read	3958	15.00	2F	14.1	9.5	-5.5	37.8	SW	.3	16.1	57.6
XEWW	MIT	3636	9.50	2F	12.5	9.5	-3.8	37.6	GG	3.2	17.5	57.4
WWV	Stanford	3980	5.00	2F	10.6	9.0	-4.8	37.8	GG	2.9	18.5	57.6
WWV	Stanford	3980	10.00	2F	10.6	9.5	-6.0	37.1	GG	3.2	11.5	48.1
WWV	Stanford	3980	15.00	2F	10.6	9.5	-6.7	37.1	GG	3.3	8.3	44.9
GLH	Riverhead	5337	13.54	2F	5.2	10.0	18.4	34.5	SW	.7	6.8	66.5
WWV	Huancayo	5670	10.00	3F	11.3	9.5	-5.8	33.9	SW	1.6	14.9	50.9
WWV	Huancayo	5670	15.00	2F	4.0	9.5	-11.6	34.3	SW	1.0	5.5	36.8
WWV	Maui, T.H.	7684	10.00	3F	5.8	9.5	-8.9	31.5	SW	1.2	13.7	44.6
WWV	Maui, T.H.	7684	15.00	3F	5.8	9.5	-8.7	31.5	SW	1.4	20.8	5 .7
VIY	Stanford	12630	12.02	6F	9.5	9.3	18.4	27.0	SW	2.1	5.3	57.9

GG - Good Ground
SW - Sea Water

Table 4

SUMMARY OF CALCULATED THEORETICAL RECEIVER INPUT VOLTAGES COMPARED TO NIGHTTIME OBSERVED RECEIVER INPUT VOLTAGES ON A YEARLY BASIS

OBSERVED RECEIVER INPUT VOLTAGE	NUMBER OF OBSERVATIONS	THEORETICAL VOLTAGE MINUS THE OBSERVED VOLTAGE
Hourly median exceeded 50% of the time	55	8.4 DB
Hourly median exceeded 1% of the time	22	0.3 DB
Hourly median exceeded 10% of the time	22	3.6 DB
Hourly median exceeded 90% of the time	22	18.1 DB
Yearly peak receiver input voltage (See Paragraph 4.c.)	38	-0.6 DB

TABLE 5

COMPARISON OF THE CALCULATED THEORETICAL INPUT VOLTAGES AND NIGHTTIME OBSERVED RECEIVER INPUT VOLTAGES

TRANSMISSION DISTANCE	FREQUENCY	YEAR	ANNUAL OBSERVED NIGHTTIME HOURLY MEDIAN INPUT VOLTAGE				CALCULATED INPUT VOLTAGE	DIFFERENCE BETWEEN CALCULATED VOLTAGE AND 1% EXCEEDED	DIFFERENCE BETWEEN CALCULATED VOLTAGE AND 10% EXCEEDED	DIFFERENCE BETWEEN CALCULATED VOLTAGE AND MEDIAN	DIFFERENCE BETWEEN CALCULATED VOLTAGE AND 90% EXCEEDED	DIFFERENCE BETWEEN 10% EXCEEDED AND 90% EXCEEDED
			TIME EXCEEDED									
			1%	10%	50%	90%						
(1)	(2)	(3)	(4)	(5)	(6)	(7)	(8)	(9)	(10)	(11)	(12)	(13)
55	2.06	1946	84.8	82.4	78.5	72.1	82.0	+2.8	-0.4	3.5	9.9	10.3
55	4.27	1946	72.1	70.6	66.2	64.5	78.0	5.9	7.4	9.8	13.5	6.1
360	1.56	1946	64.2	59.1	50.4	37.0	63.7	-0.5	4.6	13.3	26.7	22.1
581	5.00	1946	67.8	64.8	60.2	53.2	59.4	+8.4	-5.4	+0.8	6.2	11.6
581	5.00	1947	67.8	64.8	60.2	53.2	59.4	+8.4	-5.4	-0.8	6.2	11.6
591	0.70	1946	83.3	78.0	71.9	56.2	80.8	+2.5	2.8	8.9	24.6	21.8
591	6.08	1946	64.7	52.8	48.1	40.0	64.7	10.0	11.9	16.6	24.7	12.8
1617	5.00	1946	64.1	59.2	51.0	38.0	66.4	2.3	7.2	15.4	28.4	21.2
1617	10.00	1947	61.8	56.2	48.5	38.2	63.2	1.4	7.0	14.7	25.0	18.0
2494	15.00	1947	52.1	48.8	43.2	34.0	46.8	-5.3	-2.0	3.6	12.8	14.8
3010	9.50	1946	62.1	60.7	58.2	54.0	61.1	-1.0	0.4	2.9	7.1	6.7
3194	11.83	1946	61.5	58.1	53.0	44.1	54.2	-7.3	-3.9	1.2	10.1	14.0
3558	10.00	1946	50.8	47.8	42.7	34.7	59.5	8.7	11.7	16.8	24.8	13.1
3558	15.00	1946	46.1	43.0	38.0	29.6	57.6	11.5	14.6	19.6	28.0	13.4
3636	9.50	1944	55.0	51.2	43.8	34.0	57.4	2.4	6.2	13.6	23.4	17.2
3636	9.50	1945	50.2	49.2	43.0	32.4	57.4	7.2	8.2	14.4	25.0	16.8
3636	9.50	1946	59.2	55.4	49.5	37.8	57.4	-1.8	2.0	7.9	19.6	17.6
3980	5.00	1946	52.4	48.7	42.7	32.9	57.6	5.2	8.9	14.9	24.7	15.8
3980	10.00	1946	57.8	52.6	48.4	39.4	49.0	-8.8	-3.6	0.6	9.6	13.2
3980	15.00	1946	50.6	46.1	39.3	27.9	44.9	-5.7	-1.7	5.6	17.0	18.2
5670	10.00	1946	50.7	48.0	44.0	36.5	50.9	0.2	2.9	6.9	14.3	11.4
5670	15.00	1945	30.6	29.8	25.2	17.9	36.8	6.2	7.0	11.6	18.9	11.9
55	2.06	1947			77.9		82.0			4.1		
55	2.06	1948			73.6		82.0			8.4		
55	2.06	1949			60.2		82.0			21.8		
55	4.27	1947			68.6		78.0			9.4		
55	4.27	1948			68.3		78.0			9.7		
55	4.27	1949			71.4		78.0			6.6		
581	5.00	1948			61.3		59.4			-1.9		
581	5.00	1949			62.5		59.4			-3.1		
581	10.00	1947			52.4		69.1			16.7		
1176	6.08	1946			39.7		61.7			22.0		
1617	5.00	1948			59.9		66.4			6.5		
1617	5.00	1949			61.9		66.4			4.5		
1617	10.00	1948			47.5		63.2			15.7		
1617	10.00	1949			55.9		63.2			7.3		
1617	15.00	1948			47.3		63.3			16.0		
1617	15.00	1949			62.3		63.3			1.0		
2494	15.00	1946			40.6		46.8			6.2		
2494	15.00	1948			38.4		46.8			8.4		
2494	15.00	1949			43.5		46.8			3.3		
2494	20.00	1947			40.9		50.4			9.5		
2523	10.00	1946			30.2		41.0			10.8		
3000	9.50	1945			45.0		56.5			11.5		
3000	9.50	1946			48.8		56.5			7.8		
3194	11.83	1947			49.9		54.2			4.3		
3194	11.83	1948			47.2		54.2			7.0		
3194	11.83	1949			48.7		54.2			5.5		
3636	9.50	1947			49.4		57.4			8.0		
3636	9.50	1948			42.1		57.4			15.3		
3636	9.50	1949			45.1		57.4			12.3		
5337	13.52	1946			52.9		66.5			11.3		
7684	10.00	1947			36.8		44.6			7.8		
7684	15.00	1947			24.0		51.7			27.7		
12630	12.02	1946			31.2		57.9			26.7		

TABLE 6

SAMPLE SKY-WAVE RECEIVER INPUT VOLTAGE CALCULATION

NATIONAL BUREAU OF STANDARDS RECEIVING XEWW MEXICO CITY

FREQUENCY 9.5 Mc/s – TRANSMISSION DISTANCE 3010 Km

TRANSMITTING ANTENNA – λ/2 VERTICAL ELEVATED .78λ RECEIVING ANTENNA – λ/2 HORIZONTAL ELEVATED 55'

	Reference Time 90°W	F2 Layer Height – Km Figures 23 to 34	F2 – 4000 MUF – Mc/s CRPL Predictions	E 200C MUF – Mc/s CRPL Predictions	F2 Layer Critical Angle Nomogram Figure 89	E Layer Critical Angle Nomogram Figure 89	Possible Modes Nomogram Figure 85	Radiation Angles Nomogram Figure 85	Free Space Field–DB>1MV/M Nomogram Figure 56	Transmitter Antenna Gain–DB R.P.U. Tech 2 or Tech. 6	Ground Reflection Loss–DB Nomogram Figures 57 to 59	RCVG Antenna Effective Hgt R.P.U. Tech. 7 – Decibels	Transmitter Power DB > 1 Kw	Solar Zenith Angle Figures 2 to 13	12 Month Moving Average Sunspot Number; CRPL Pred.	Absorption Index "I" Nomogram Figure 87	Gyro Frequency at 100 Km Figure 51 – Mc/s	Wave Frequency plus 1.4 Mc Gyro Frequency	Sky-wave Absorption – DB Nomogram Figure 88	Σ(9), (10), (11), (12), (13), (19)	Theoretical Median Receiver Input Voltage Max (20)–8.4
	(1)	(2)	(3)	(4)	(5)	(6)	(7)	(8)	(9)	(10)	(11)	(12)	(13)	(14)	(15)	(16)	(17)	(18)	(19)	(20)	(21)
June 1946	0000	285	17.6	–	25°	–	1F	3°	39.8	-9.0	–	7.4							–	47.7	
							2F	16°	39.1	-2.5	0.2	18.4	9.5	–	87	–	1.4	10.9	–	64.3	55.9
	1200	385	23.0	18.4	52°	18°	2F	22°	38.9	-3.6	0.2	20.2							33.4	31.4	23.0
							3F	33°	38.0	-5.8	7.6	20.4	9.5	6°	87	1.32	1.4	10.9	36.0	18.5	
							2E	4°	39.7	-6.8	.8	9.8							72.0	-20.6	
December 1946	0000	275	14.2	–	20°	–	1F	3°	39.8	-9.0	–	7.4							–	47.7	
							2F	15°	39.2	-2.2	0.2	18.4	9.5	–	126	–	1.4	10.9	–	64.7	56.3
	1200	245	33.0	16.8	70°	16°	2F	13°	39.1	-2.0	0.3	17.4							34.0	29.7	21.3
							3F	22°	38.9	-3.6	6.2	20.2	9.5	53°	126	.92	1.4	10.9	34.8	24.0	
							2E	4°	39.7	-7.0	0.8	9.0							49.8	0.6	

Table 7

EXAMPLE OF DIURNAL VARIATION OF RECEIVER INPUT VOLTAGES
LOUISIANA STATE UNIVERSITY RECEIVING WASHINGTON, D. C.
MARCH 1949

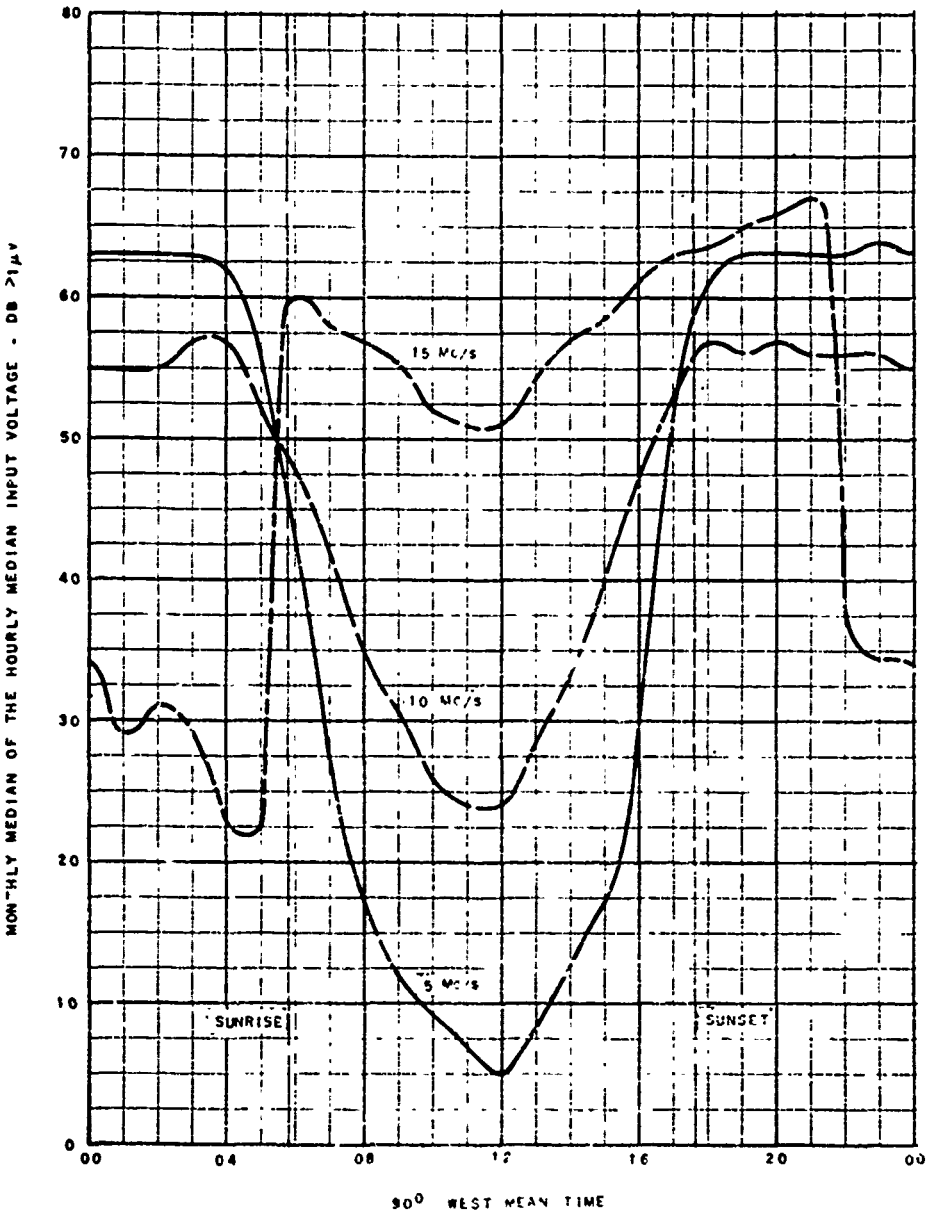

Figure 1

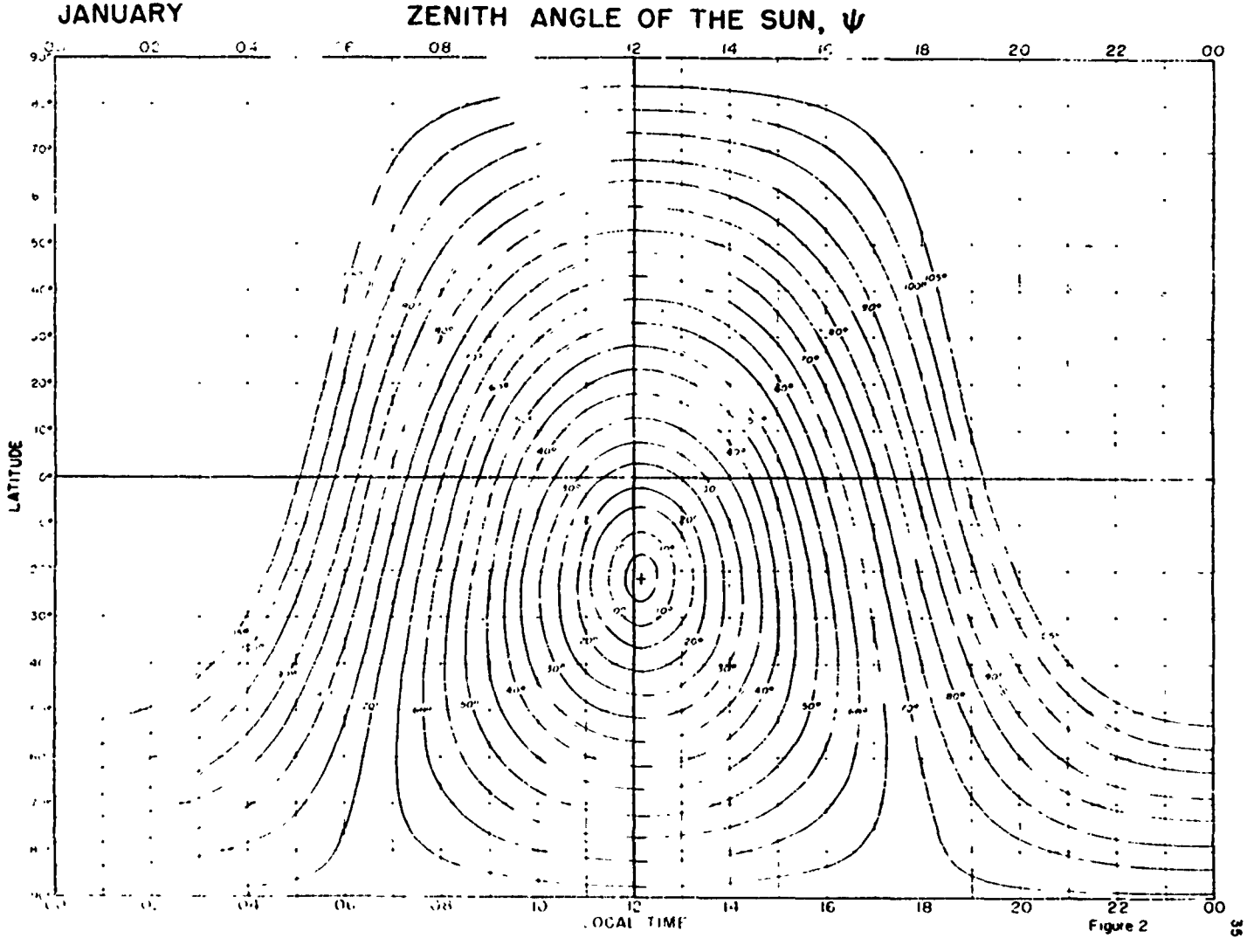
JANUARY
ZENITH ANGLE OF THE SUN, ψ
LATITUDE
LOCAL TIME
00
02
04
06
08
10
12
14
16
18
20
22

Figure 2

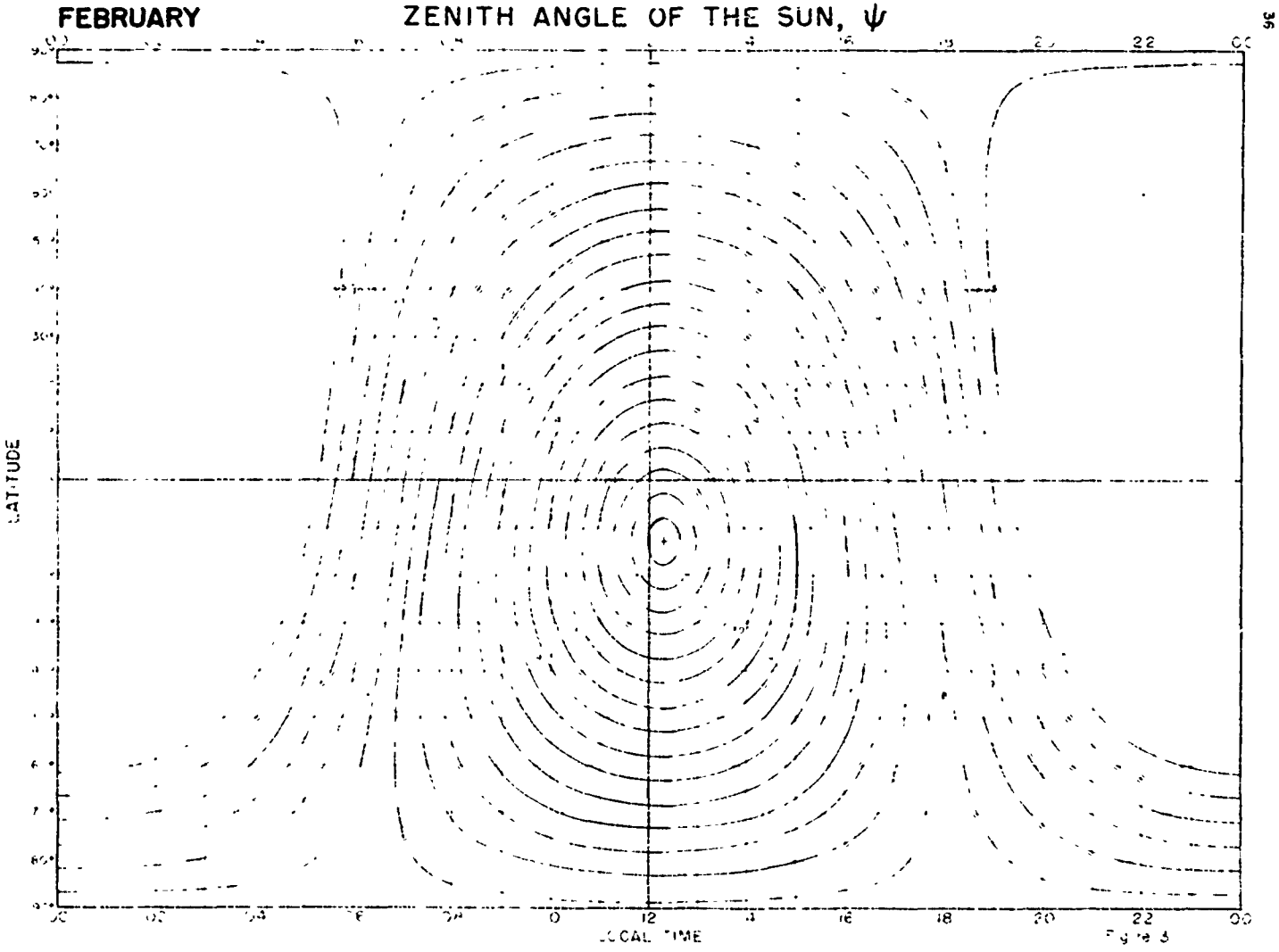
FEBRUARY
ZENITH ANGLE OF THE SUN, ψ
LATITUDE
LOCAL TIME
0
12
18
22
00

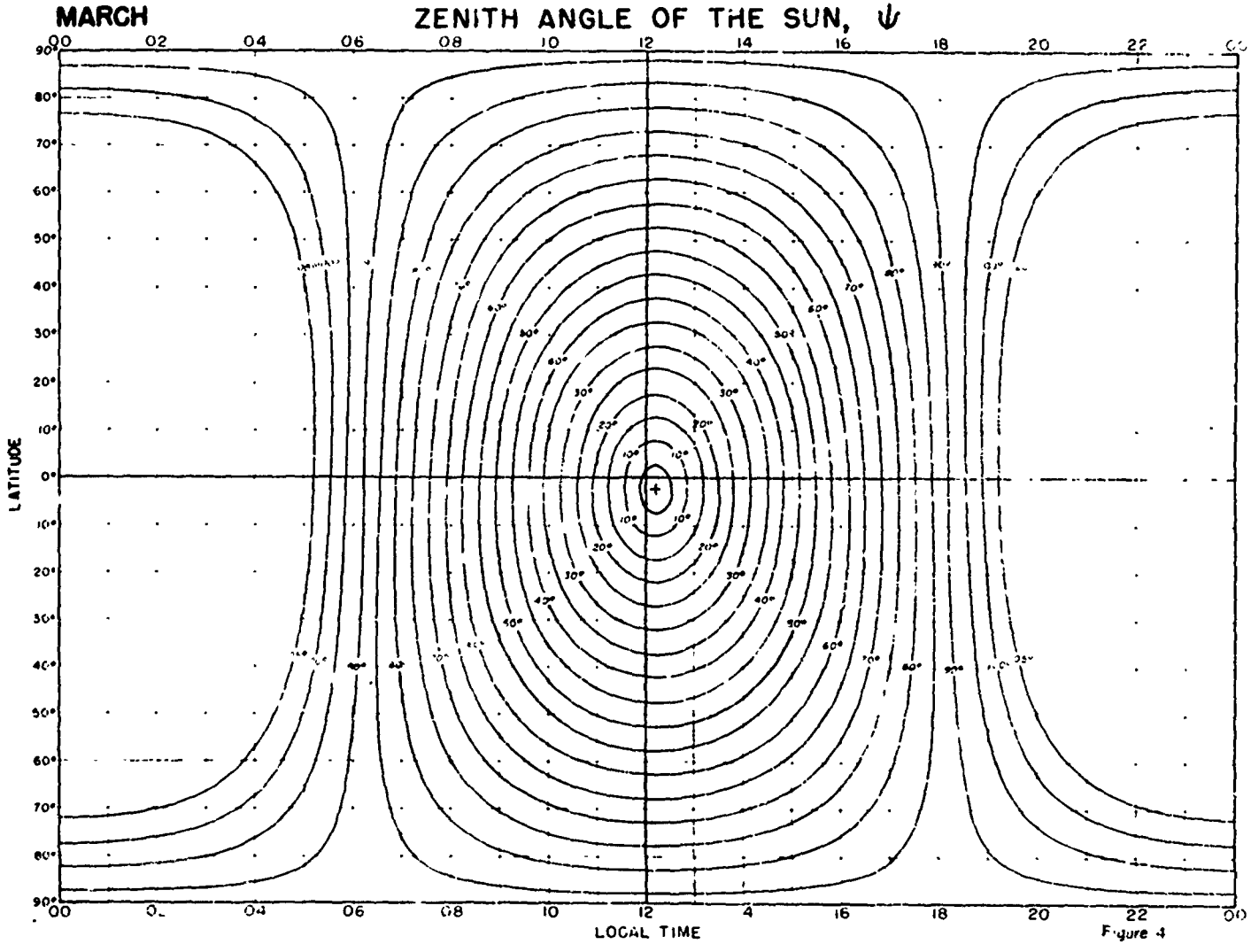

Figure 4

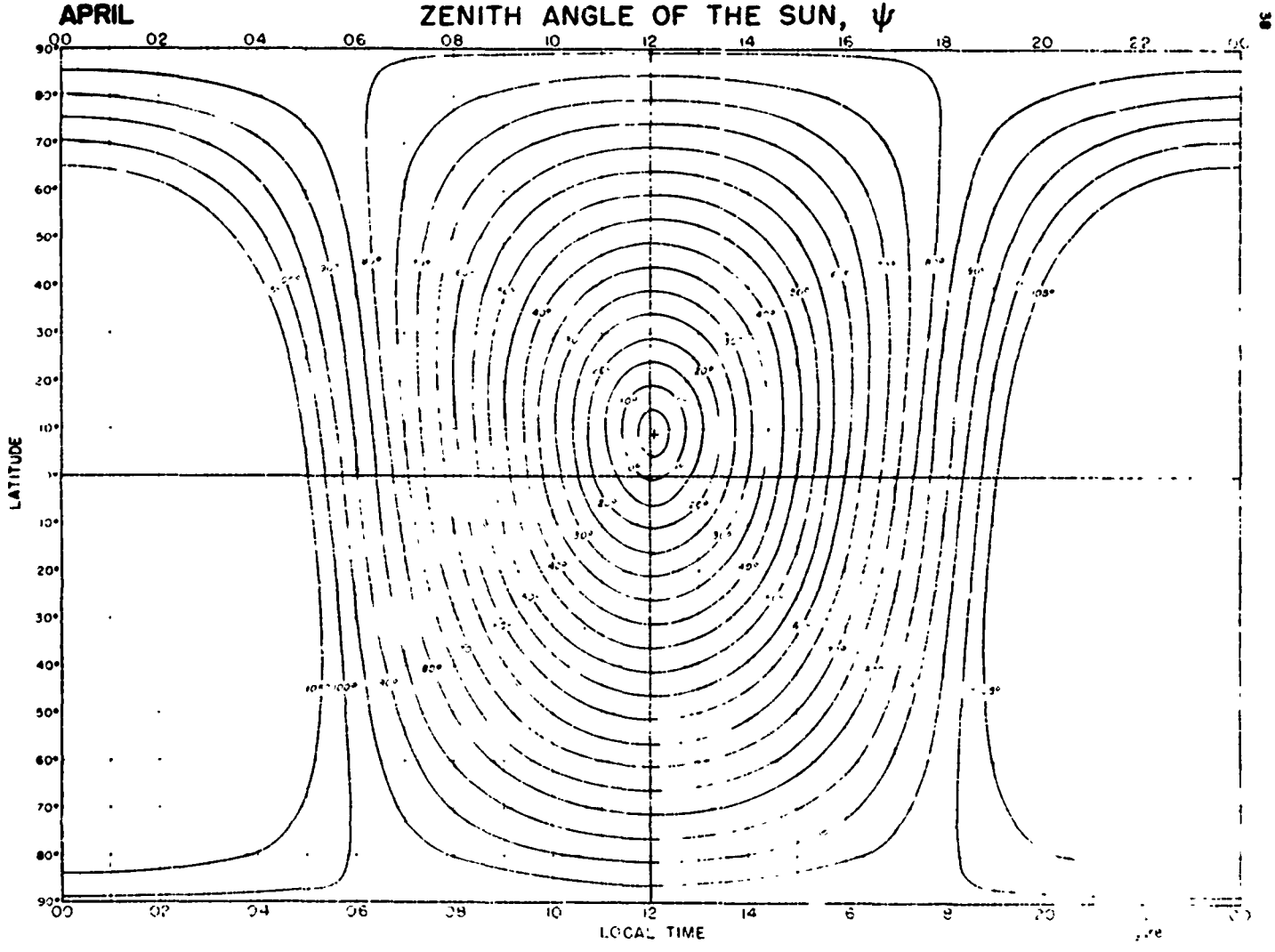
APRIL
ZENITH ANGLE OF THE SUN, ψ
LATITUDE
LOCAL TIME

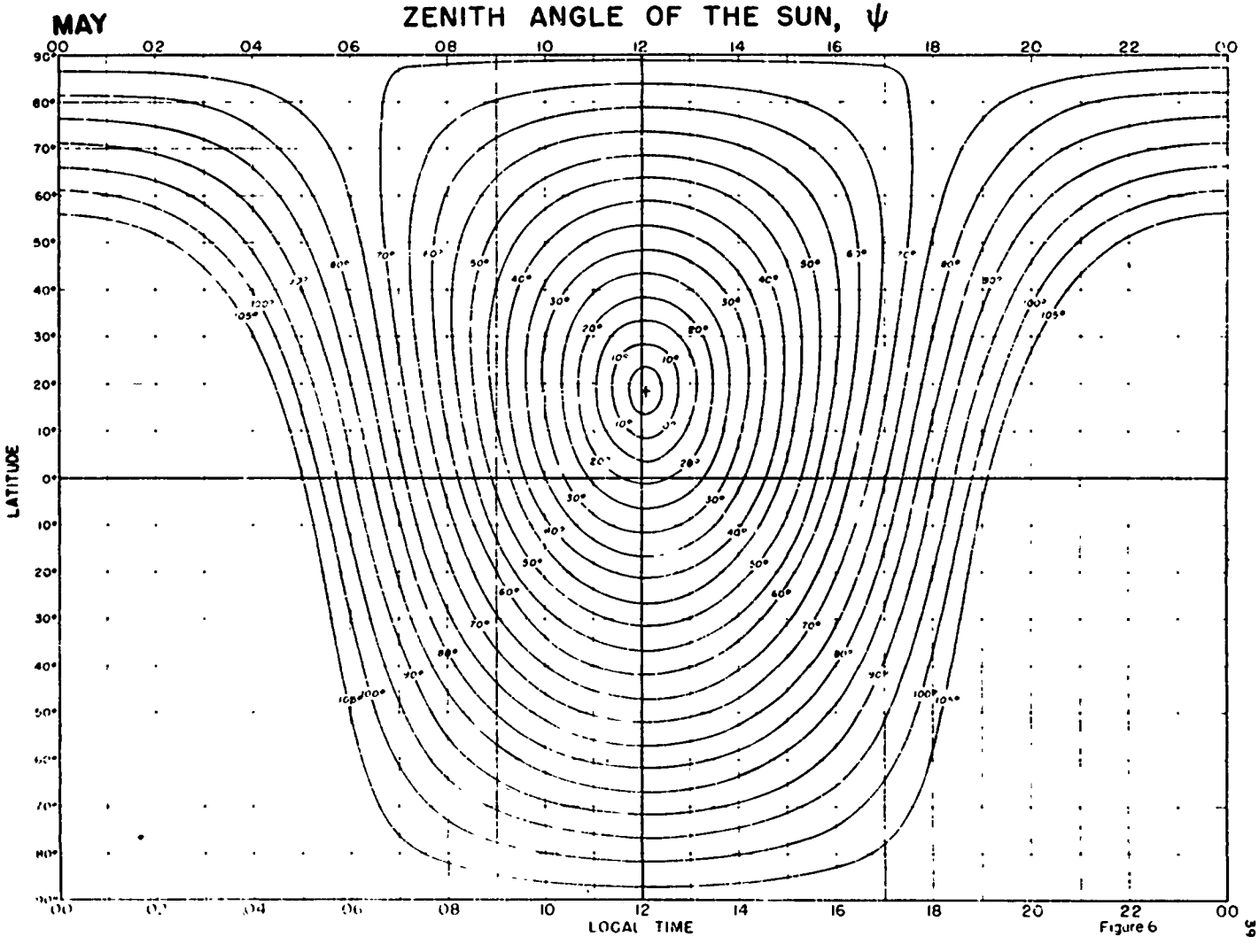
MAY
ZENITH ANGLE OF THE SUN, ψ
LATITUDE
LOCAL TIME
00
02
04
06
08
10
12
14
16
18
20
22
00
90°
80°
70°
60°
50°
40°
30°
20°
10°
0°

Figure 6

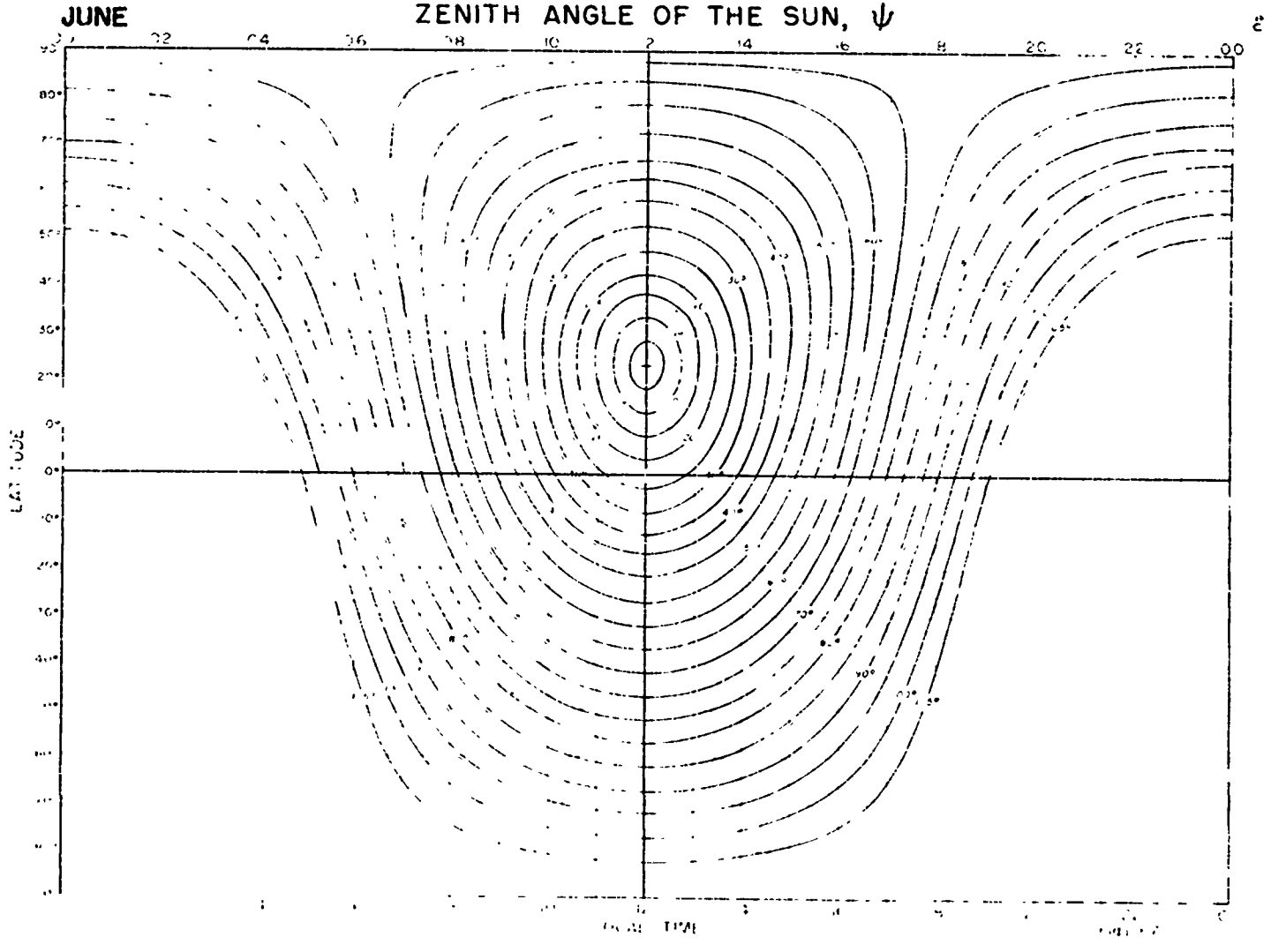
JUNE
ZENITH ANGLE OF THE SUN, ψ
22
24
02
04
06
08
10
12
14
16
18
20
22
24
80°
70°
60°
50°
40°
30°
20°
0°
0°
10°
20°
30°
40°
50°
60°
70°
80°
90°
100°
110°
120°
130°
140°
150°
160°
170°
180°

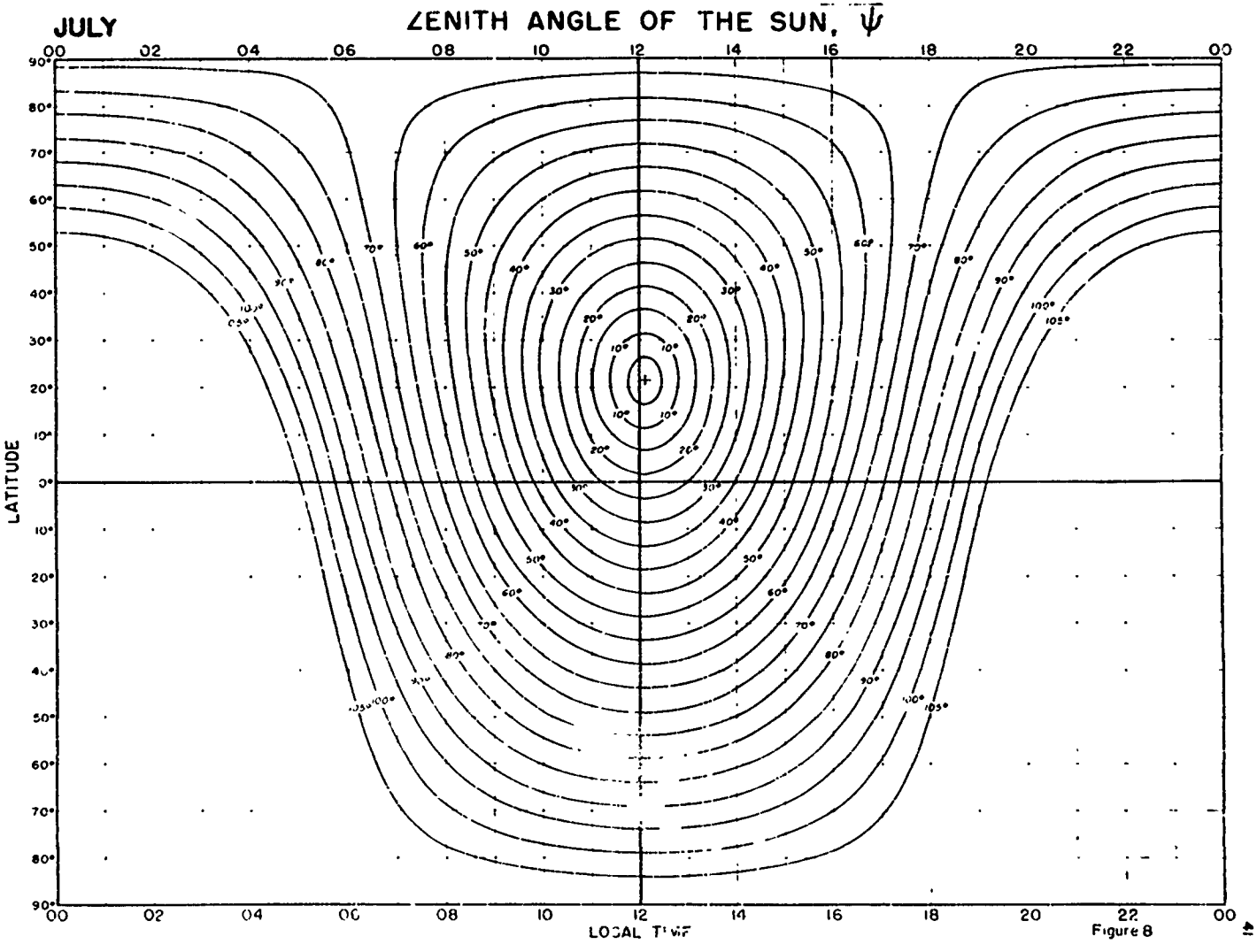
JULY
ZENITH ANGLE OF THE SUN, ψ
LATITUDE
LOCAL TIME
00
02
04
06
08
10
12
14
16
18
20
22
00
90°
80°
70°
60°
50°
40°
30°
20°
10°
0°

Figure 8

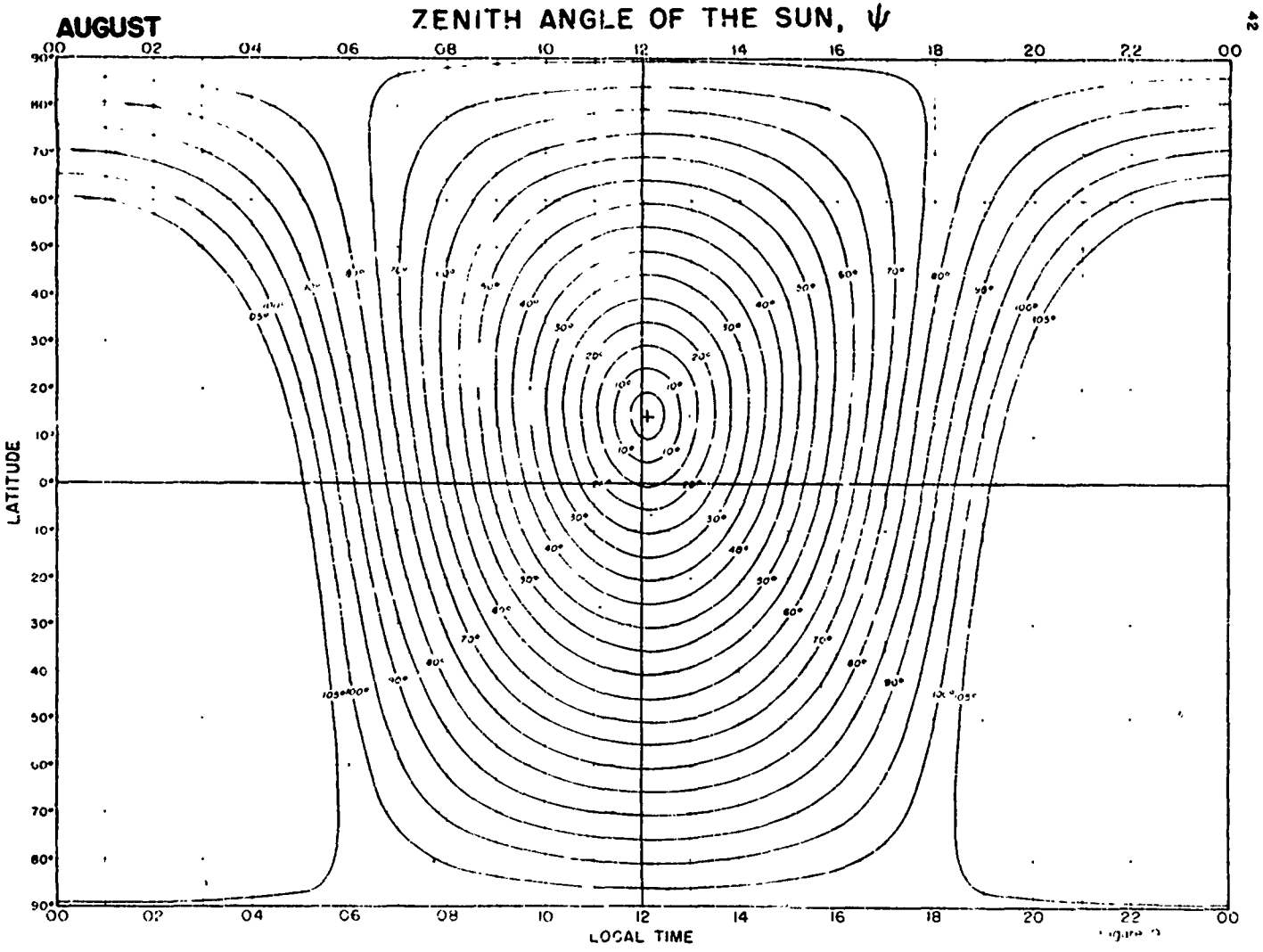
AUGUST
ZENITH ANGLE OF THE SUN, ψ
LATITUDE
LOCAL TIME
00
02
04
06
08
10
12
14
16
18
20
22
00

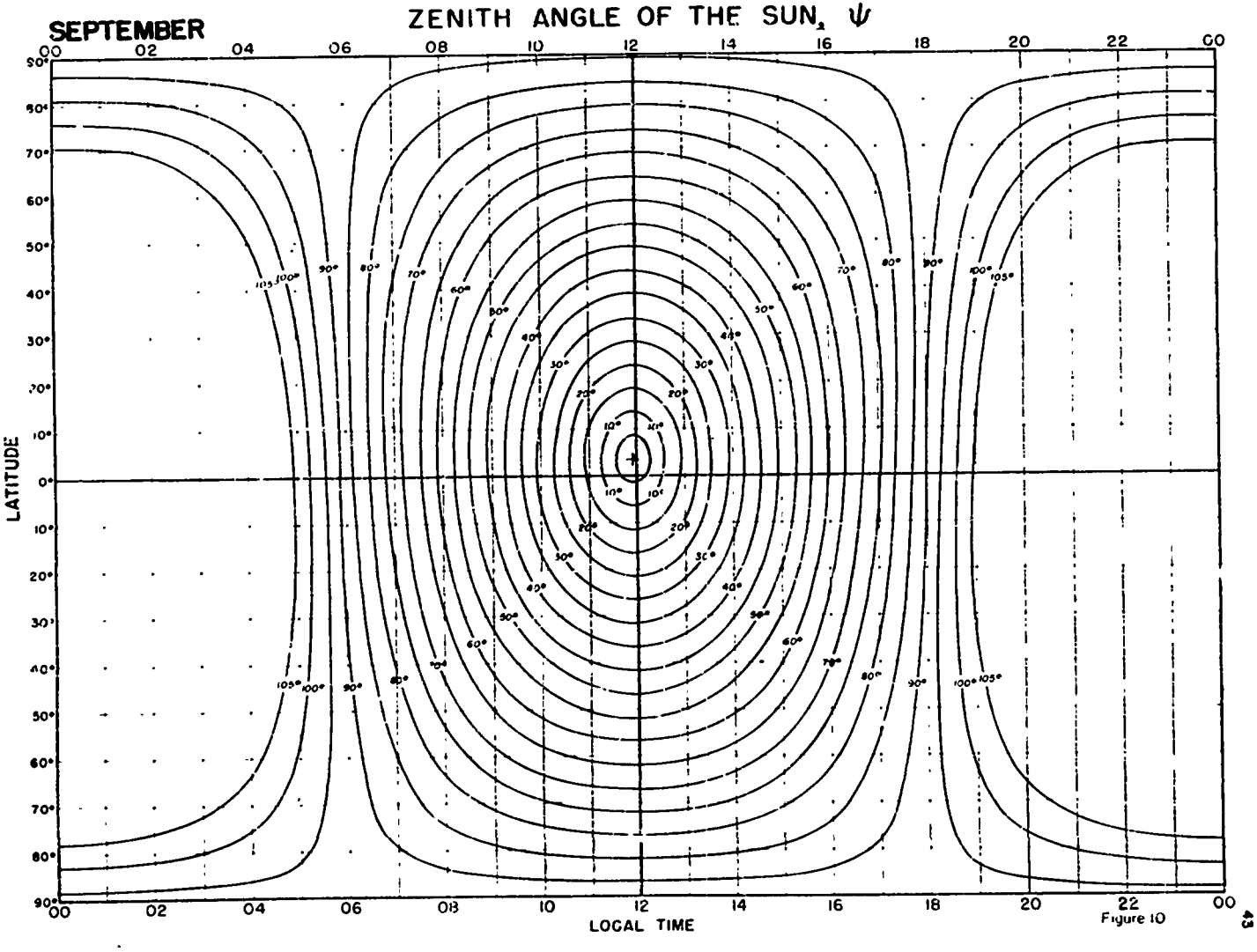
SEPTEMBER
ZENITH ANGLE OF THE SUN, ψ
LATITUDE
LOCAL TIME
00
02
04
06
08
10
12
14
16
18
20
22
90°
80°
70°
60°
50°
40°
30°
20°
10°
0°
105°
100°
90°
80°
70°
60°
50°
40°
30°
20°
10°

Figure 10

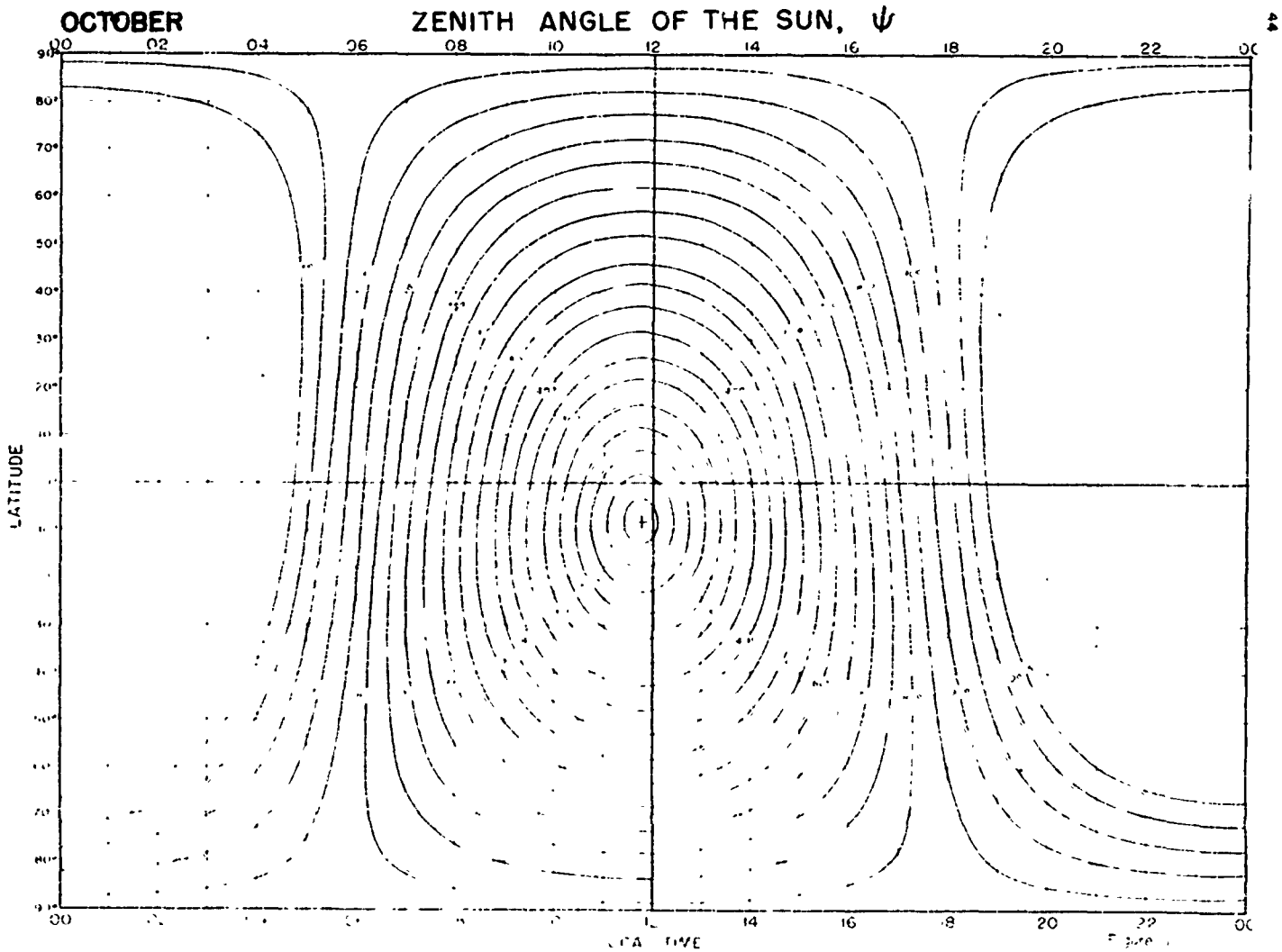
OCTOBER
ZENITH ANGLE OF THE SUN, ψ
00
02
04
06
08
10
12
14
16
18
20
22
00
90°
80°
70°
60°
50°
40°
30°
20°
LATITUDE
14
16
18
20
22
00

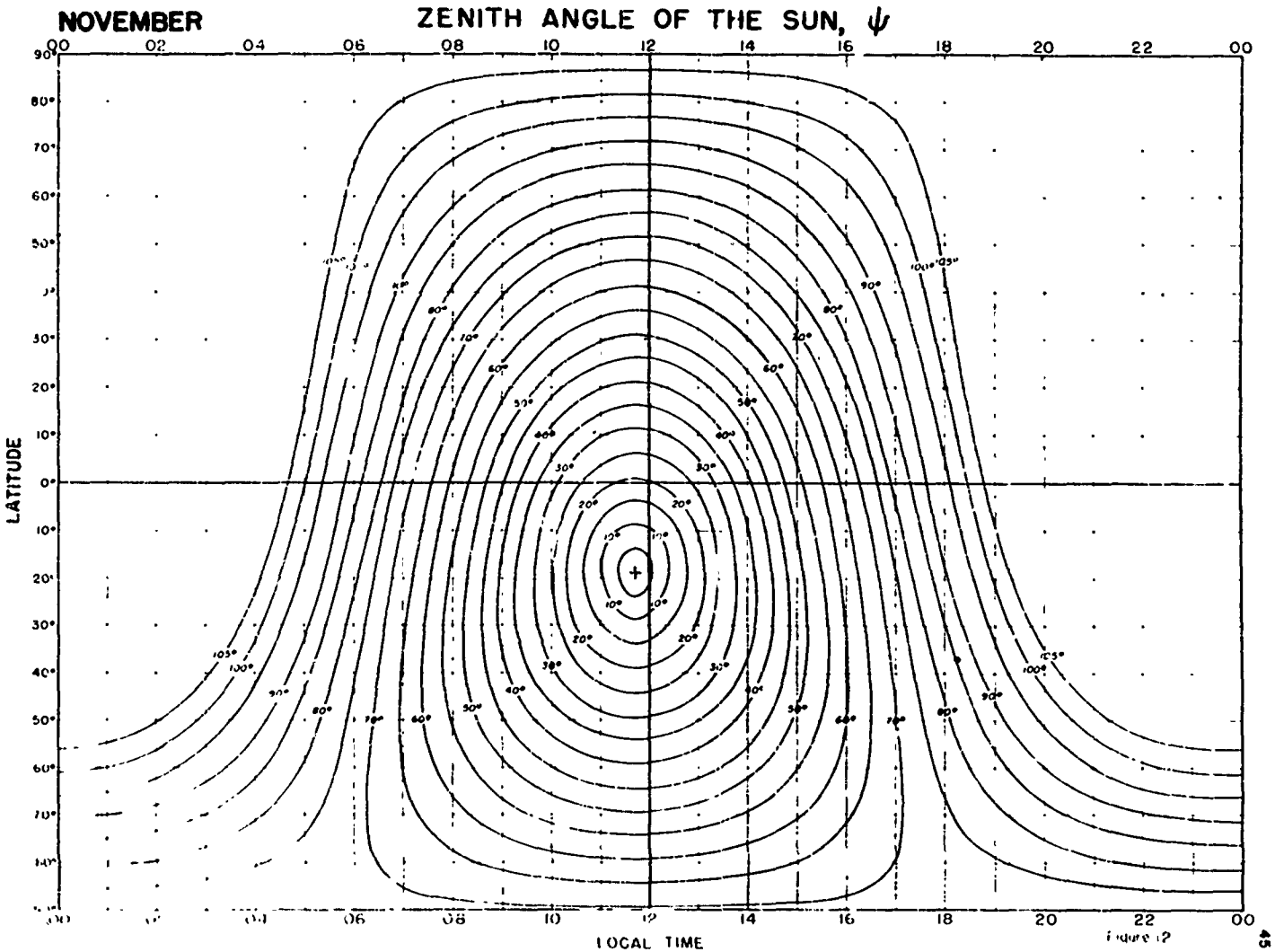
NOVEMBER
ZENITH ANGLE OF THE SUN, ψ
LATITUDE
LOCAL TIME
00
02
04
06
08
10
12
14
16
18
20
22
00
90°
80°
70°
60°
50°
40°
30°
20°
10°
0°

Figure 12

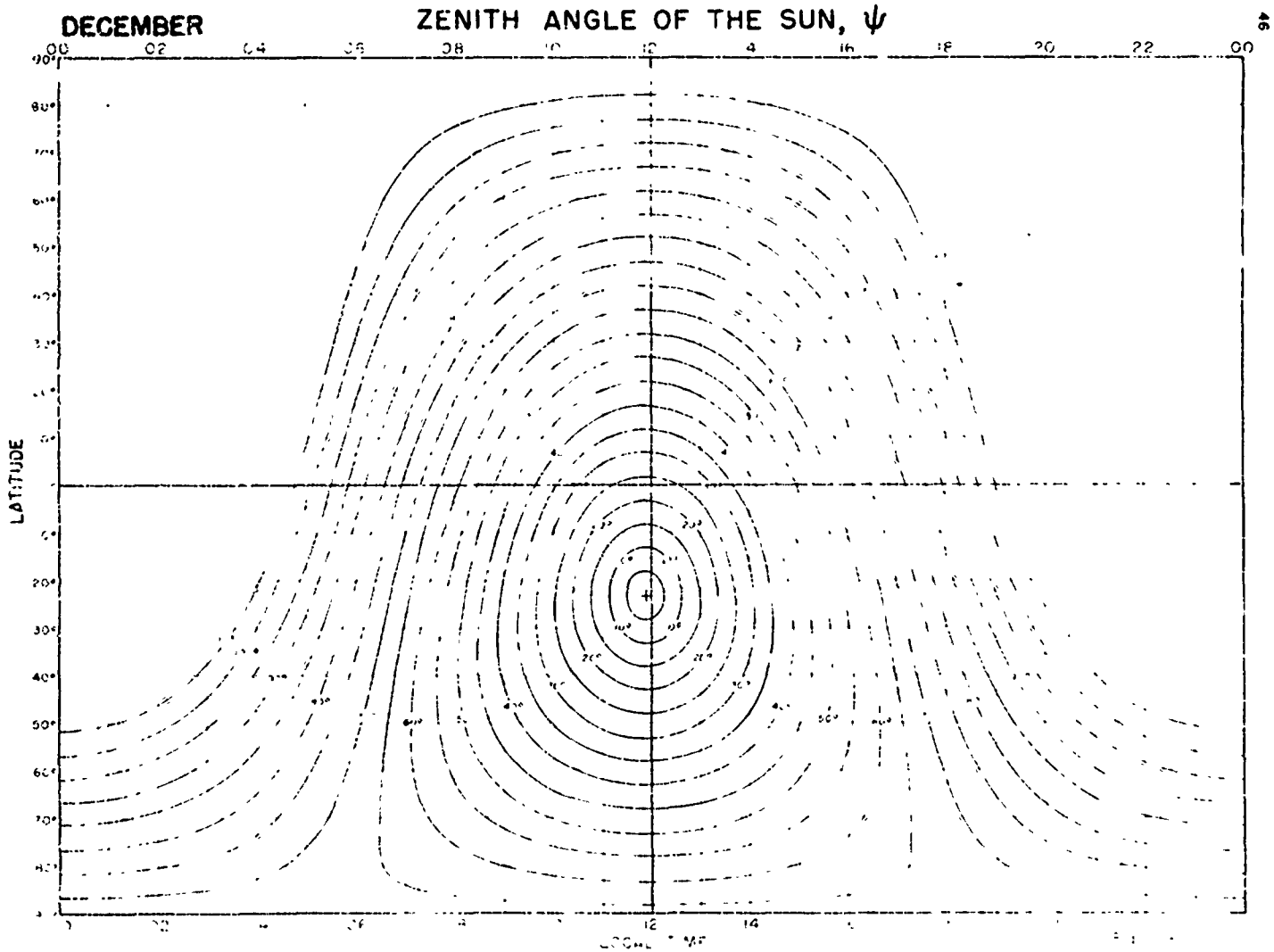
DECEMBER
ZENITH ANGLE OF THE SUN, ψ
LATITUDE
00
02
04
06
08
10
12
14
16
18
20
22
00

ZENITH ANGLE OF THE SUN AT ONSET OF SKY-WAVE ABSORPTION
APPARENTLY BEGINS AND CEASES

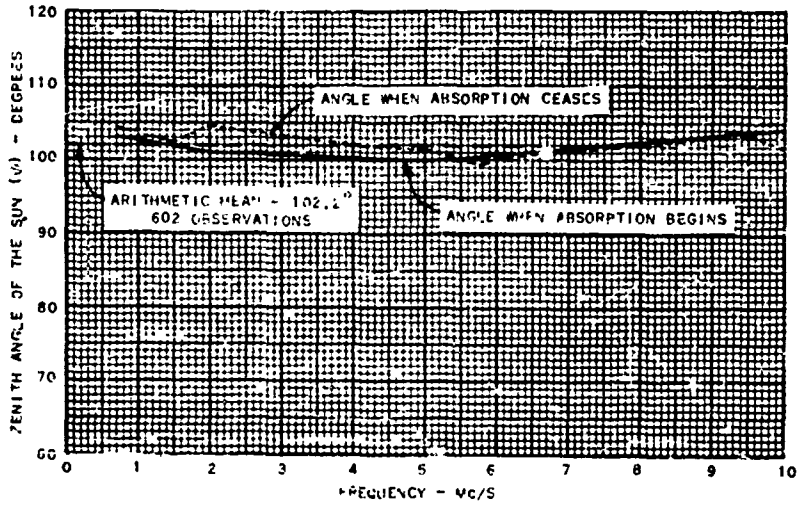

Figure 14

ZENITH ANGLE OF THE SUN AT DAWN AND SUNSET
CORRECTED FOR ATMOSPHERIC REFRACTION AND ELEVATION ABOVE EARTH

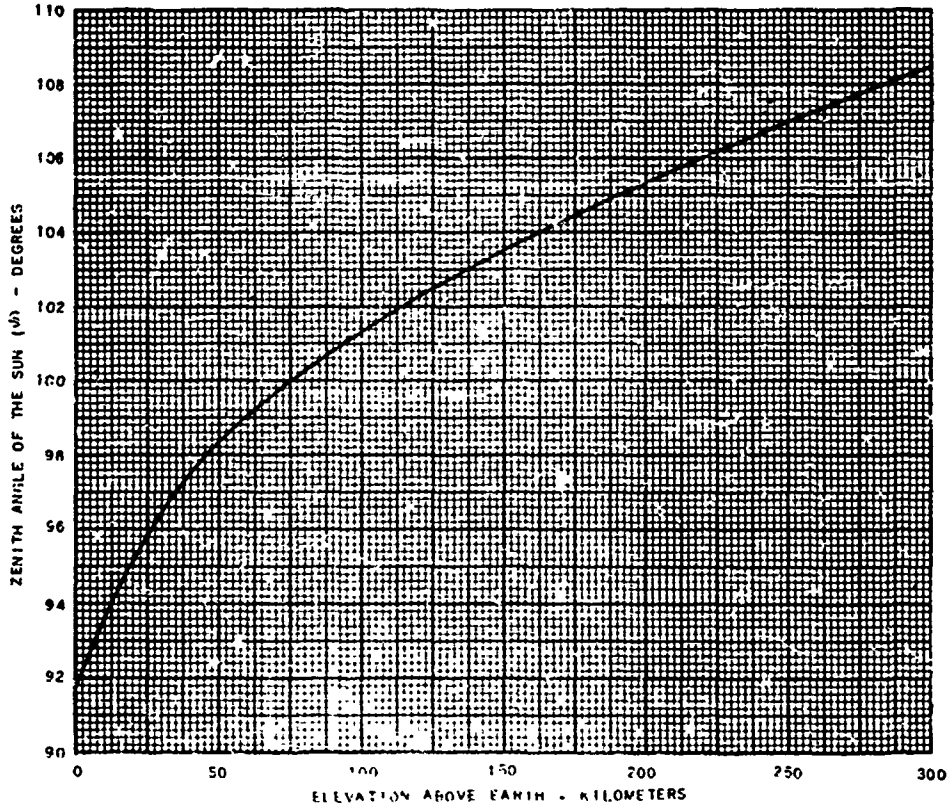

Figure 15

ZENITH ANGLE OF THE SUN AT WHICH SKY-WAVE ABSORPTION BEGINS OR CEASES
MASS PLOT OF 602 OBSERVATIONS

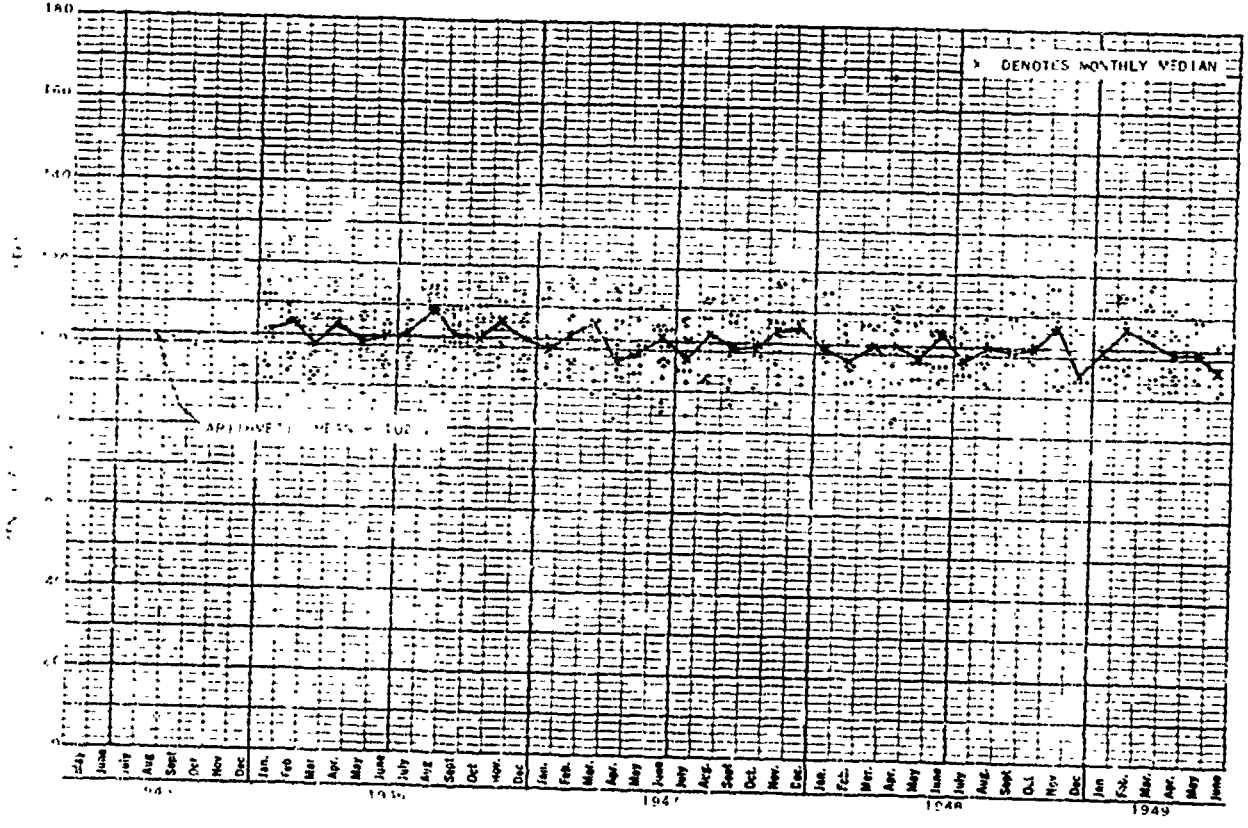

Figure 16

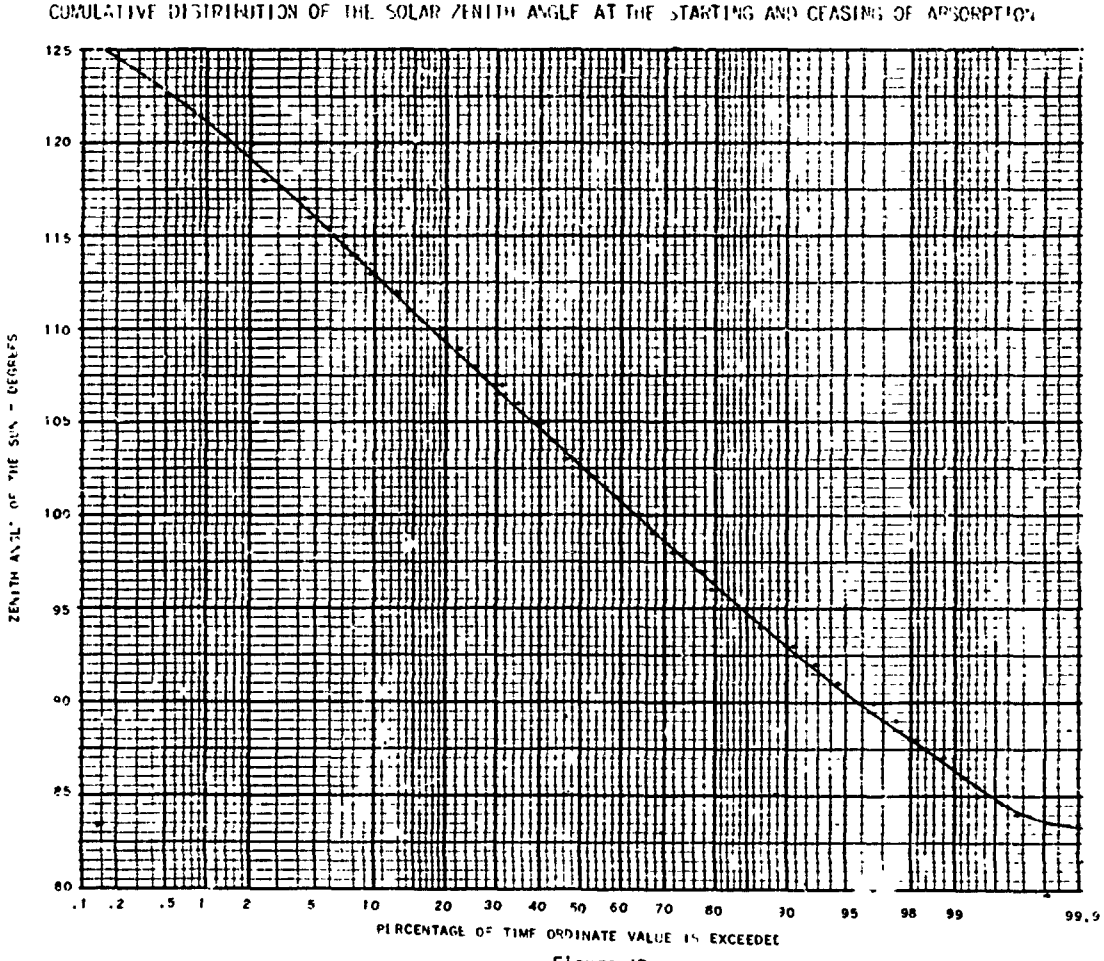
CUMULATIVE DISTRIBUTION OF THE SOLAR ZENITH ANGLE AT THE STARTING AND CEASING OF ABSORPTION
ZENITH ANGLE OF THE SUN - DEGREES
125
120
115
110
105
100
95
90
85
80
.1
.2
.5
1
2
5
10
20
30
40
50
60
70
80
90
95
98
99
99.9
PERCENTAGE OF TIME ORDINATE VALUE IS EXCEEDED

Figure 17

SAMPLE HOURLY MEDIAN RECEIVER INPUT VOLTAGE PLOTTED AGAINST COS .88 ψ
FOR BOTH MORNING AND AFTERNOON

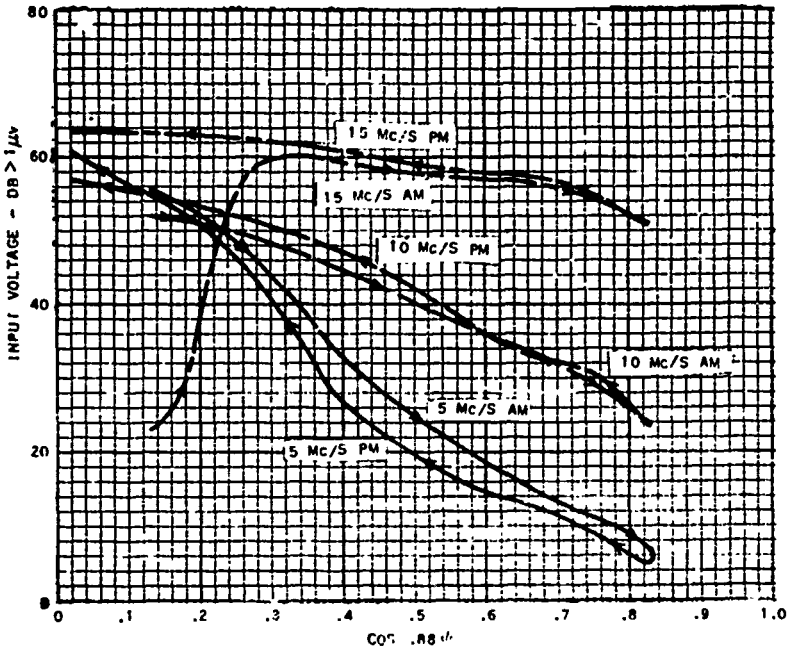

Figure 18

SAMPLE ABSORPTION CALCULATION FROM SMOOTHED INPUT VOLTAGE CURVES

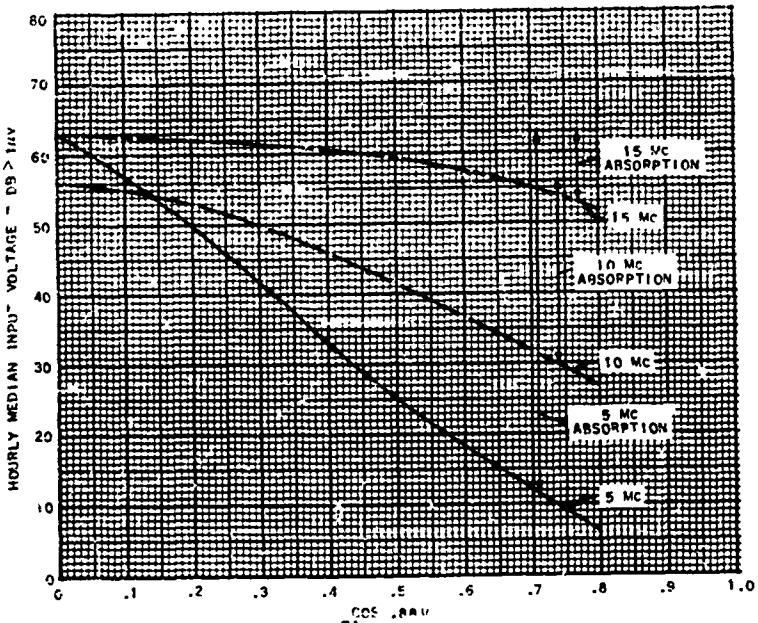

Figure 19

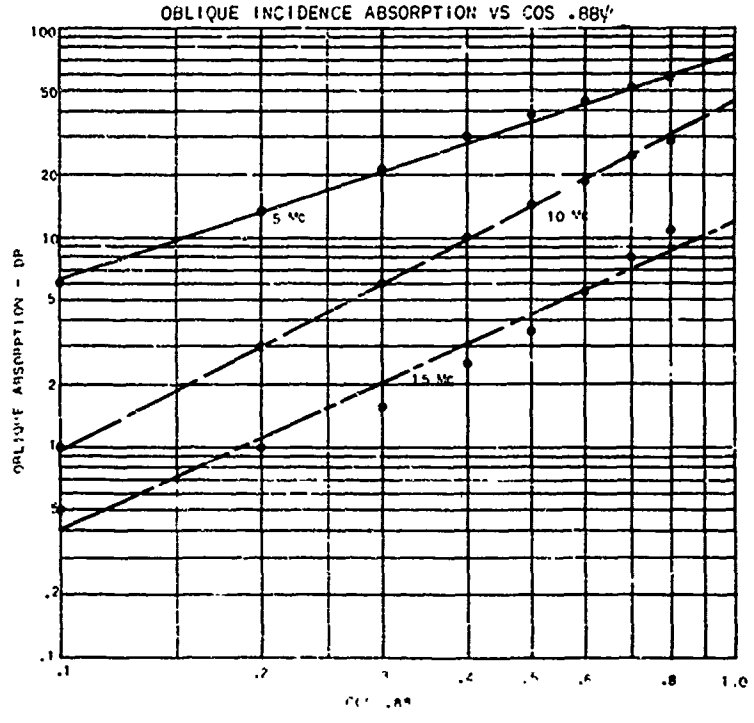

Figure 20

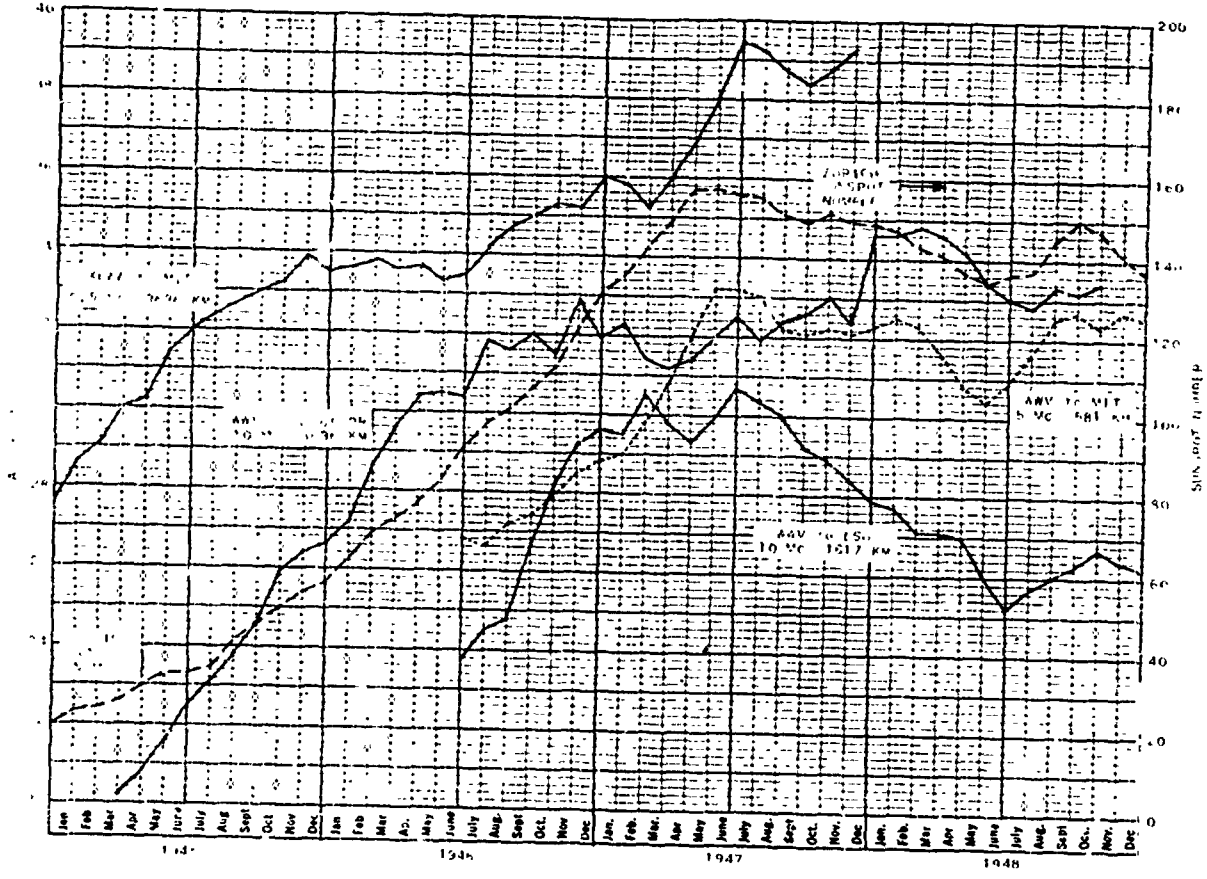
ZURICH
SUNSPOT
NUMBER
AAV TO MIT
5 Vc 681 KM
AAV TO ESO
10 Vc 1617 KM
Jan Feb Mar Apr May June July Aug Sept Oct Nov Dec
1946
1947
1948

Figure 21

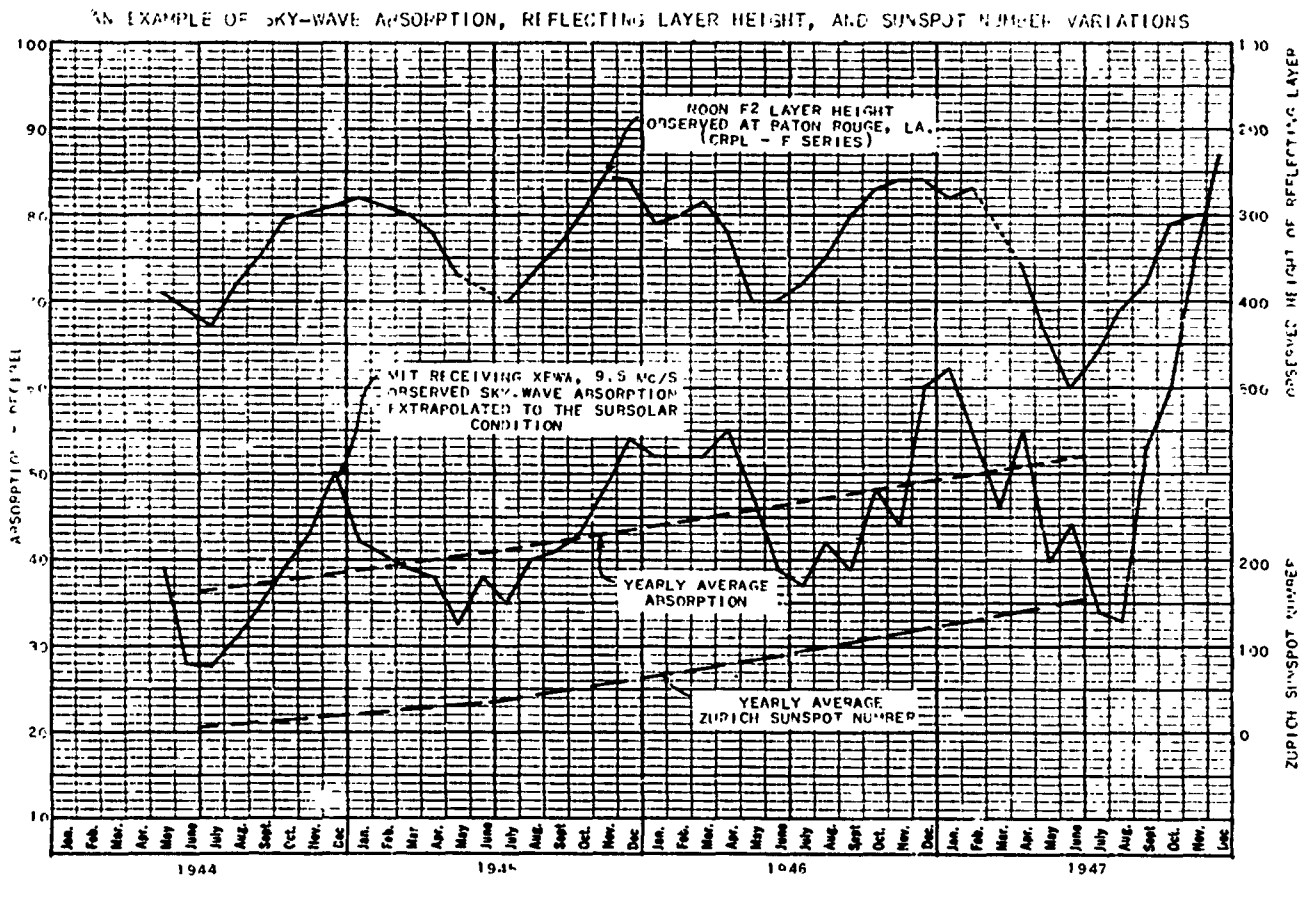
AN EXAMPLE OF SKY-WAVE ABSORPTION, REFLECTING LAYER HEIGHT, AND SUNSPOT NUMBER VARIATIONS
NOON F2 LAYER HEIGHT OBSERVED AT BATON ROUGE, LA. (CRPL - F SERIES)
MIT RECEIVING XFWA, 9.5 MC/S OBSERVED SKY-WAVE ABSORPTION EXTRAPOLATED TO THE SUBSOLAR CONDITION
YEARLY AVERAGE ABSORPTION
YEARLY AVERAGE ZURICH SUNSPOT NUMBER
ABSORPTION - DECIBELS
OBSERVED HEIGHT OF REFLECTING LAYER
ZURICH SUNSPOT NUMBER
100
90
80
70
60
50
40
30
20
10
500
400
300
200
100
0
Jan. Feb. Mar. Apr. May June July Aug. Sept. Oct. Nov. Dec.
1944
1945
1946
1947

Figure 22

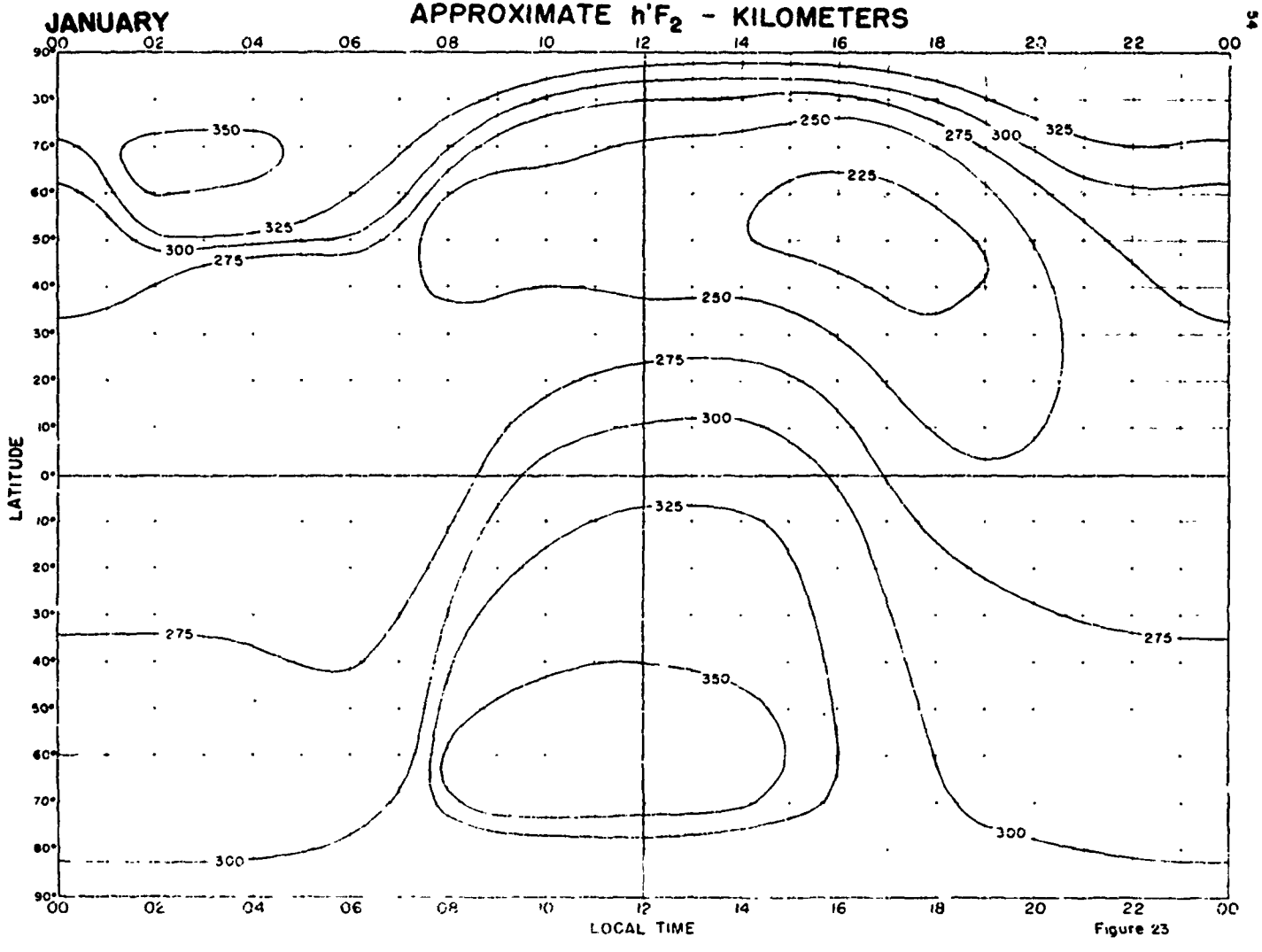
JANUARY
APPROXIMATE h'F2 - KILOMETERS
LATITUDE
LOCAL TIME
00
02
04
06
08
10
12
14
16
18
20
22
00
90°
80°
70°
60°
50°
40°
30°
20°
10°
0°
350
325
300
275
250
225

Figure 23

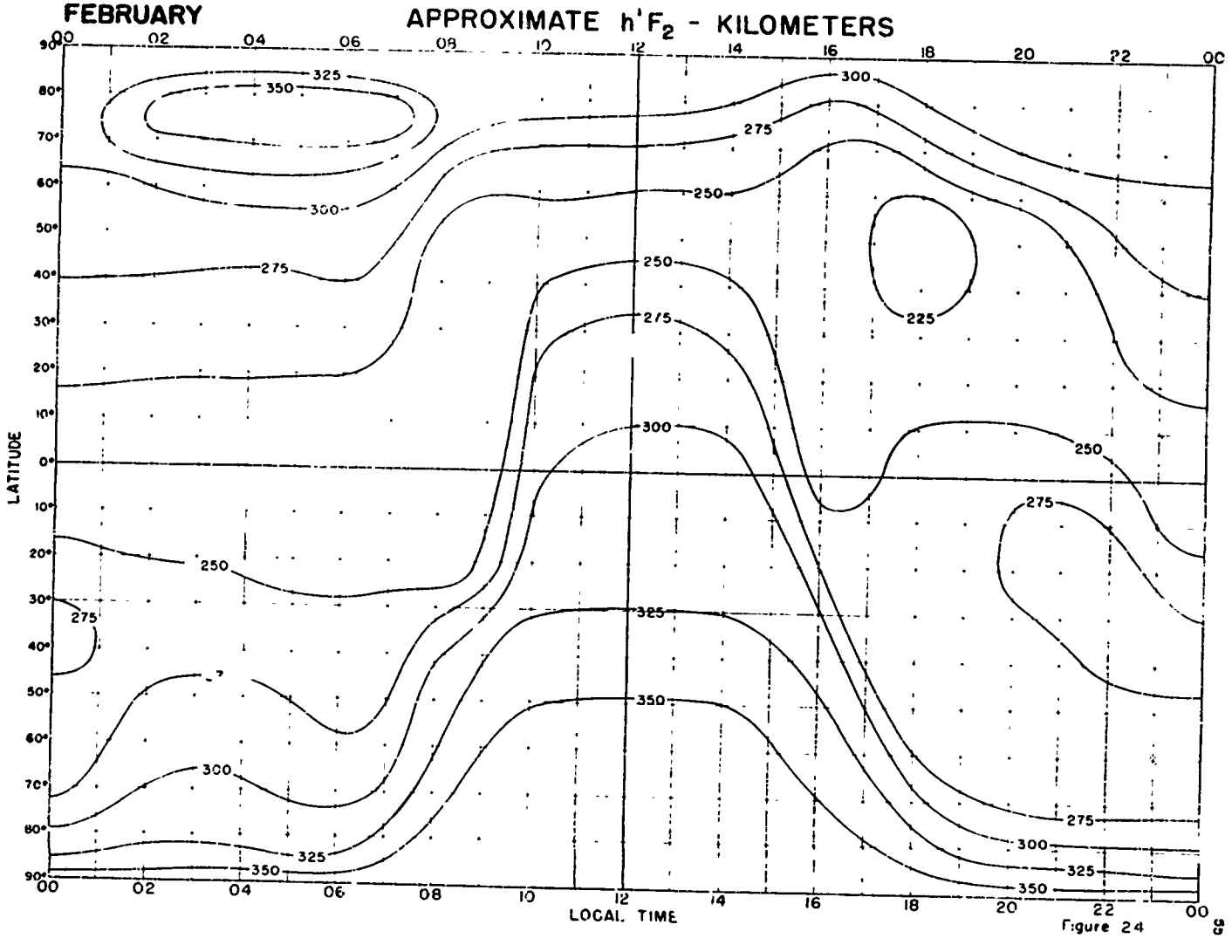
FEBRUARY
APPROXIMATE h'F2 - KILOMETERS
LATITUDE
LOCAL TIME
00
02
04
06
08
10
12
14
16
18
20
22
90°
80°
70°
60°
50°
40°
30°
20°
10°
0°
325
350
300
275
250
225

Figure 24

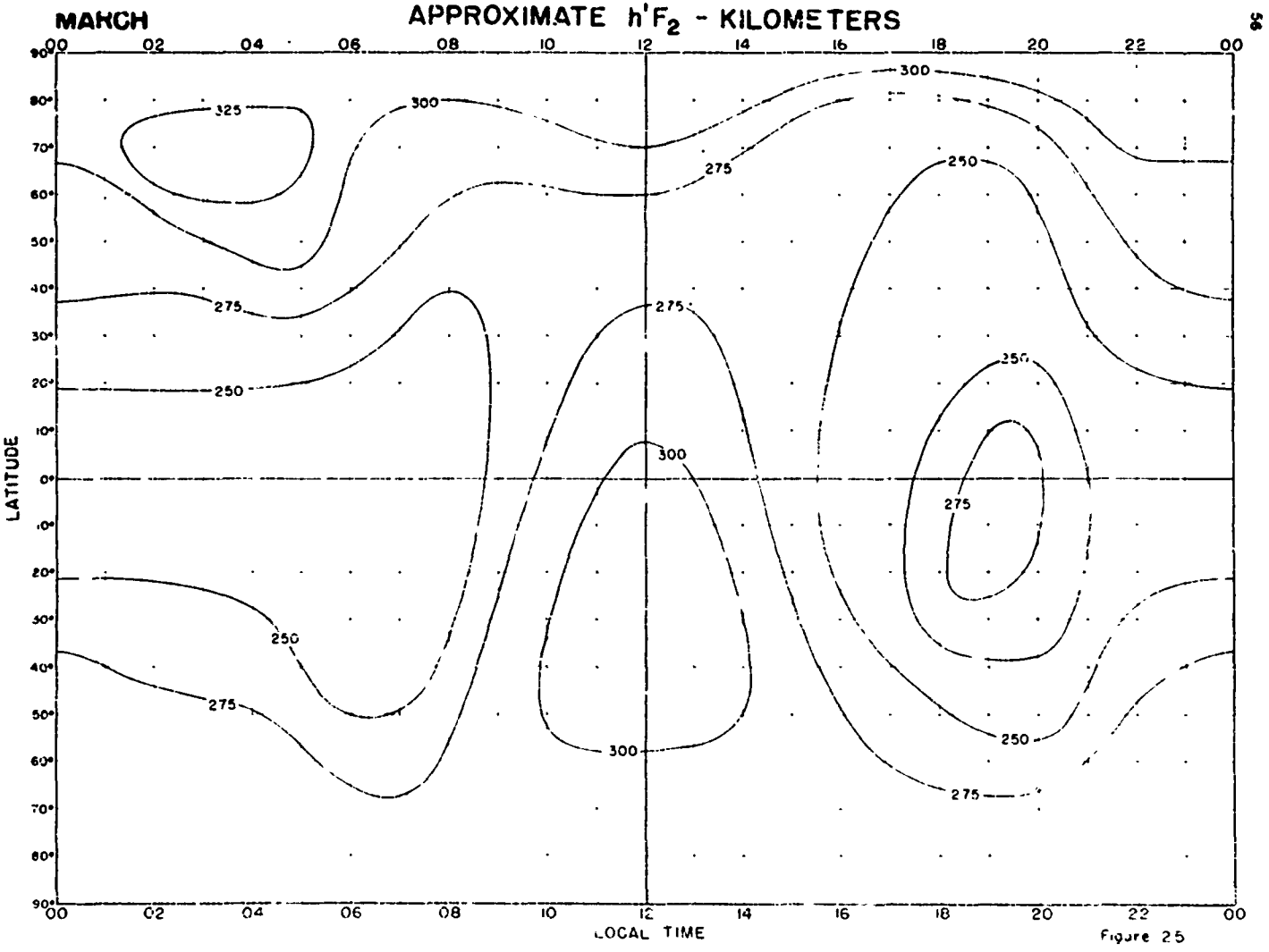
MARCH
APPROXIMATE h'F2 - KILOMETERS
LATITUDE
LOCAL TIME
00
02
04
06
08
10
12
14
16
18
20
22
90°
80°
70°
60°
50°
40°
30°
20°
10°
0°
325
300
275
250

Figure 25

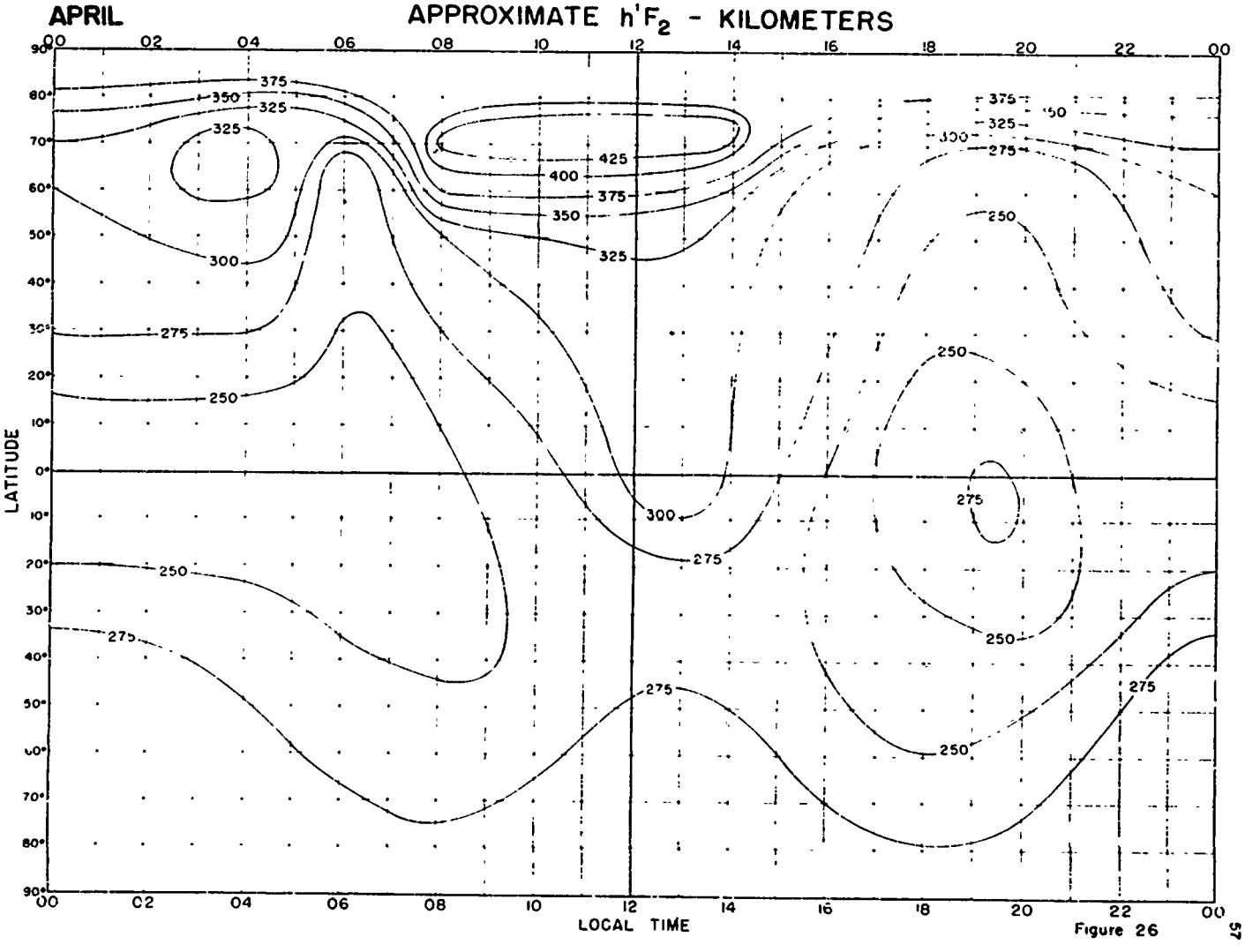
APRIL
APPROXIMATE h'F2 - KILOMETERS
LATITUDE
LOCAL TIME
00
02
04
06
08
10
12
14
16
18
20
22
90°
80°
70°
60°
50°
40°
30°
20°
10°
0°
375
350
325
425
400
300
275
250

Figure 26

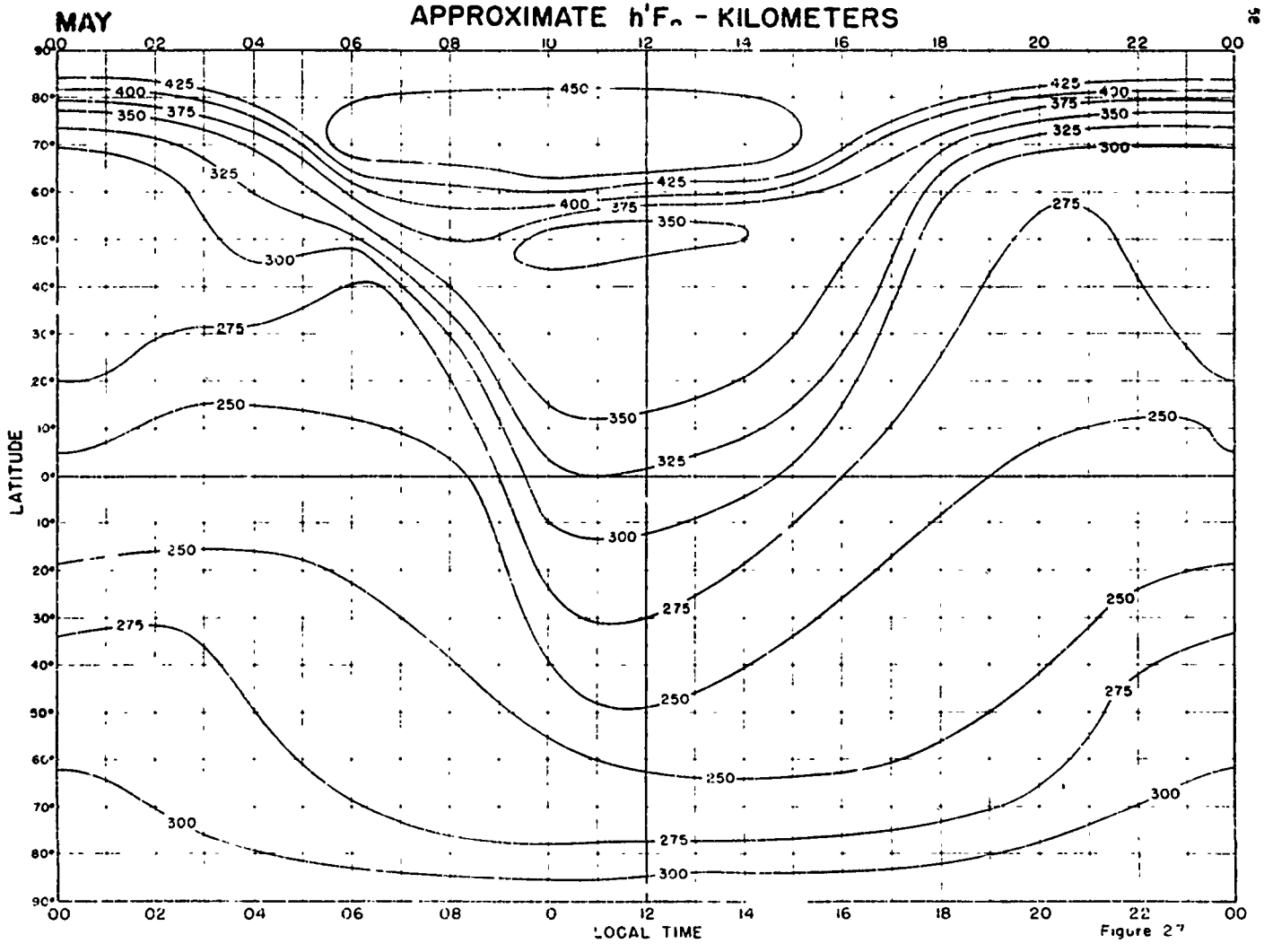
MAY
APPROXIMATE h'F2 - KILOMETERS
LATITUDE
LOCAL TIME
00
02
04
06
08
10
12
14
16
18
20
22
90°
80°
70°
60°
50°
40°
30°
20°
10°
0°
425
400
375
350
325
300
275
250
450

Figure 27

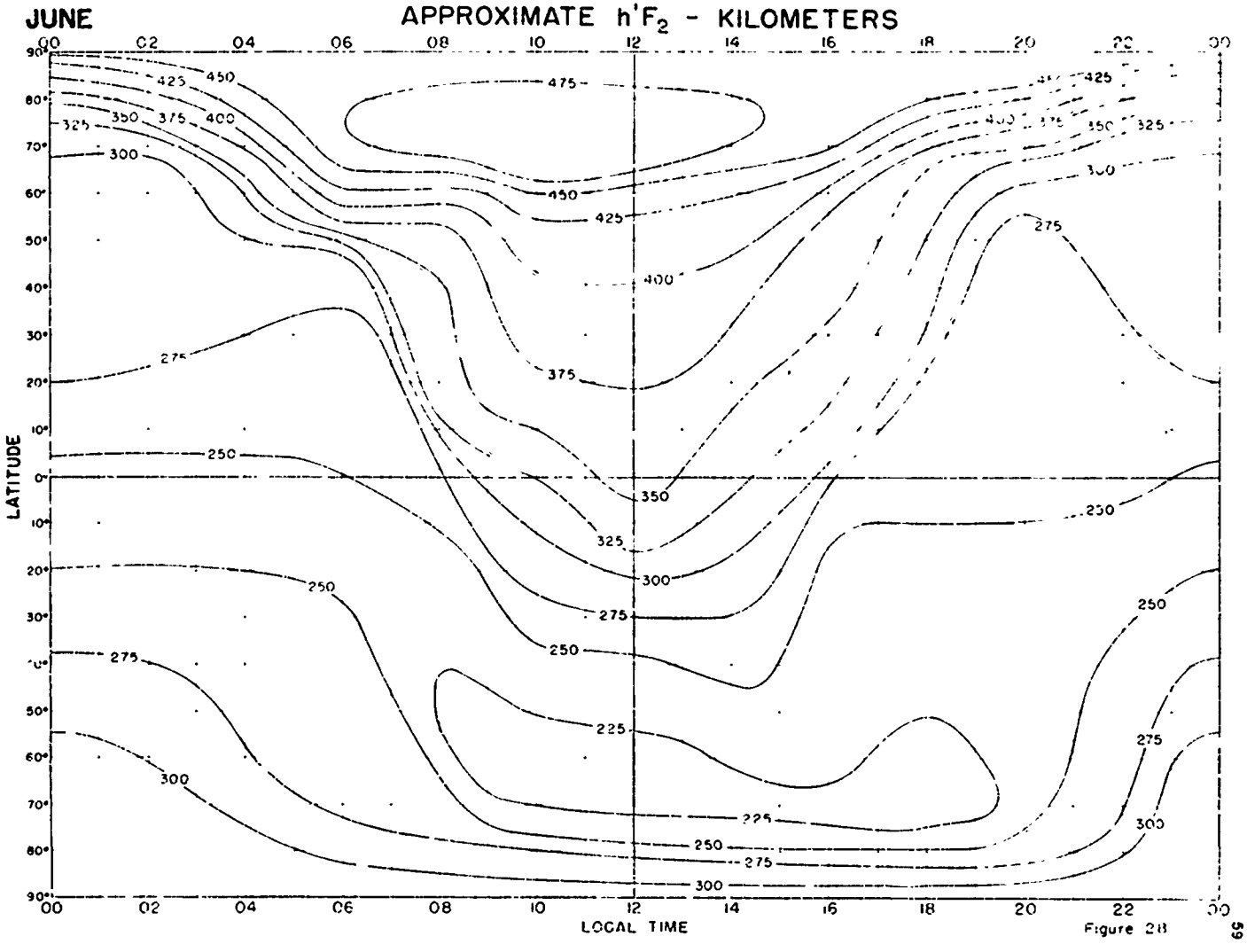
JUNE
APPROXIMATE h'F2 - KILOMETERS
LATITUDE
LOCAL TIME
00
02
04
06
08
10
12
14
16
18
20
22
00
90°
80°
70°
60°
50°
40°
30°
20°
10°
0°
475
450
425
400
375
350
325
300
275
250
225

Figure 28

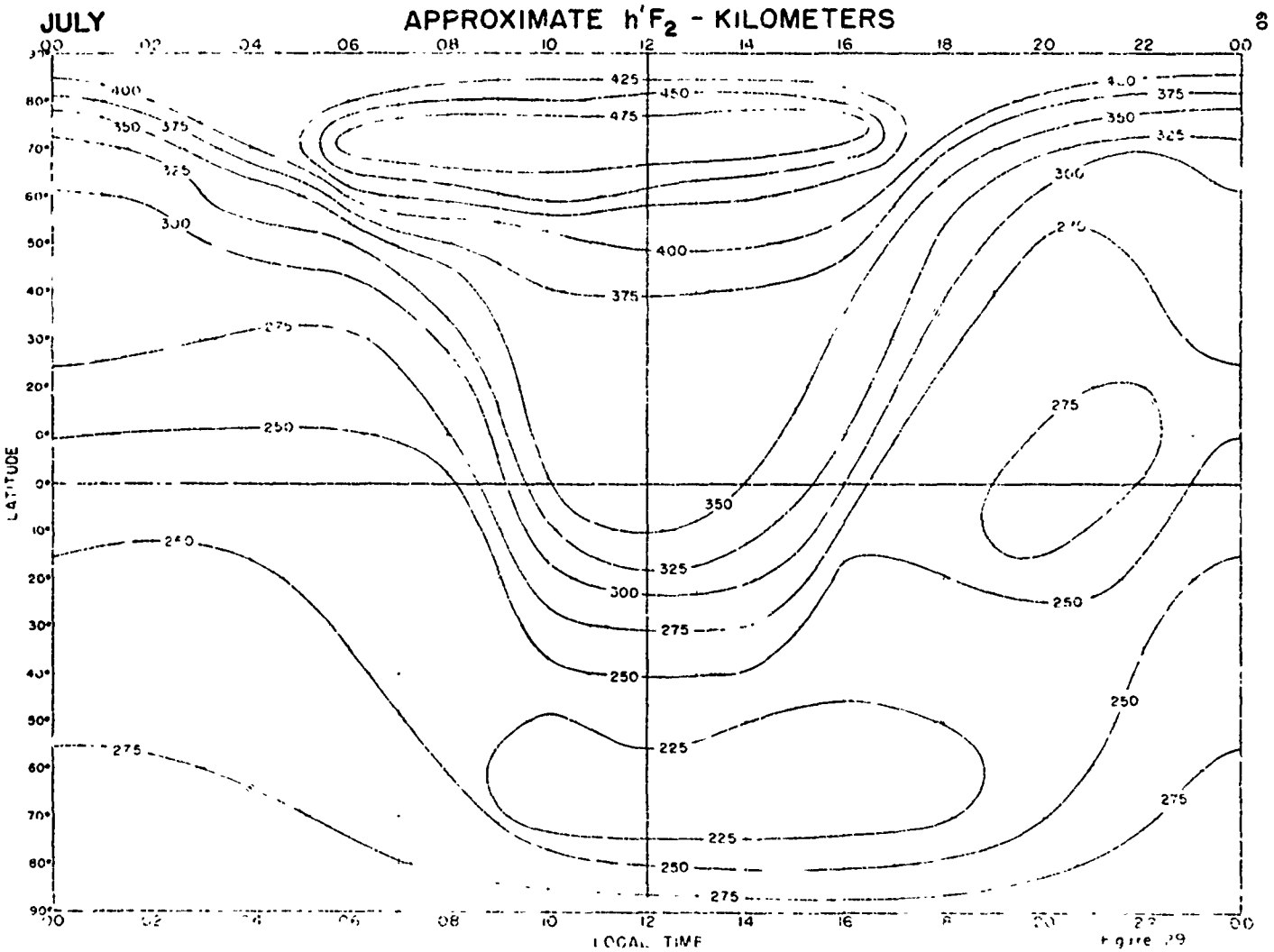
JULY
APPROXIMATE h'F2 - KILOMETERS
LATITUDE
LOCAL TIME
00
02
04
06
08
10
12
14
16
18
20
22
00
425
450
475
400
375
350
325
300
275
250
225

Figure 29

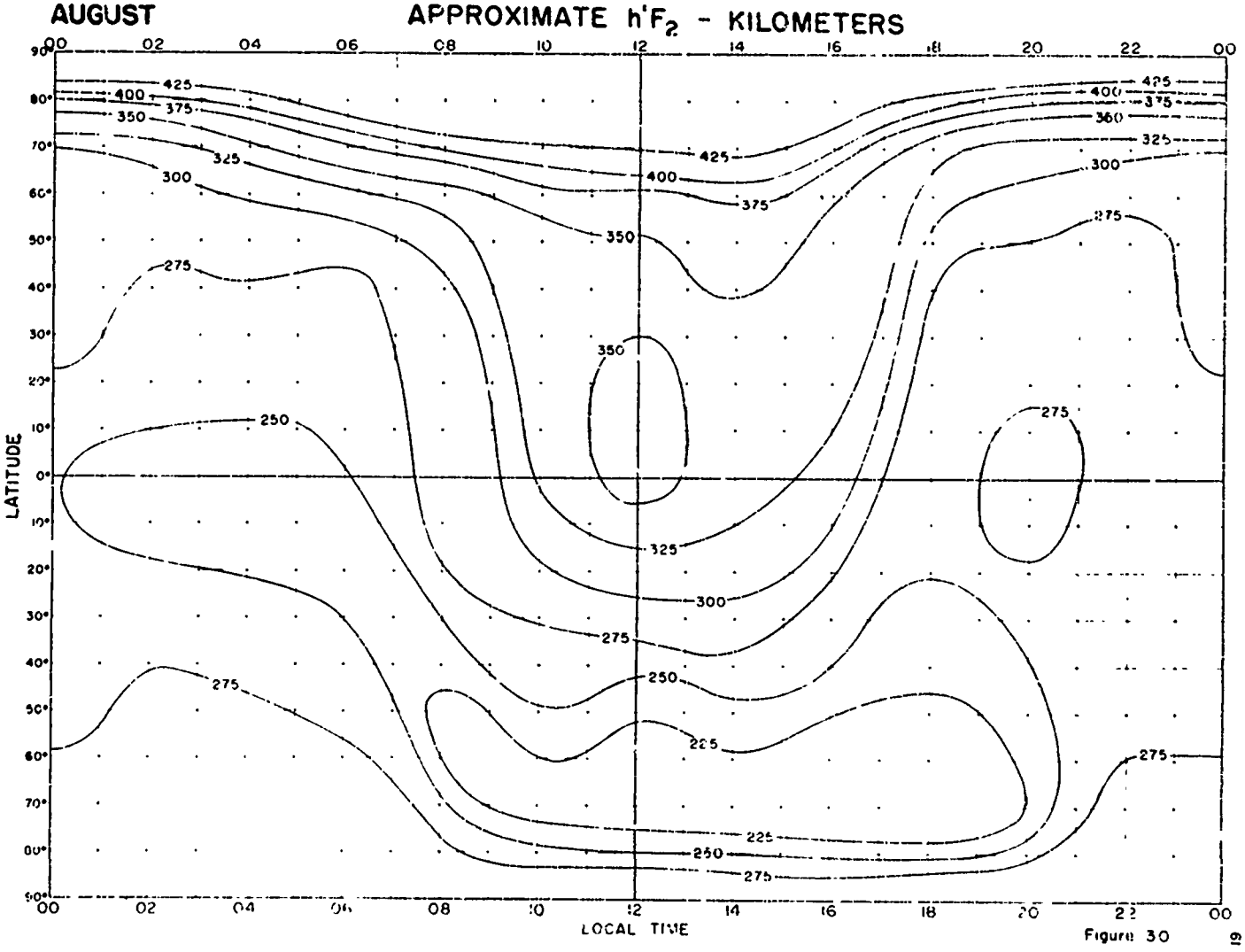
AUGUST
APPROXIMATE h'F2 - KILOMETERS
LATITUDE
LOCAL TIME
00
02
04
06
08
10
12
14
16
18
20
22
00
90°
80°
70°
60°
50°
40°
30°
20°
10°
0°
425
400
375
350
325
300
275
250
225

Figure 30

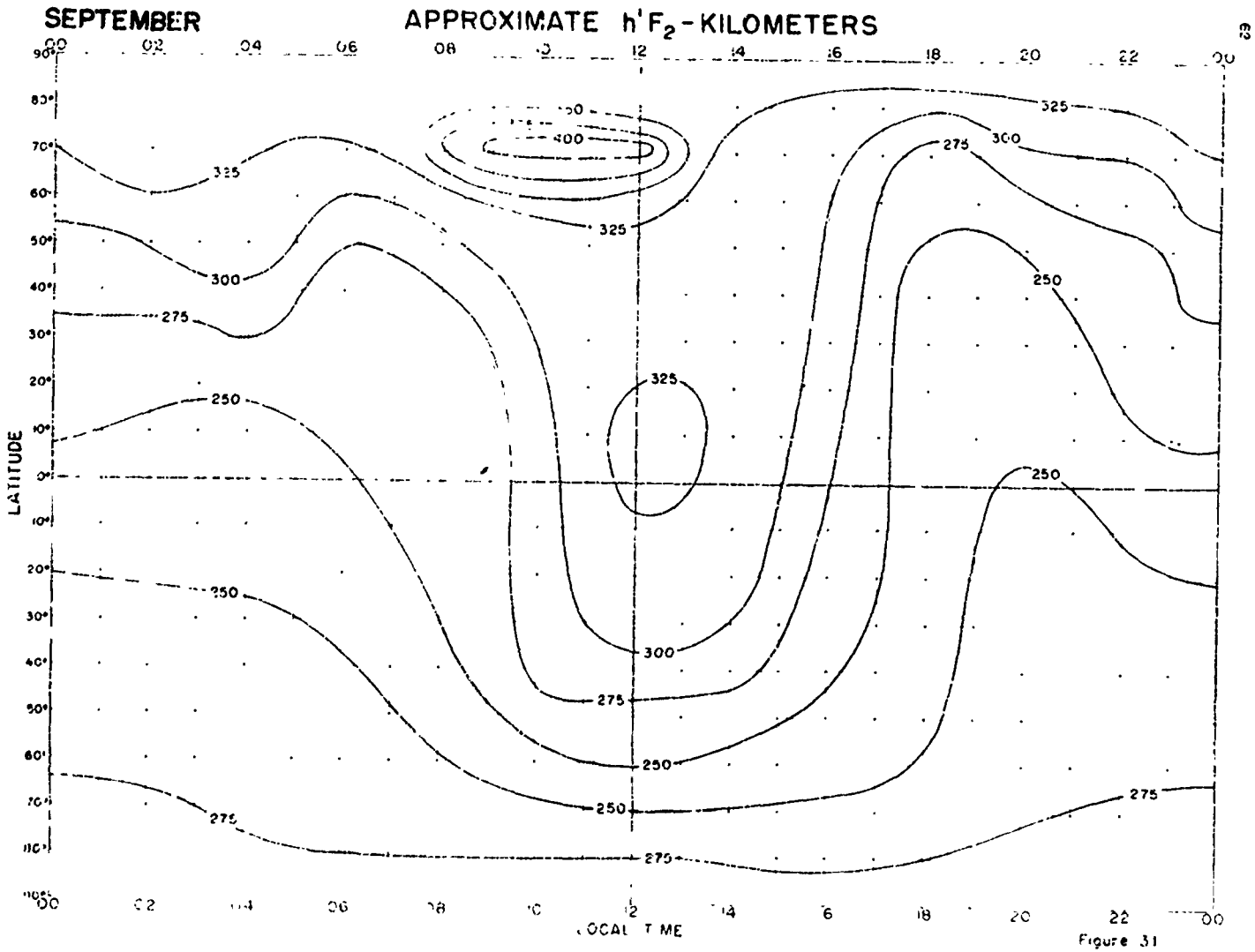
SEPTEMBER
APPROXIMATE h'F2 - KILOMETERS
LATITUDE
LOCAL TIME
00
02
04
06
08
10
12
14
16
18
20
22
00
90°
80°
70°
60°
50°
40°
30°
20°
10°
0°
400
325
300
275
250

Figure 31

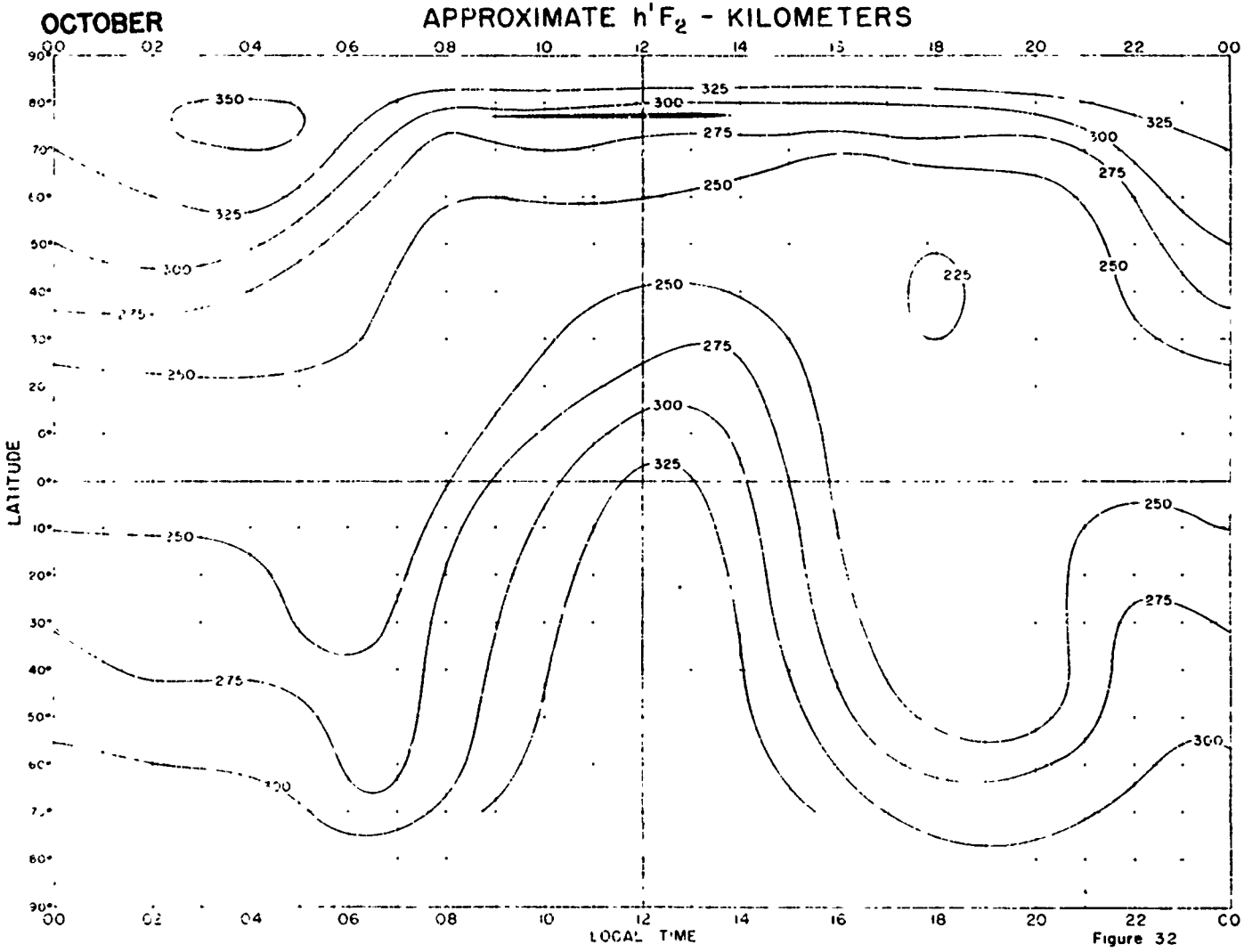
OCTOBER
APPROXIMATE h'F2 - KILOMETERS
LATITUDE
LOCAL TIME
00
02
04
06
08
10
12
14
16
18
20
22
00
90°
80°
70°
60°
50°
40°
30°
20°
10°
0°
350
325
300
275
250
225

Figure 32

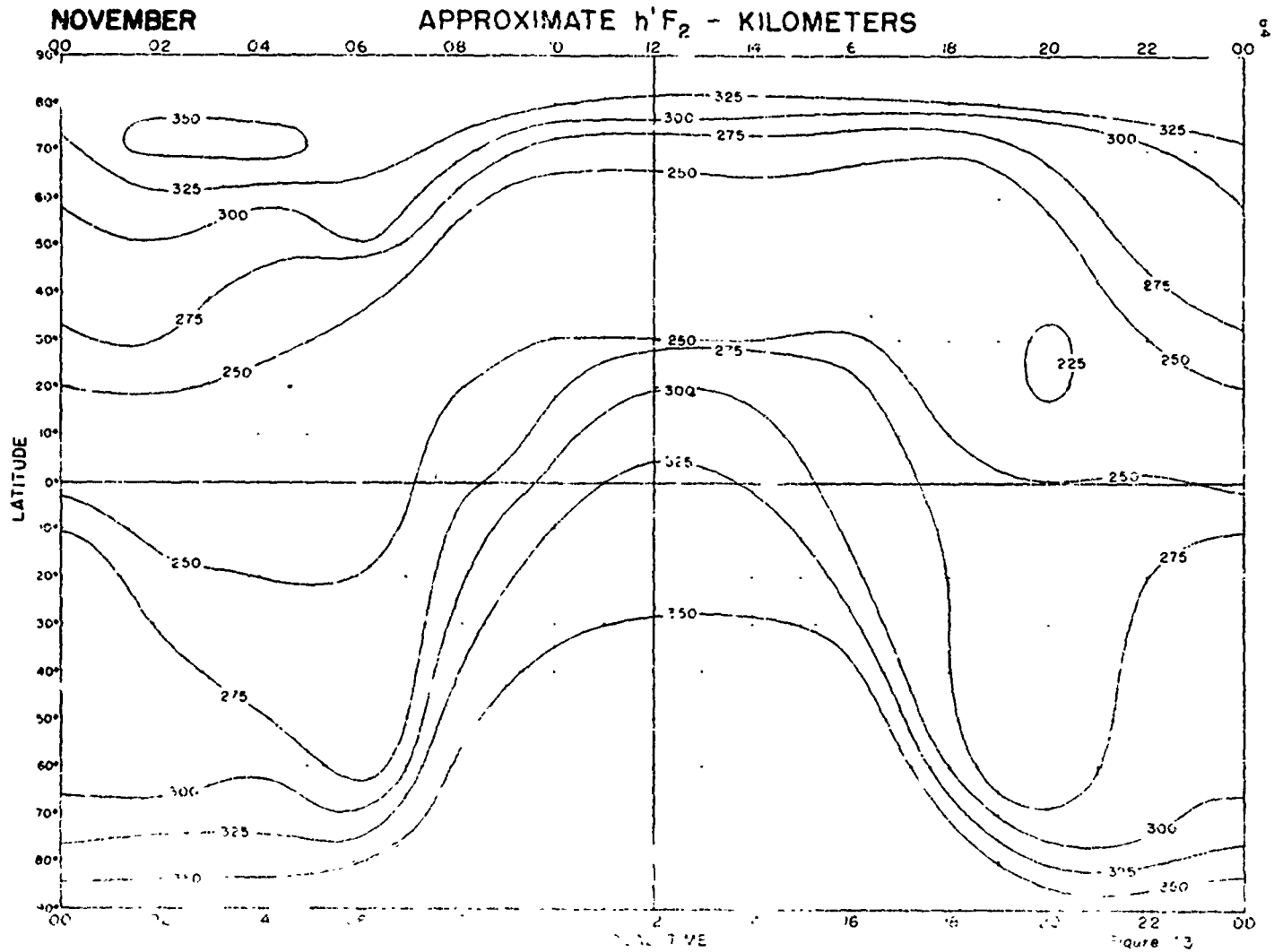
NOVEMBER
APPROXIMATE h'F2 - KILOMETERS
LATITUDE
00 02 04 06 08 10 12 14 16 18 20 22 00
90° 80° 70° 60° 50° 40° 30° 20° 10° 0° 10° 20° 30° 40° 50° 60° 70° 80° 90°
350
325
300
275
250
225

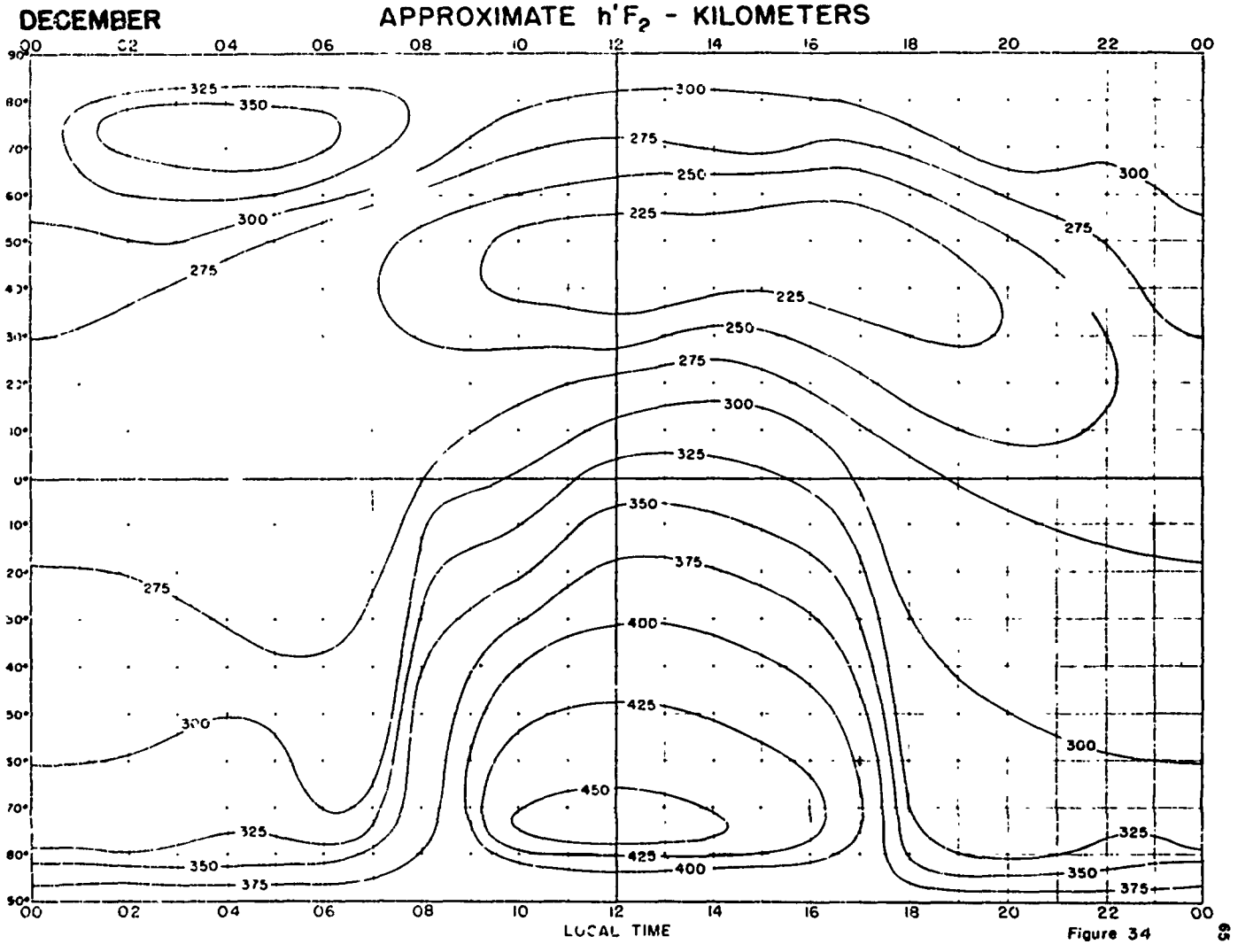
DECEMBER
APPROXIMATE h'F2 - KILOMETERS
00 02 04 06 08 10 12 14 16 18 20 22 00
90°
80°
70°
60°
50°
40°
30°
20°
10°
0°
10°
20°
30°
40°
50°
60°
70°
80°
90°
325
350
300
275
250
225
375
400
425
450
LOCAL TIME

Figure 34

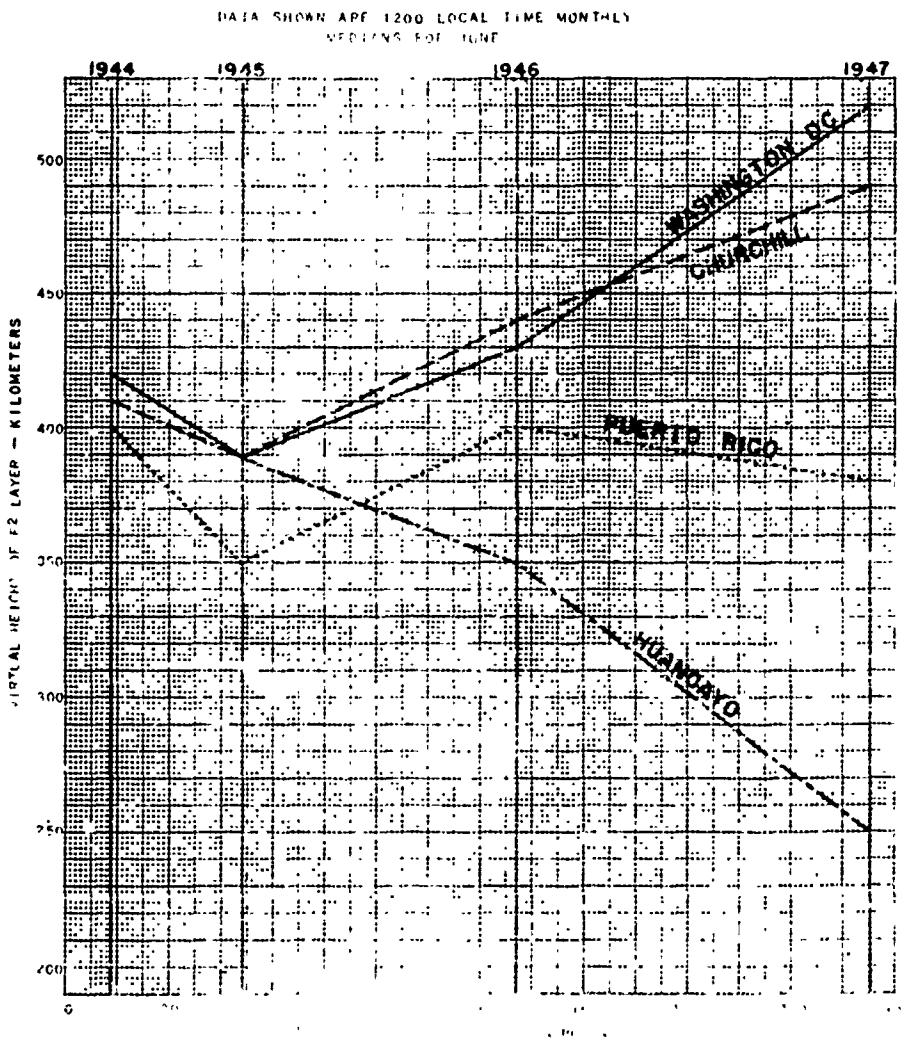
DATA SHOWN ARE 1200 LOCAL TIME MONTHLY
1944
1945
1946
1947
500
450
400
350
300
250
200
WASHINGTON, DC
CHURCHILL
PUERTO RICO
HUANCAYO

VARIATION OF F2 LAYER VIRTUAL HEIGHTS AT WASHINGTON, D. C. 1200 EASTERN STANDARD TIME

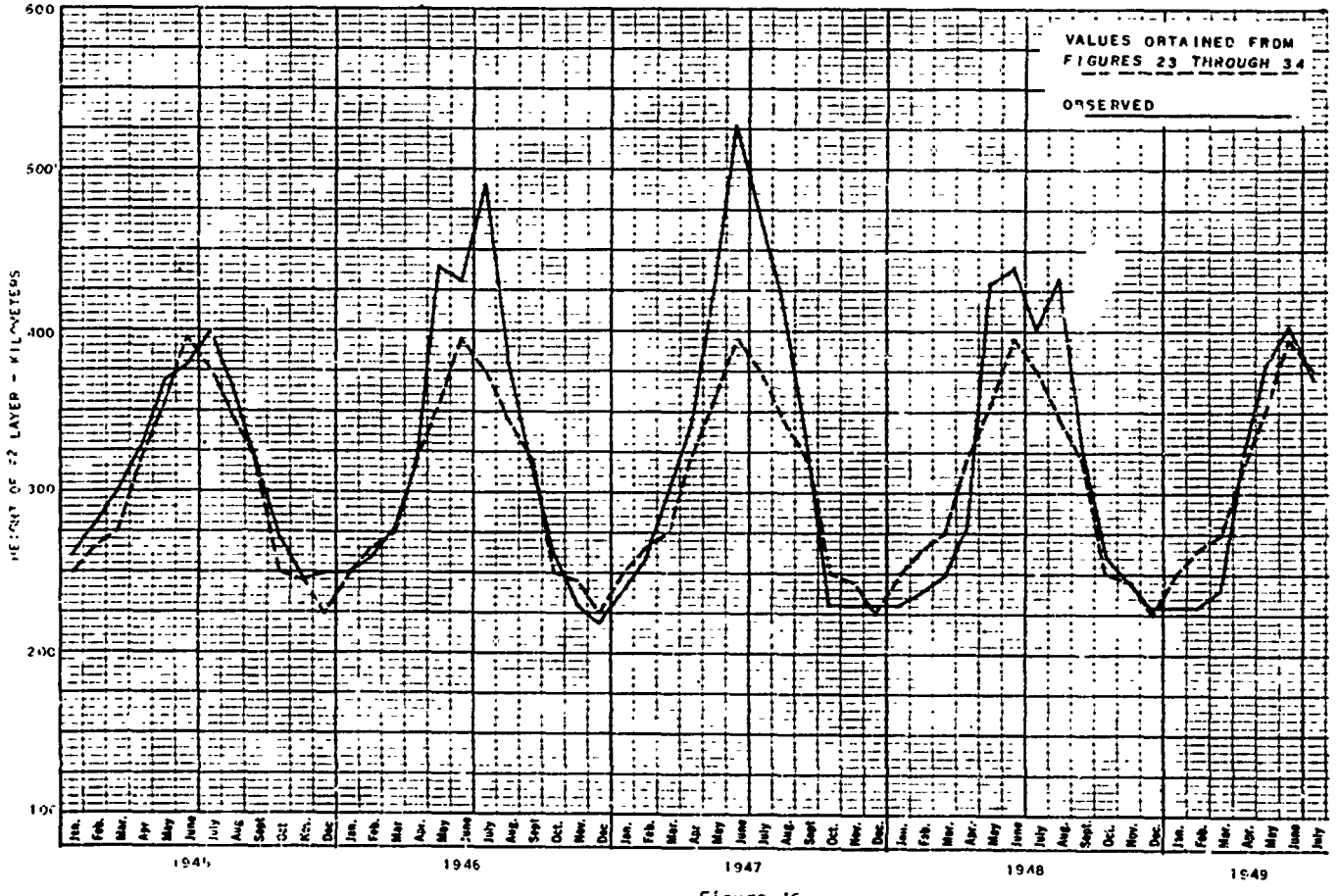

Figure 36

E-LAYER MINIMUM VIRTUAL HEIGHTS OBSERVED AT WASHINGTON, D. C. DURING 1940

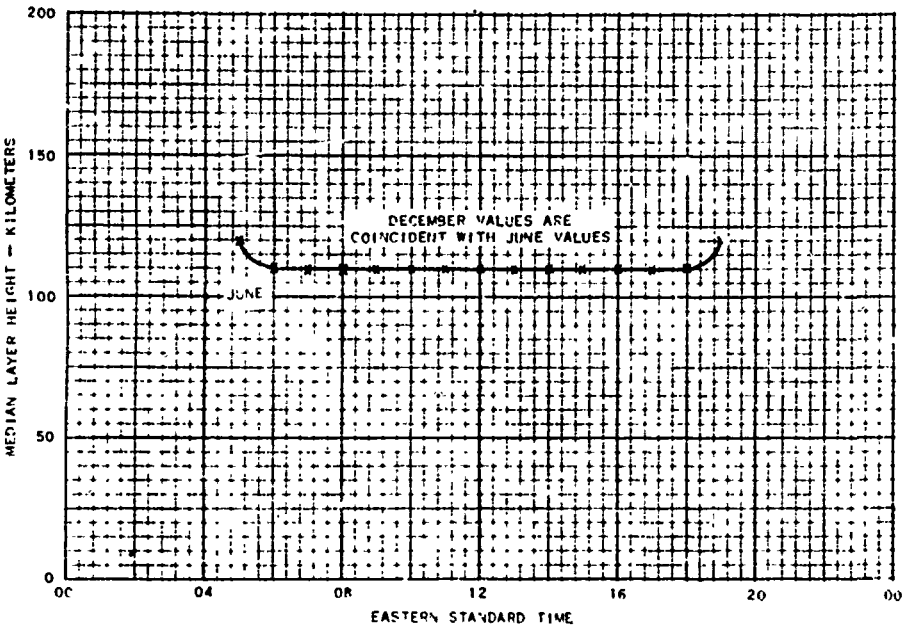

Figure 37

SECANT ϕ AND RADIATION ANGLE (α) FOR GREAT CIRCLE DISTANCE
FROM 100 TO 1000 KILOMETERS FOR VARIED SPECIFIC LAYER HEIGHT (H_L)

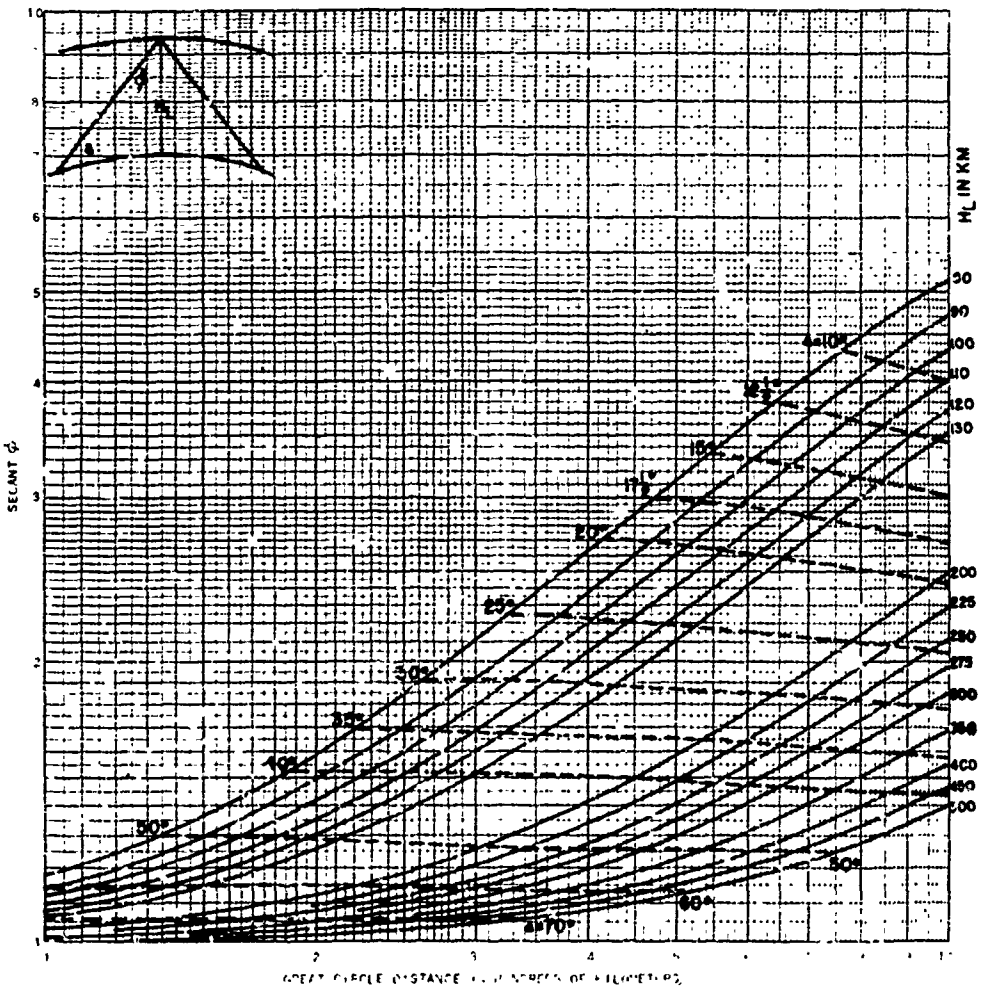

Figure 38-A

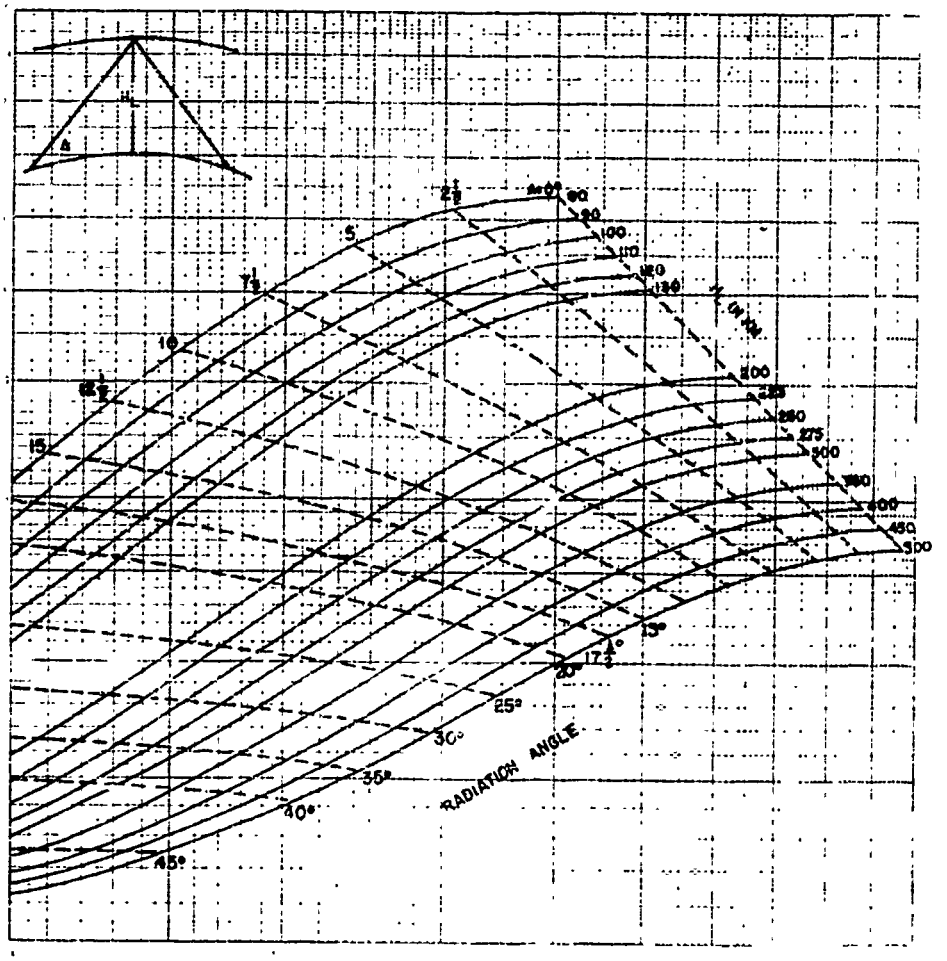
2½
5
7½
10
12½
15
90
100
110
120
130
200
250
275
300
350
400
450
500
13°
17½°
20°
25°
30°
35°
40°
45°
RADIATION ANGLE

MAXIMUM USABLE AND PENETRATION FREQUENCIES USED TO DETERMINE POSSIBLE MODES OF PROPAGATION BETWEEn WASHINGTON, D. C. AND LOUISIANA STATE UNIVERSITY FOR MARCH 1949

THESE DATA WERE DERIVED FROM OBSERVATIONS AT WASHINGTON, D.C. AND BATON ROUGE, LOUISIANA AS REPORTED IN 'IONOSPHERIC DATA' CRPL-F REPORTS

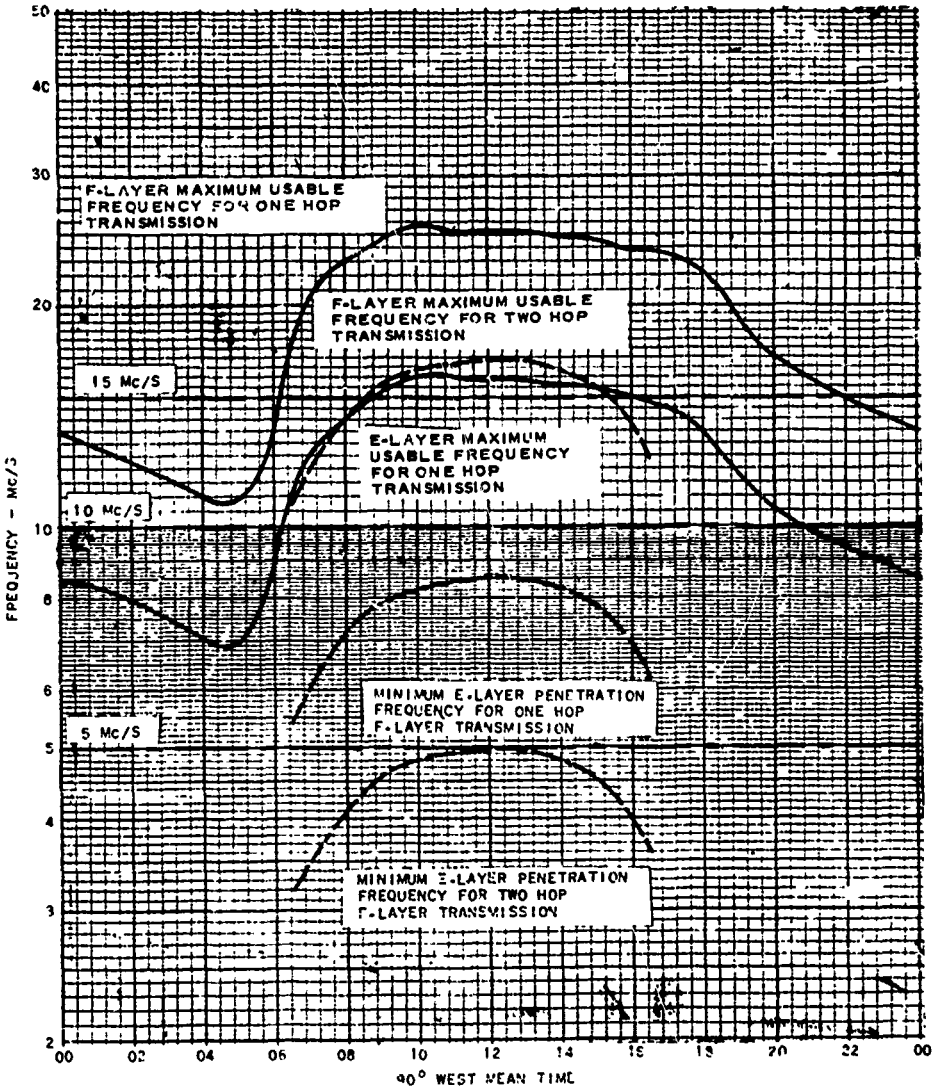

Figure 39

EXAMPLE OF OBLIQUE INCIDENCE ABSORPTION DATA
REDUCED TO VERTICAL INCIDENCE AND SUNSPOT ZERO
LOUISIANA STATE UNIVERSITY RECEIVING WWV, MARCH 1949

12 Month Moving Average Sunspot Number = 134
Solar Activity Factor = (1 + .0037 x 134) = 1.496

FREQUENCY	COSINE .88 ψ	OBLIQUE INCIDENCE ABSORPTION AT SSN = 134	ASSUMED MODE OF TRANSMISSION	RADIATION ANGLE (Δ)	SECANT ϕ FOR RADIATION ANGLE (Δ)	VERTICAL INCIDENCE ABSORPTION AT SSN = 134 (2) ÷ (5)	VERTICAL INCIDENCE ABSORPTION AT SSN = 0 (6) ÷ 1.496
	(1)	(2)	(3)	(4)	(5)	(6)	(7)
5 MEGACYCLES	0.1	8.0	1F	4.0	5.30	1.13	0.76
	0.2	13.0	1E	4.0	5.30	2.45	1.64
	0.3	21.0	1E	4.0	5.30	3.96	2.65
	0.4	30.0	1E	4.0	5.30	5.66	3.78
	0.5	38.0	1E	4.0	5.30	7.17	4.79
	0.6	44.5	1E	4.0	5.30	8.40	5.61
	0.7	51.0	1E	4.0	5.30	9.62	6.43
	0.8	57.0	1E	4.0	5.30	10.75	7.19
10 MEGACYCLES	0.1	1.0	2F	28.4	4.00	.25	.17
	0.2	3.0	2F	28.4	4.00	.75	.50
	0.3	6.0	2F	28.4	4.00	1.50	1.00
	0.4	10.0	2F	28.9	3.94	2.54	1.70
	0.5	14.5	2F	29.4	3.92	3.70	2.47
	0.6	19.0	2F	29.9	3.86	4.92	3.29
	0.7	24.0	2F	30.9	3.76	6.38	4.26
	0.8	29.0	2F	31.3	3.72	7.80	5.21
15 MEGACYCLES	0.1	0.5	1F	12.6	3.61	.14	.09
	0.2	1.0	1F	12.6	3.61	.28	.19
	0.3	1.5	1F	12.6	3.61	.42	.28
	0.4	2.5	1F	12.9	3.56	.70	.47
	0.5	3.5	1F	13.2	3.51	1.00	.67
	0.6	5.5	1F	13.5	3.46	1.59	1.06
	0.7	8.0	1F	14.2	3.35	2.39	1.60
	0.8	11.0	1F	14.5	3.31	3.32	2.22

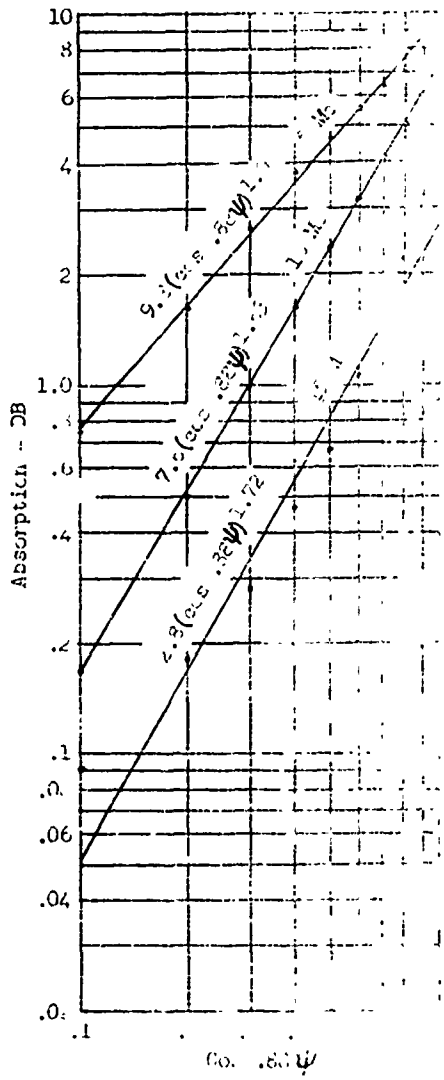

Figure 40

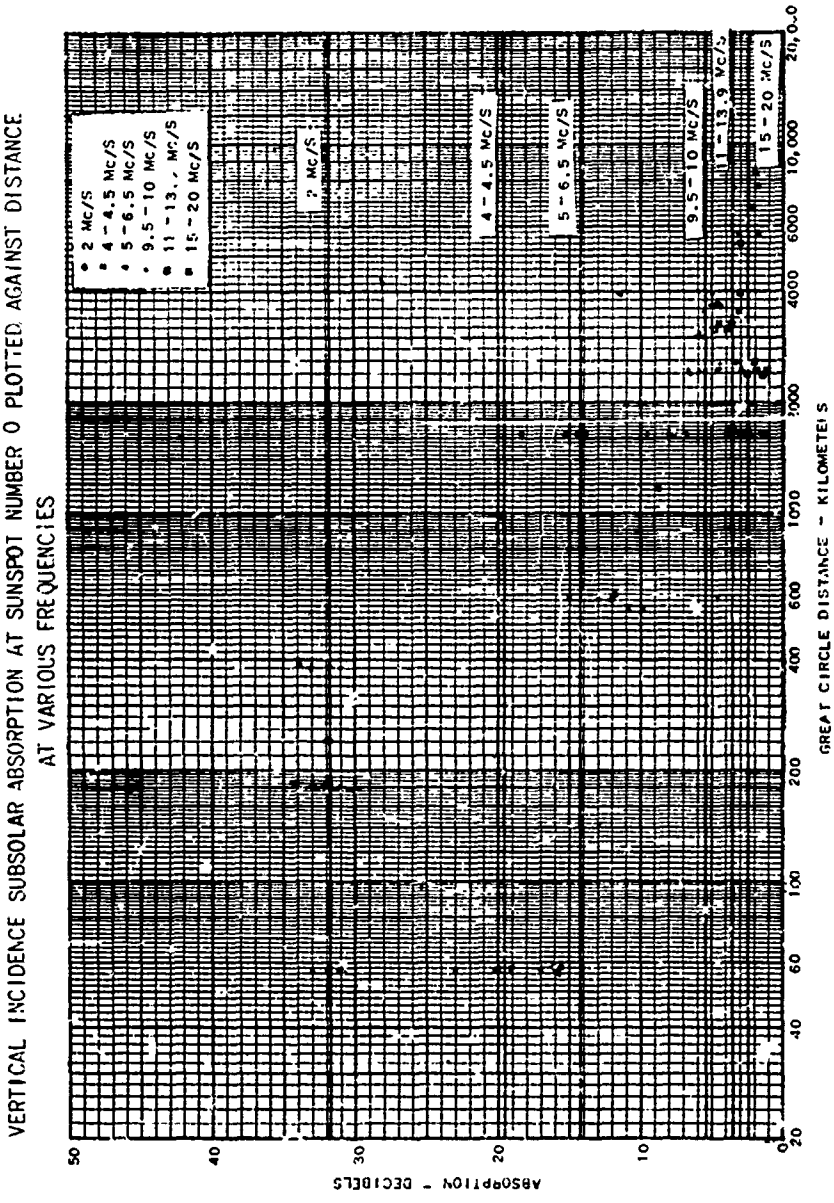
VERTICAL INCIDENCE SUBSOLAR ABSORPTION AT SUNSPOT NUMBER 0 PLOTTED AGAINST DISTANCE
AT VARIOUS FREQUENCIES
2 Mc/S
4 - 4.5 Mc/S
5 - 6.5 Mc/S
9.5 - 10 Mc/S
11 - 13.9 Mc/S
15 - 20 Mc/S
2 Mc/S
4 - 4.5 Mc/S
5 - 6.5 Mc/S
9.5 - 10 Mc/S
11 - 13.9 Mc/S
15 - 20 Mc/S
ABSORPTION - DECIBELS
GREAT CIRCLE DISTANCE - KILOMETERS
0
10
20
30
40
50
20
40
60
100
200
400
600
1000
2000
4000
6000
10,000
20,000

Figure 41

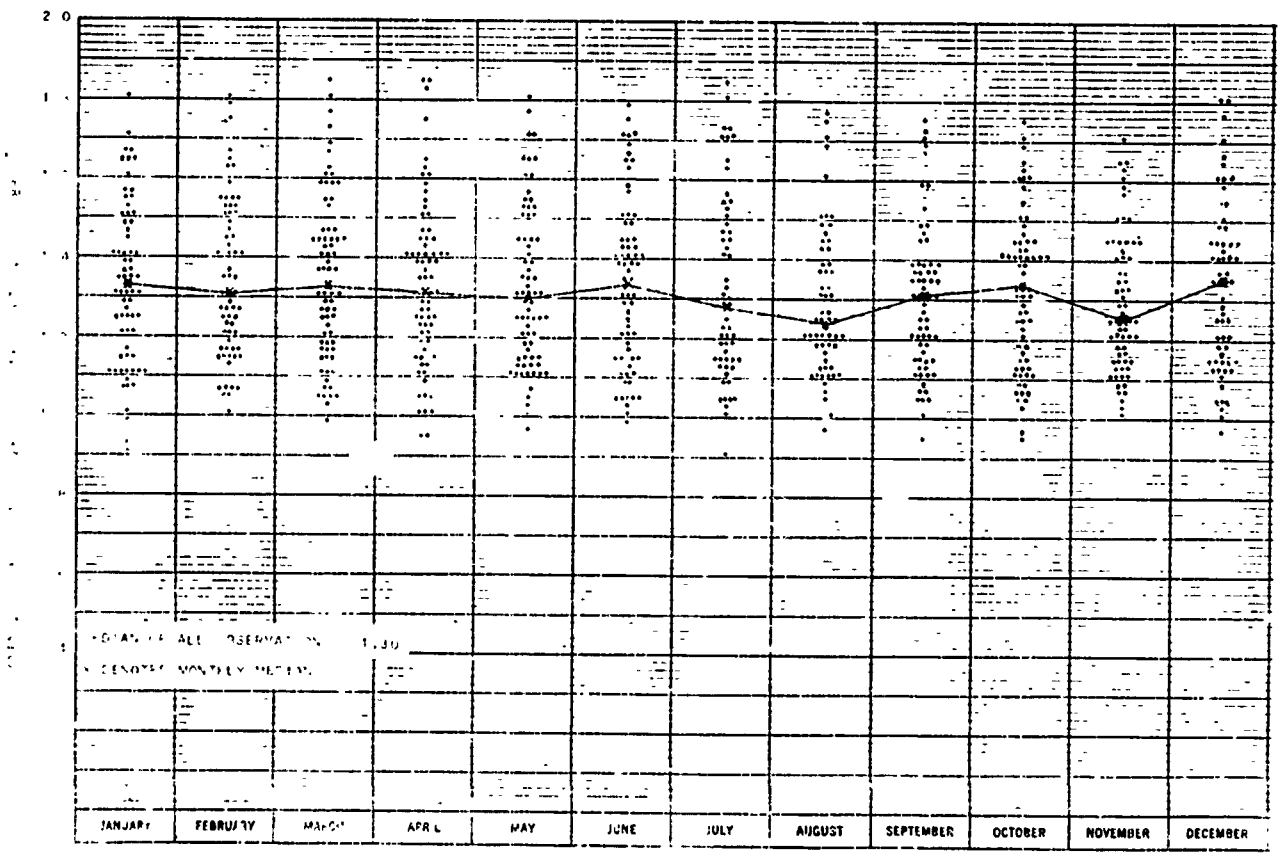
2.0
1.
.4
JANUARY
FEBRUARY
MARCH
APRIL
MAY
JUNE
JULY
AUGUST
SEPTEMBER
OCTOBER
NOVEMBER
DECEMBER

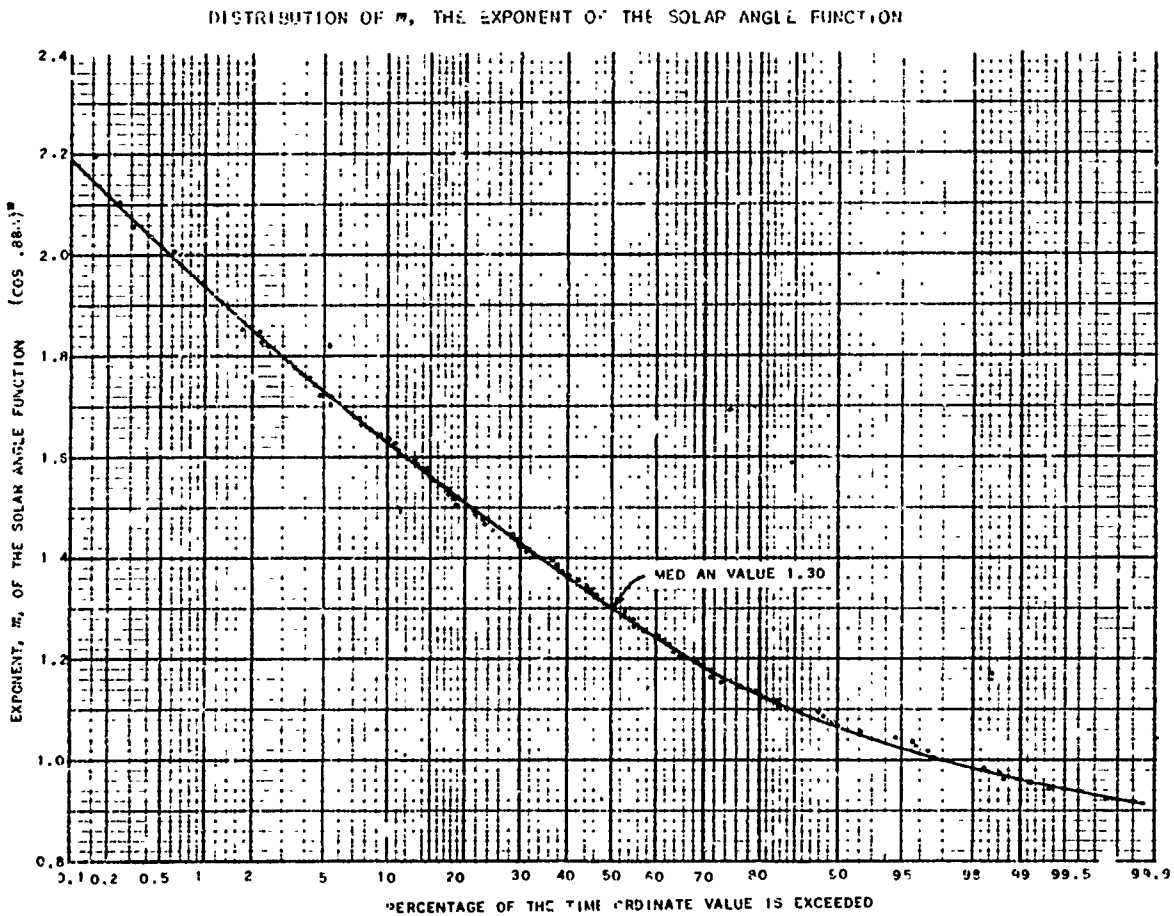
DISTRIBUTION OF m, THE EXPONENT OF THE SOLAR ANGLE FUNCTION
EXPONENT, m, OF THE SOLAR ANGLE FUNCTION (COS .88.)^m
2.4
2.2
2.0
1.8
1.6
1.4
1.2
1.0
0.8
MEDIAN VALUE 1.30
0.1 0.2 0.5 1 2 5 10 20 30 40 50 60 70 80 90 95 98 99 99.5 99.9
PERCENTAGE OF THE TIME ORDINATE VALUE IS EXCEEDED

Figure 43

THE EXPONENT, m, OF THE SOLAR ZENITH ANGLE FUNCTION PLOTTED AGAINST FREQUENCY

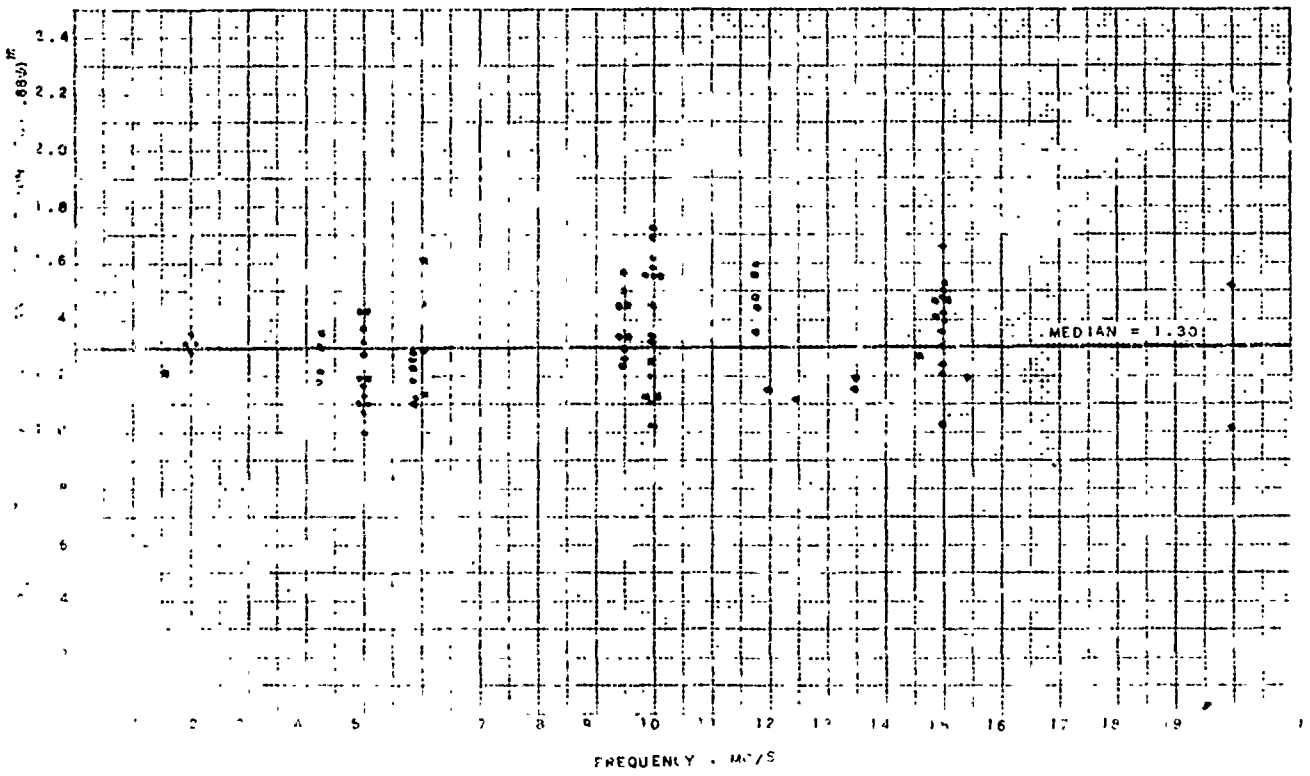

Figure 1

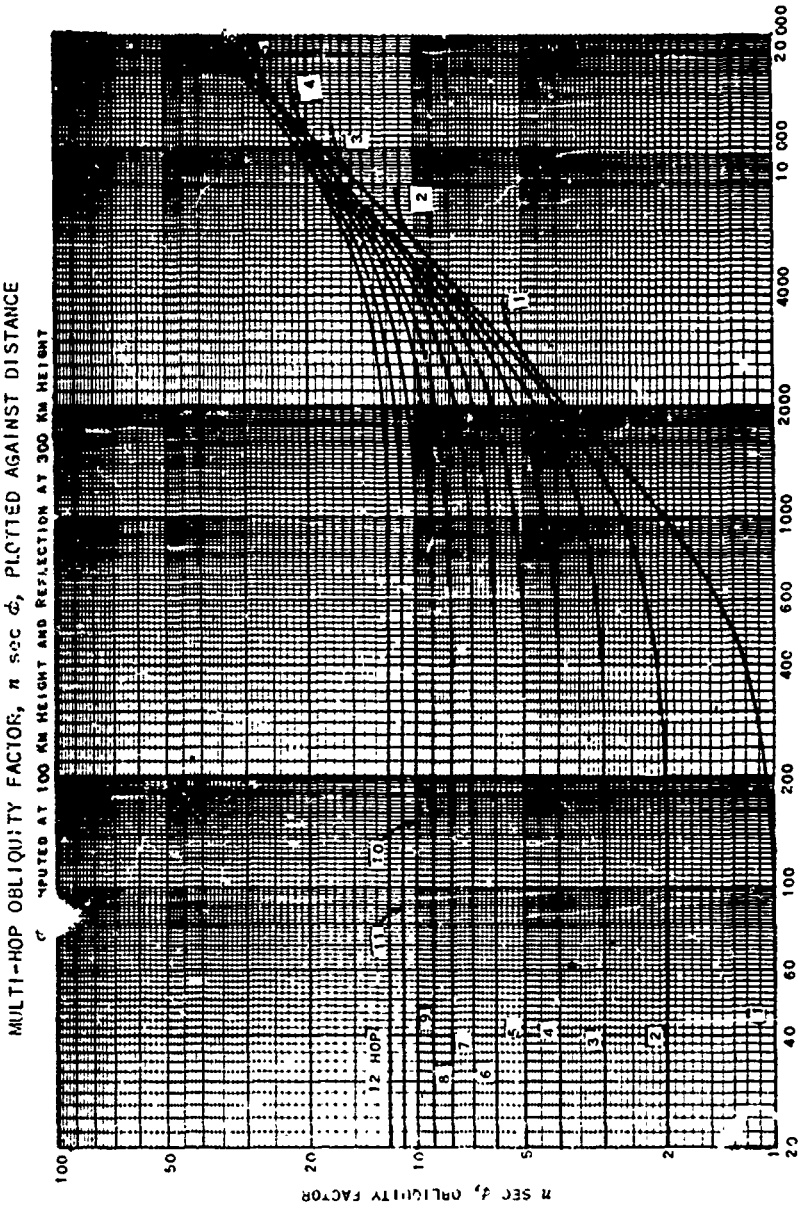
MULTI-HOP OBLIQUITY FACTOR, n sec φ, PLOTTED AGAINST DISTANCE
COMPUTED AT 100 KM HEIGHT AND REFLECTION AT 300 KM HEIGHT
n SEC φ, OBLIQUITY FACTOR
GREAT CIRCLE DISTANCE — KILOMETERS
12 HOP
11
10
9
8
7
6
5
4
3
2
1
100
50
20
10
5
2
1
20
40
60
100
200
400
600
1000
2000
4000
10 000
20 000

Figure 45

FACTOR TO APPROX MATE THE EFFECT OF THE EARTH'S MAGNETIC FIELD UPON ABSORPTION OF THE ORDINARY RAY

ABSORPTION = $I_{vo}\frac{K}{f^2}$

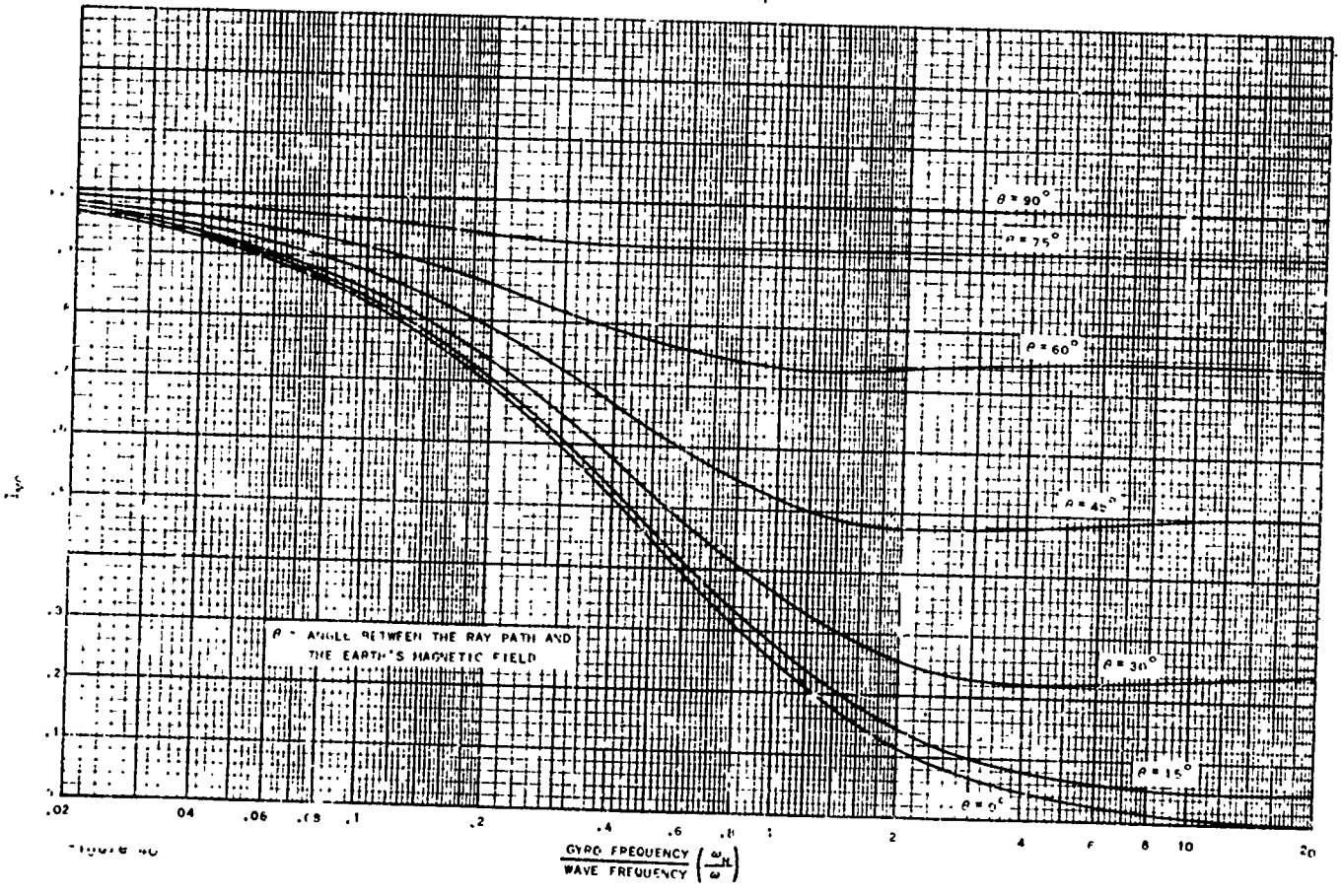

Figure 40

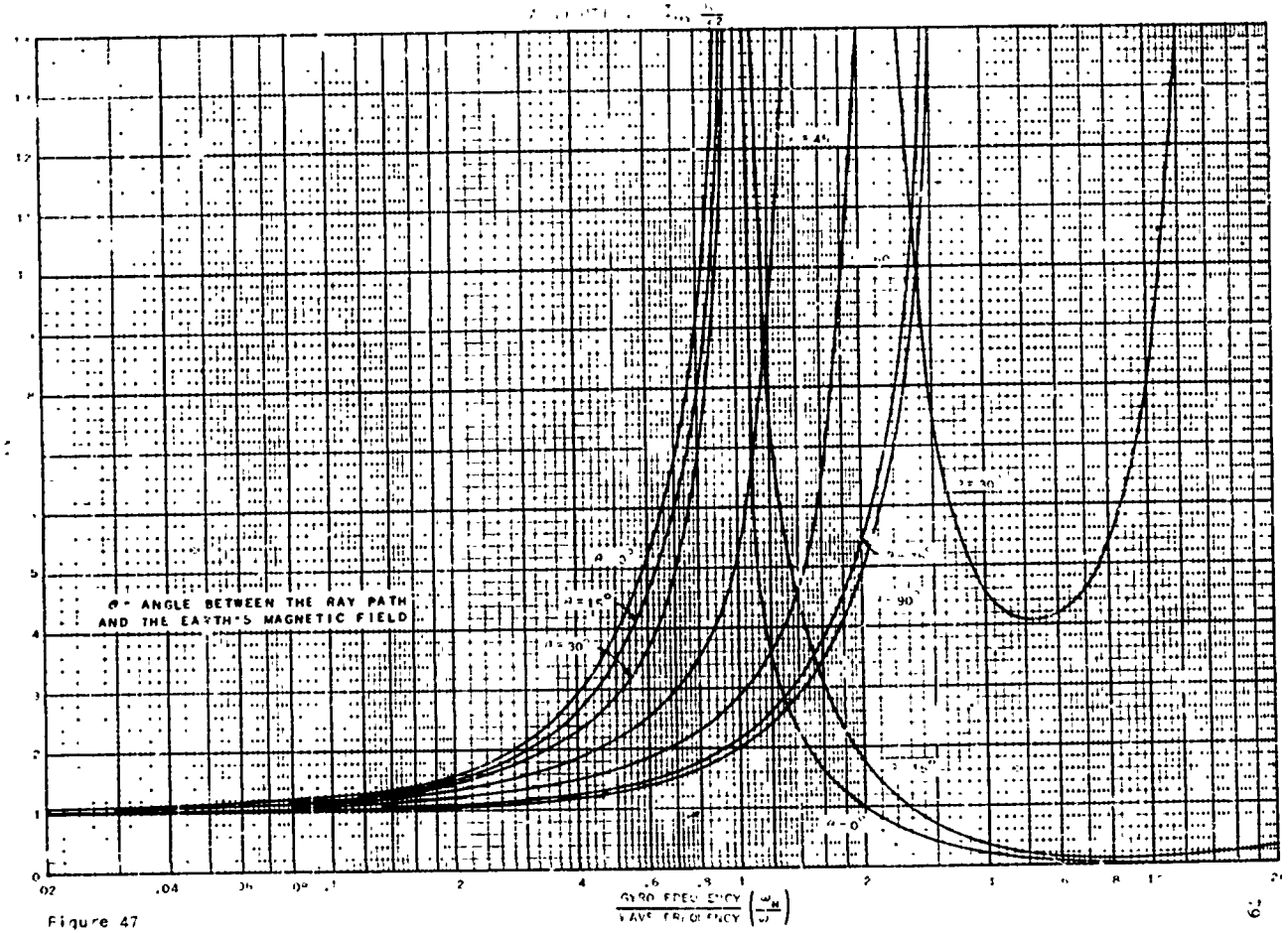
θ = ANGLE BETWEEN THE RAY PATH AND THE EARTH'S MAGNETIC FIELD
θ = 0°
θ = 15°
θ = 30°
θ = 45°
θ = 90°
.02
.04
.06
.08
.1
.2
.4
.6
.8
1
2
4
6
8
10
20
GYRO FREQUENCY / WAVE FREQUENCY (ω_H/ω)

Figure 47

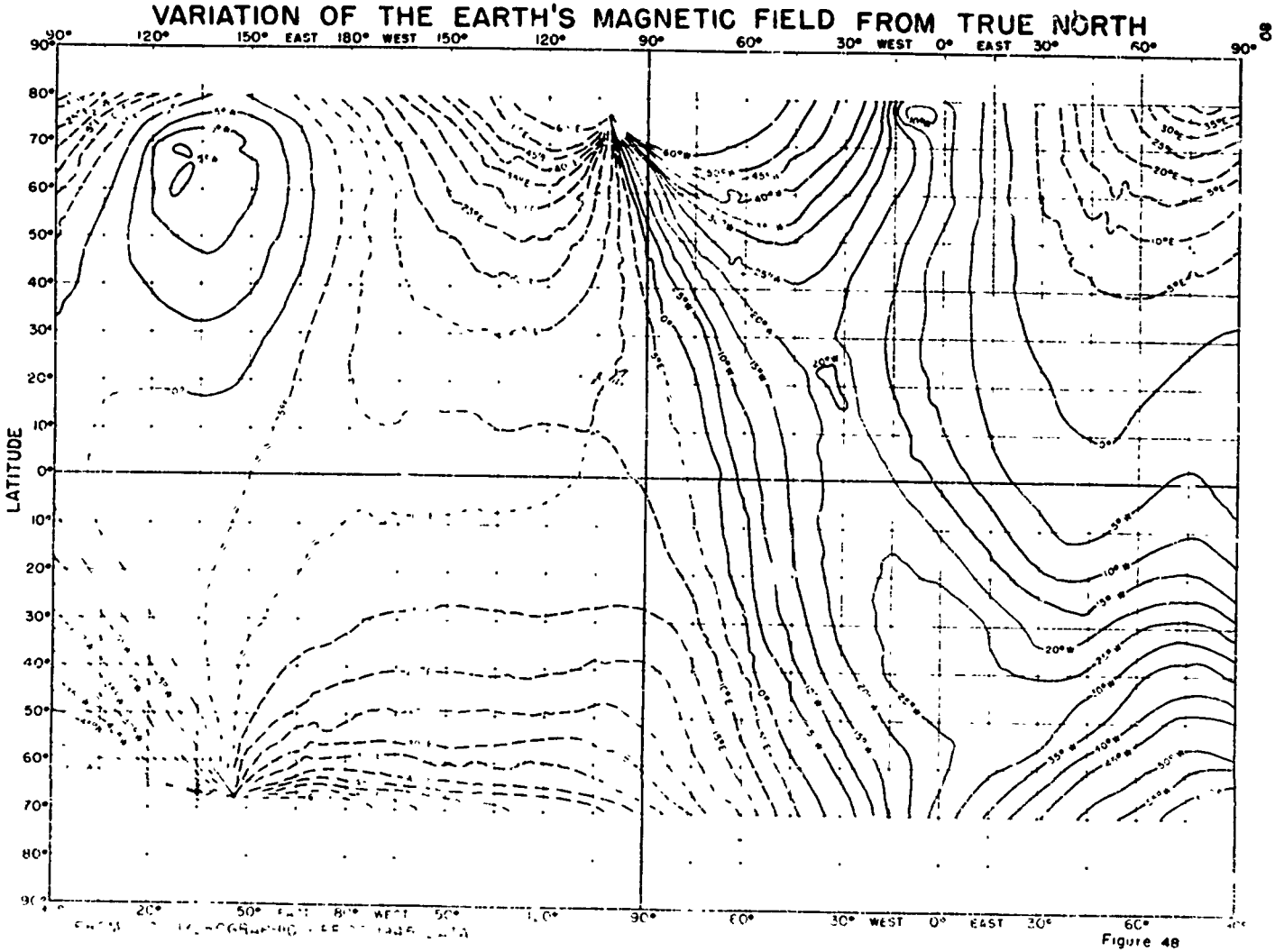
VARIATION OF THE EARTH'S MAGNETIC FIELD FROM TRUE NORTH
LATITUDE
90° 120° 150° EAST 180° WEST 150° 120° 90° 60° 30° WEST 0° EAST 30° 60° 90°
80° 70° 60° 50° 40° 30° 20° 10° 0° 10° 20° 30° 40° 50° 60° 70° 80° 90°
90° 60° 30° WEST 0° EAST 30° 60°

Figure 48

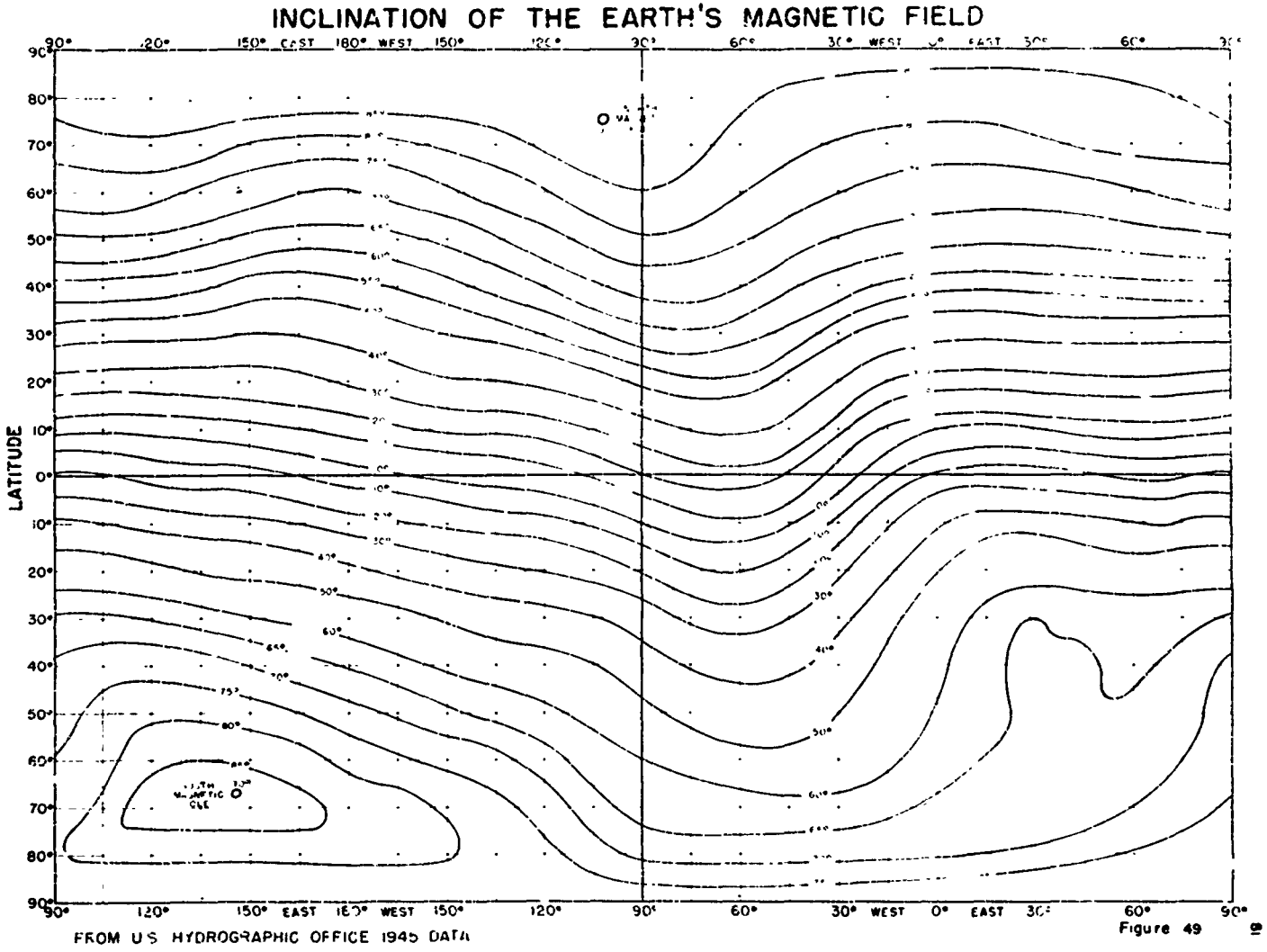
INCLINATION OF THE EARTH'S MAGNETIC FIELD
LATITUDE
90°
120°
150° EAST
180° WEST
150°
120°
90°
60°
30° WEST
0° EAST
30°
60°
90°
80°
70°
60°
50°
40°
30°
20°
10°
0°
FROM U S HYDROGRAPHIC OFFICE 1945 DATA

Figure 49

BEARING CHART

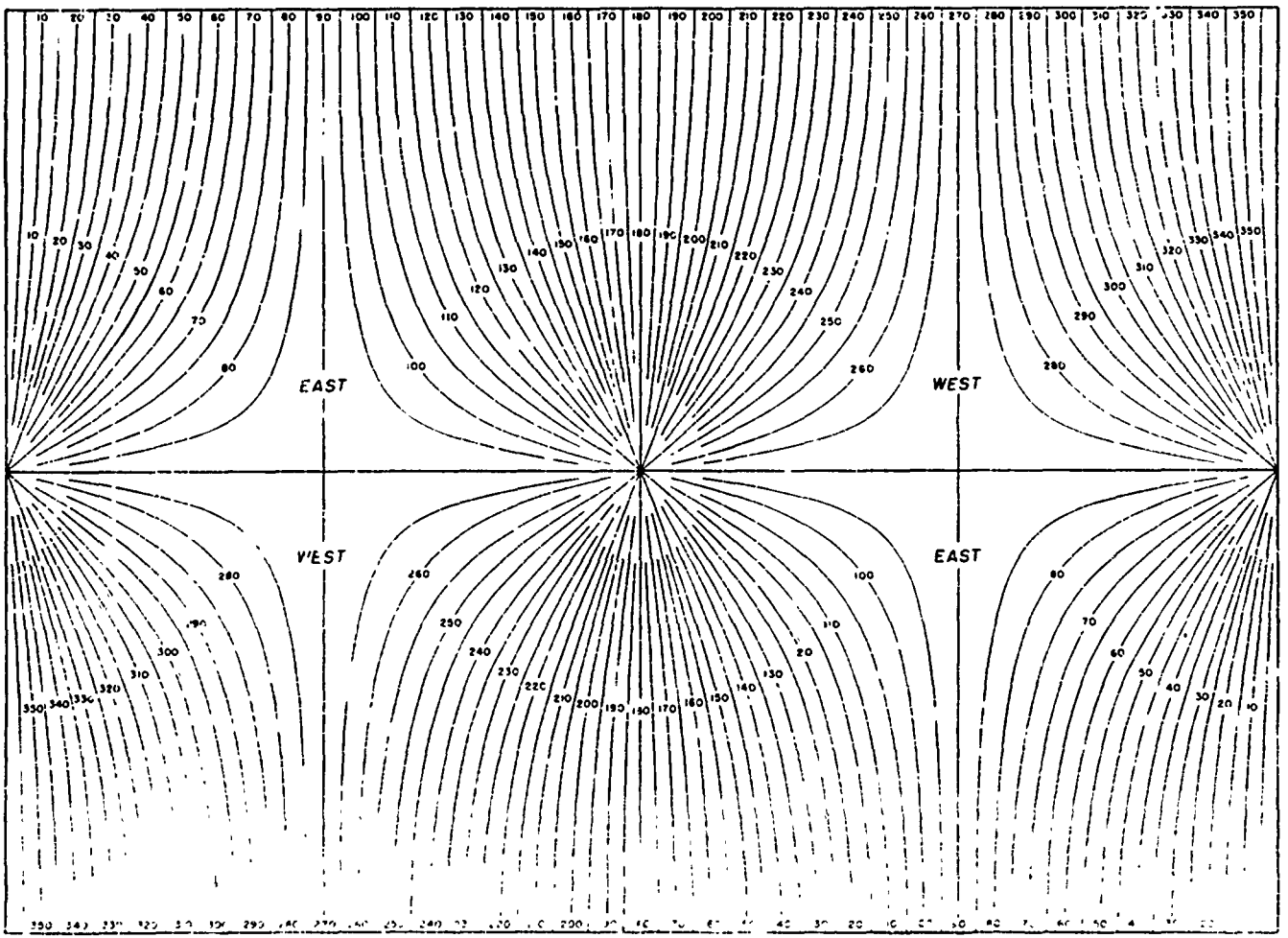

EAST AND WEST ON THE CHART CORRESPOND TO THE GENERAL PATH DIRECTION

Figure 50

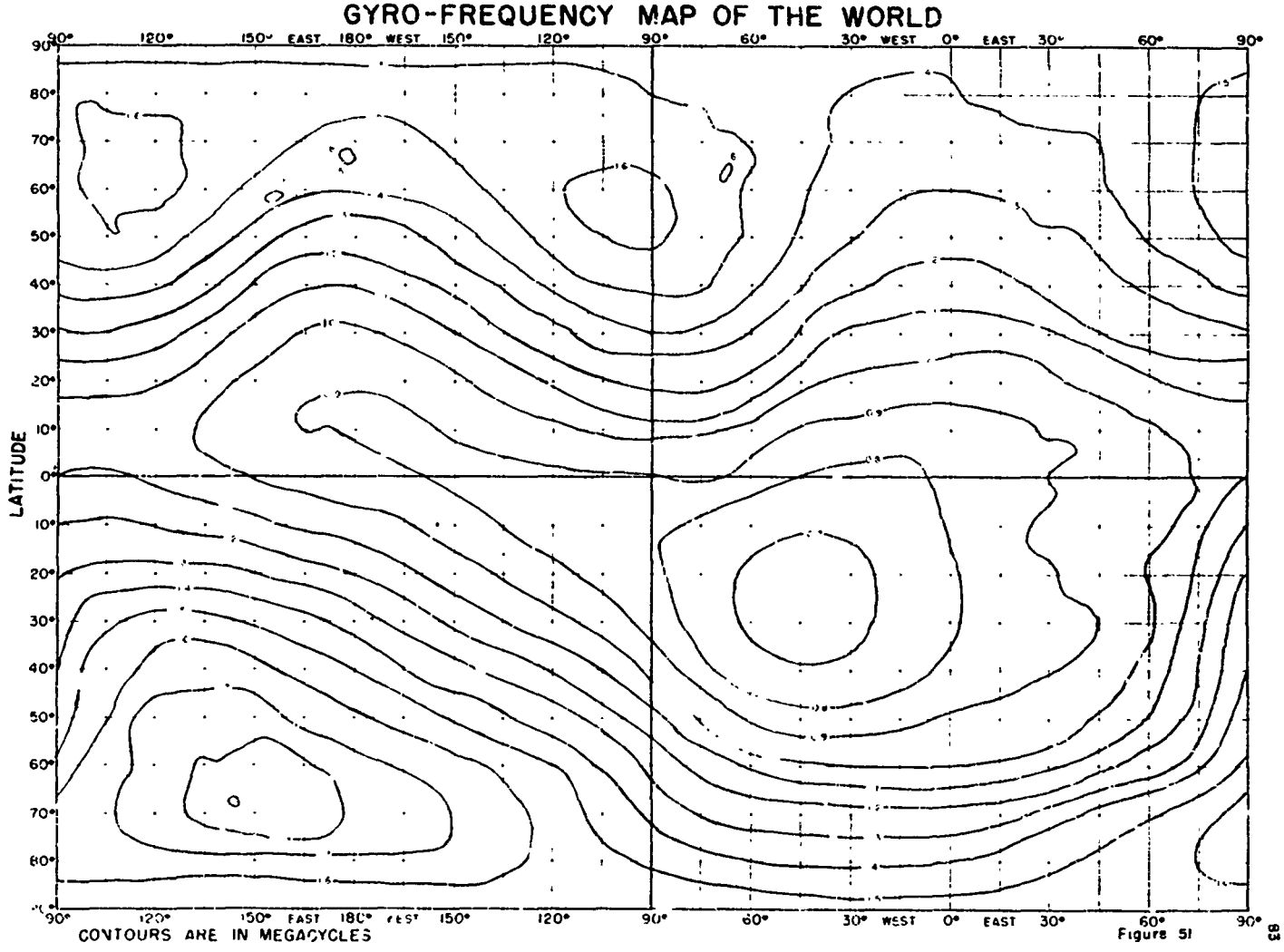
GYRO-FREQUENCY MAP OF THE WORLD
90° 120° 150° EAST 180° WEST 150° 120° 90° 60° 30° WEST 0° EAST 30° 60° 90°
LATITUDE
90° 80° 70° 60° 50° 40° 30° 20° 10° 0° 10° 20° 30° 40° 50° 60° 70° 80° 90°
CONTOURS ARE IN MEGACYCLES

Figure 51

NOMOGRAM (AFTER D'OCAGNE) TO DETERMINE THE ANGLE (τ) BETWEEN A RAY PATH AND THE EARTH'S MAGNETIC FIELD

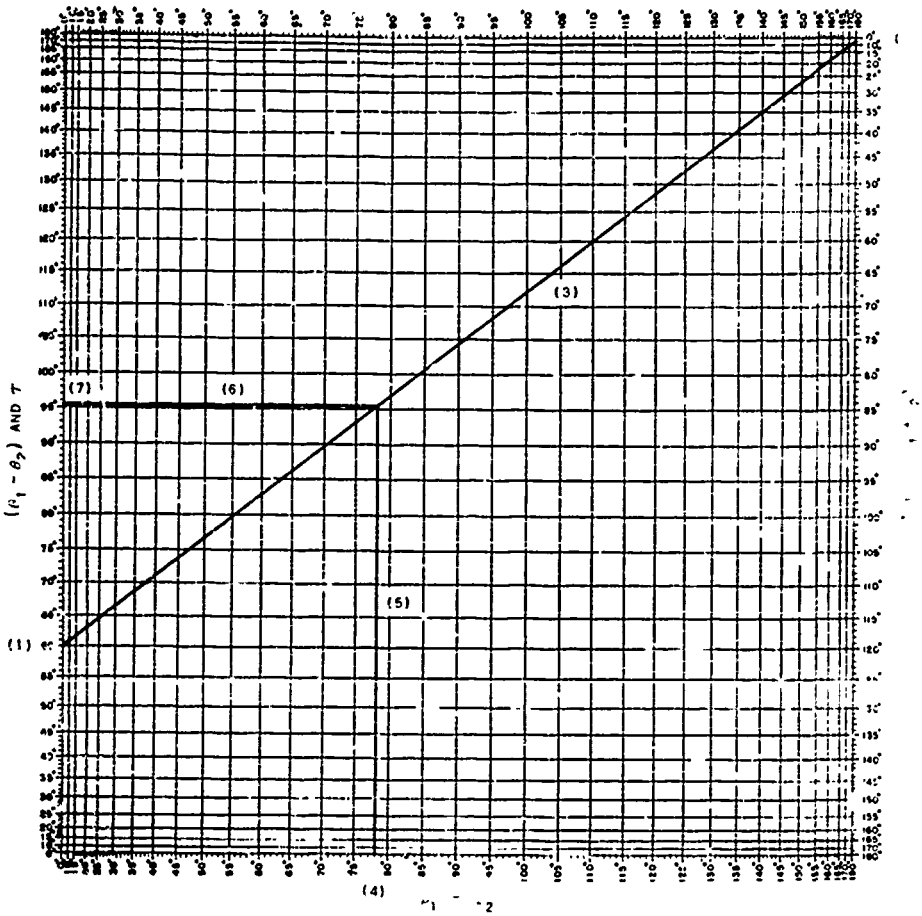

θ_1 = 90° PLUS THE INCLINATION OF THE EARTH'S MAGNETIC FIELD

θ_2 = ANGLE OF THE RAY PATH WITH THE IONOSPHERE AT 100 KILOMETER HEIGHT

ϕ_1 = VARIATION OF THE EARTH'S MAGNETIC FIELD

ϕ_2 = BEARING OF RAY PATH AT CONTROL POINT

EXAMPLE

BEARING OF RAY PATH = 86°, MAGNETIC INCLINATION = 32°, VARIATION = 8°, ANGLE OF RAY PATH AT IONOSPHERE = 32°:

1) ENTER LEFT SCALE WITH DIFFERENCE BETWEEN θ_1 AND θ_2 (60°)
2) ENTER RIGHT SCALE WITH DIFFERENCE BETWEEN 180° AND $(\theta_1 + \theta_2)$ (4°)
3) JOIN THESE ENTRIES WITH A STRAIGHT LINE
4) ENTER BOTTOM SCALE WITH THE DIFFERENCE BETWEEN ϕ_1 AND ϕ_2
5) DRAW A VERTICAL LINE TO INTERSECT LINE (3)
6) DRAW A HORIZONTAL LINE FROM INTERSECTION TO THE LEFT SCALE
7) READ τ ON LEFT SCALE (95.6°)

Figure 52

VERTICAL INCIDENCE SUBSOLAR ABSORPTION AT SSN 0

AT THE [illegible] EFFECT OF THE EARTH'S MAGNETIC FIELD REMOVED.

[illegible] APPLICATION OF [illegible] FACTOR TO THE ORDINARY RAY

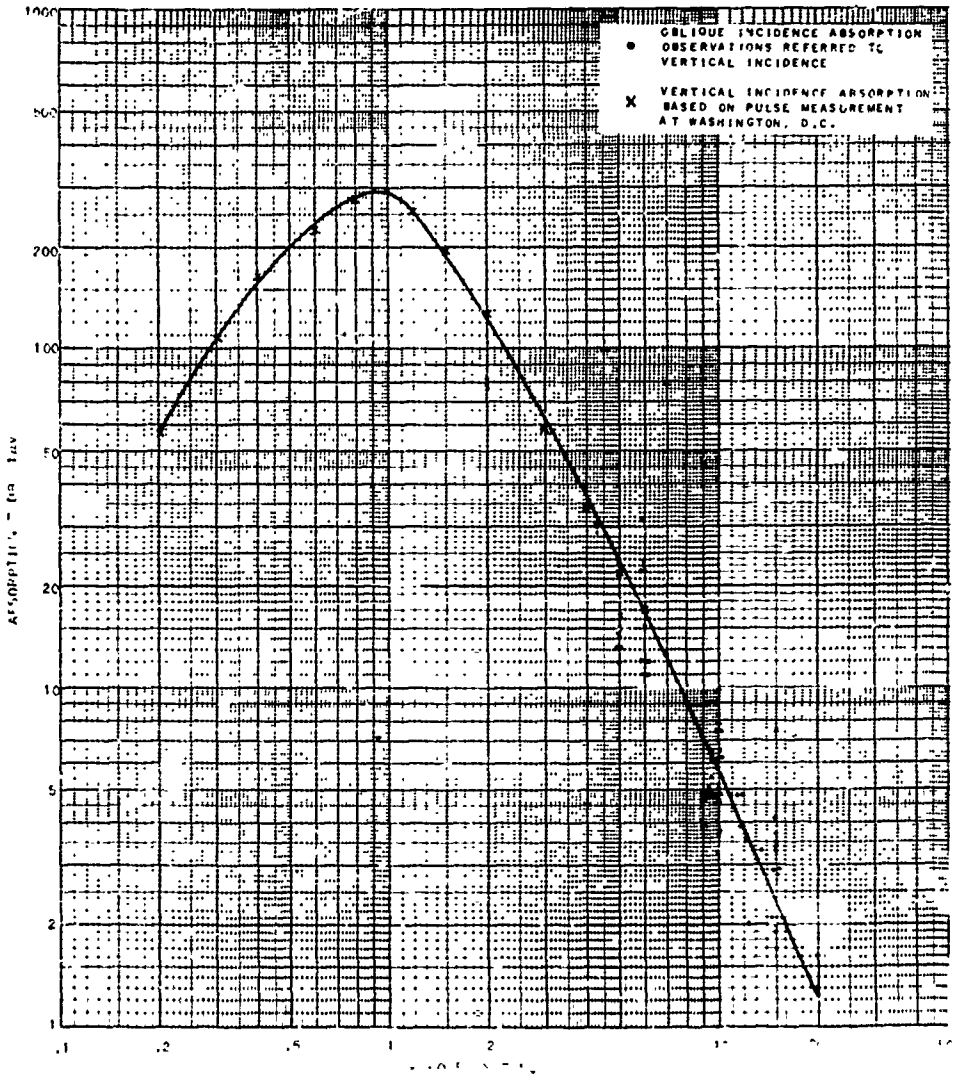

Figure 53

VERTICAL INCIDENCE SKY-WAVE ABSORPTION AT THE SUBSOLAR POINT

FOR SUNSPOT NUMBER ZERO

ABSORPTION OF SKY WAVES OBSERVED AT OBLIQUE INCIDENCE, REDUCED TO VERTICAL INCIDENCE EXTRAPOLATED TO THE SUBSOLAR POINT AND FACTORED TO SUNSPOT NUMBER ZERO.

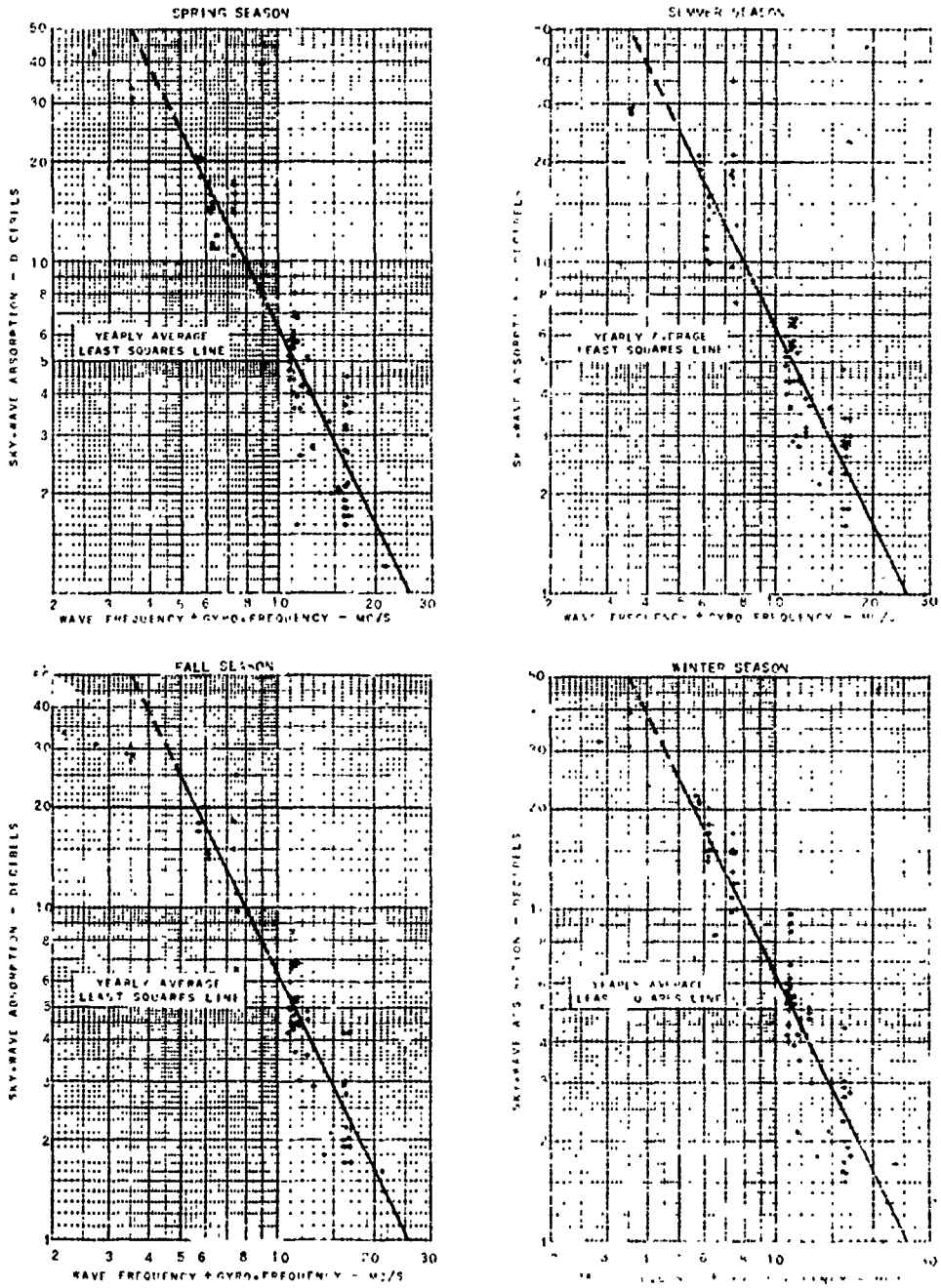

Figure 54

VERTICAL INCIDENCE SKY-WAVE ABSORPTION
AT THE SUBSOLAR POINT FOR SUNSPOT NUMBER ZERO
YEARLY AVERAGE VALUES

ABSORPTION OF SKY-WAVES OBSERVED AT OBLIQUE INCIDENCE, REDUCED TO VERTICAL INCIDENCE, EXTRAPOLATED TO THE SUBSOLAR POINT AND FACTORED TO SUNSPOT NUMBER ZERO

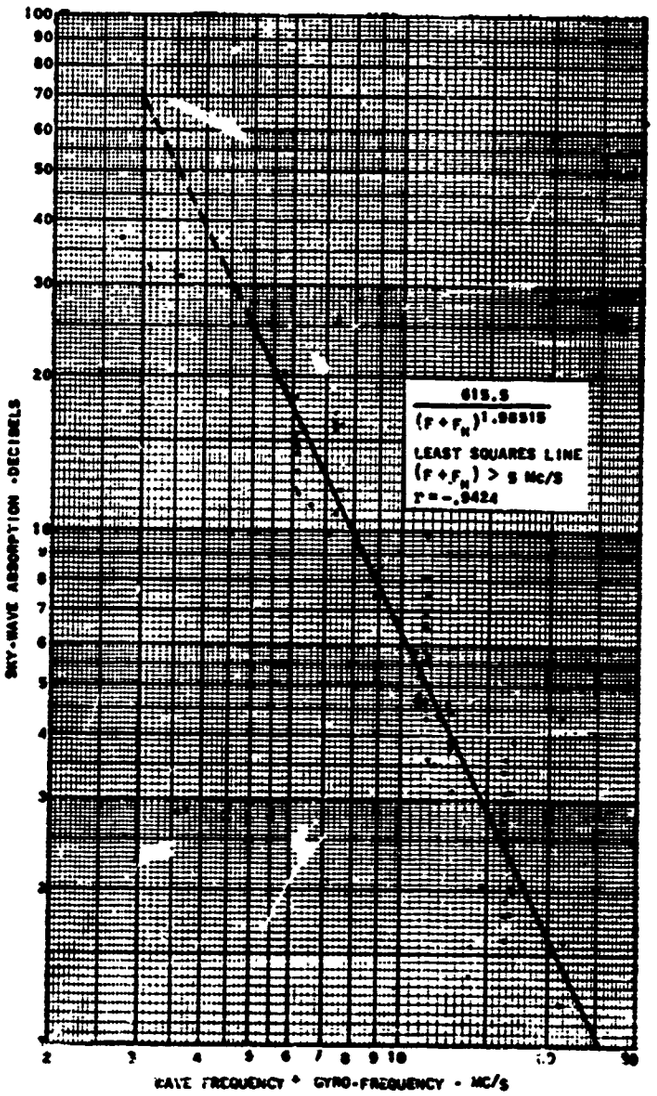

Figure 55

FREE SPACE FIELD

REFERENCE INTENSITY - 300 MILLIVOLTS PER METER AT ONE KILOMETER

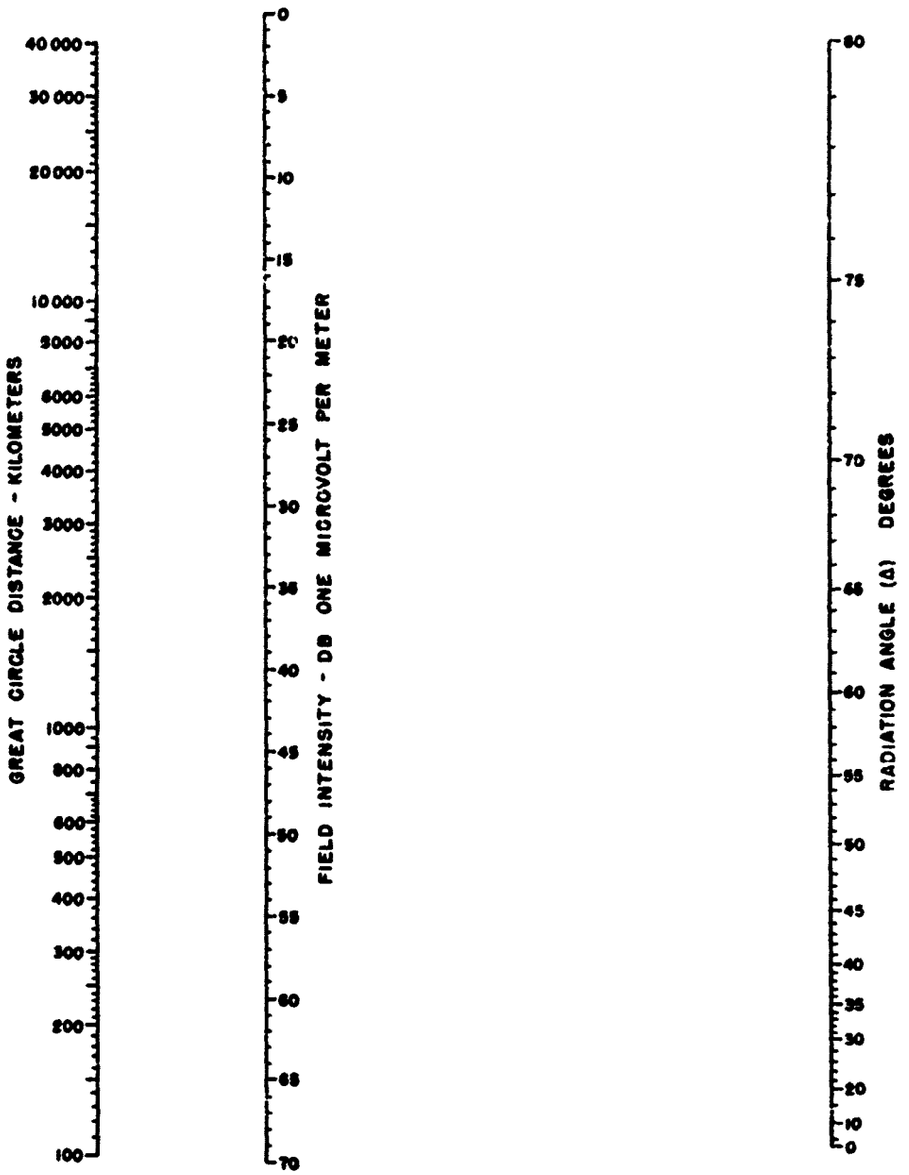

Figure 56.

GROUND LOSSES FOR MULTIHOP PROPAGATION OF RANDOMLY POLARIZED WAVES OVER "GOOD" EARTH

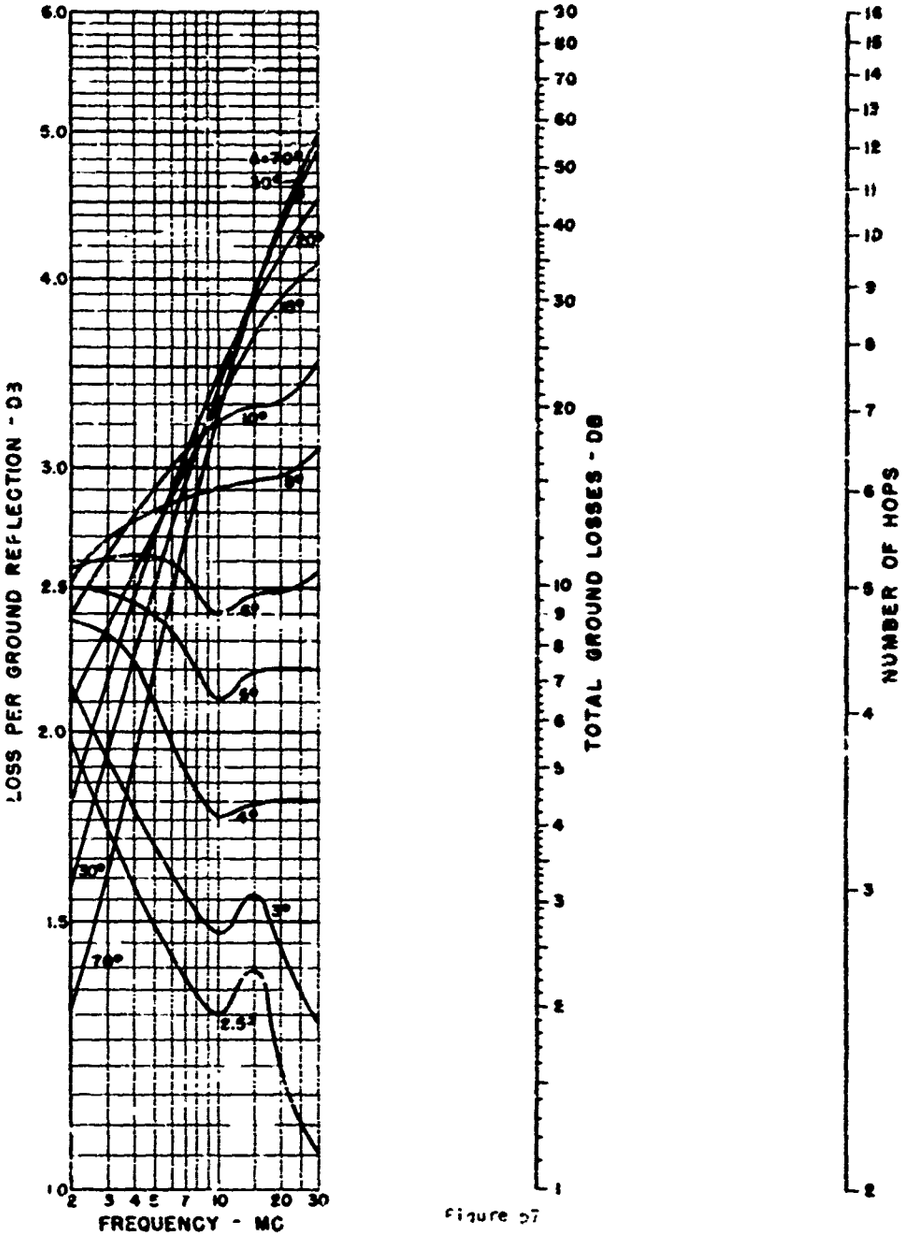

Figure 57

GROUND LOSSES FOR MULTIHOP PROPAGATION OF RANDOMLY POLARIZED WAVES OVER "POOR" EARTH

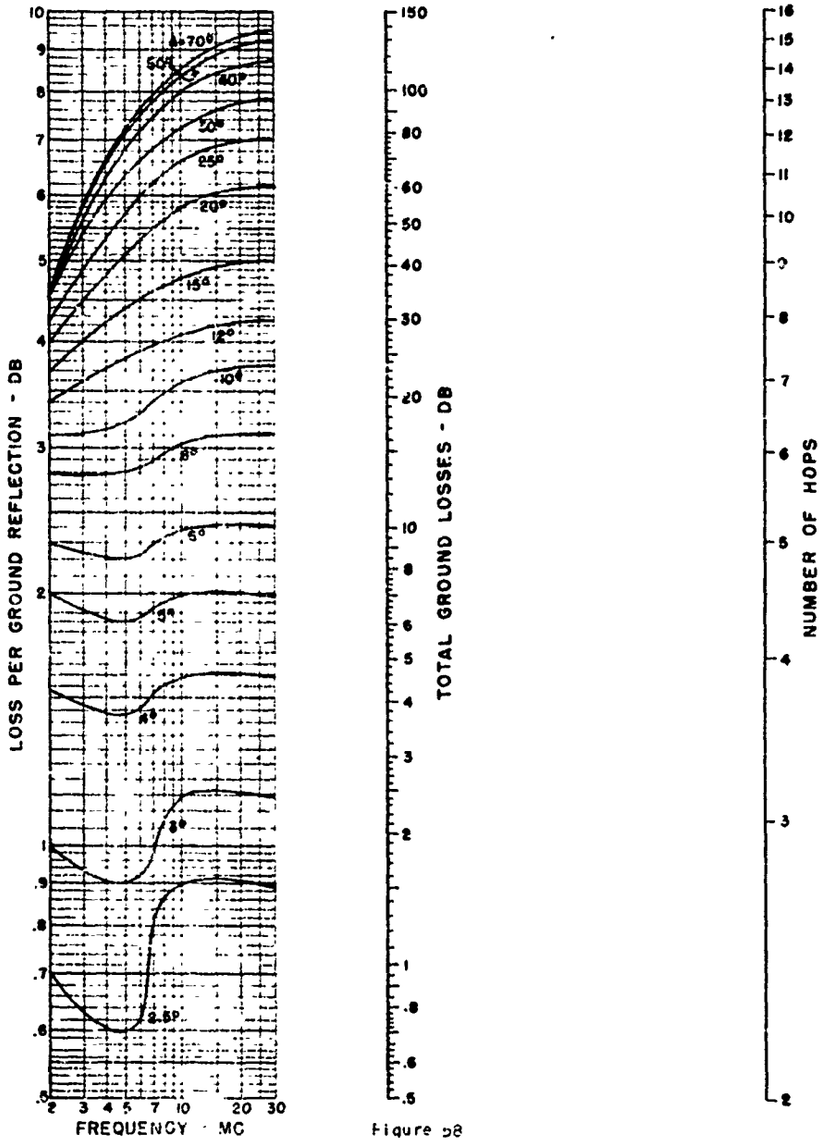

Figure 58

GROUND LOSSES FOR MULTIHOP PROPAGATION OF RANDOMLY POLARIZED WAVES OVER SEA WATER

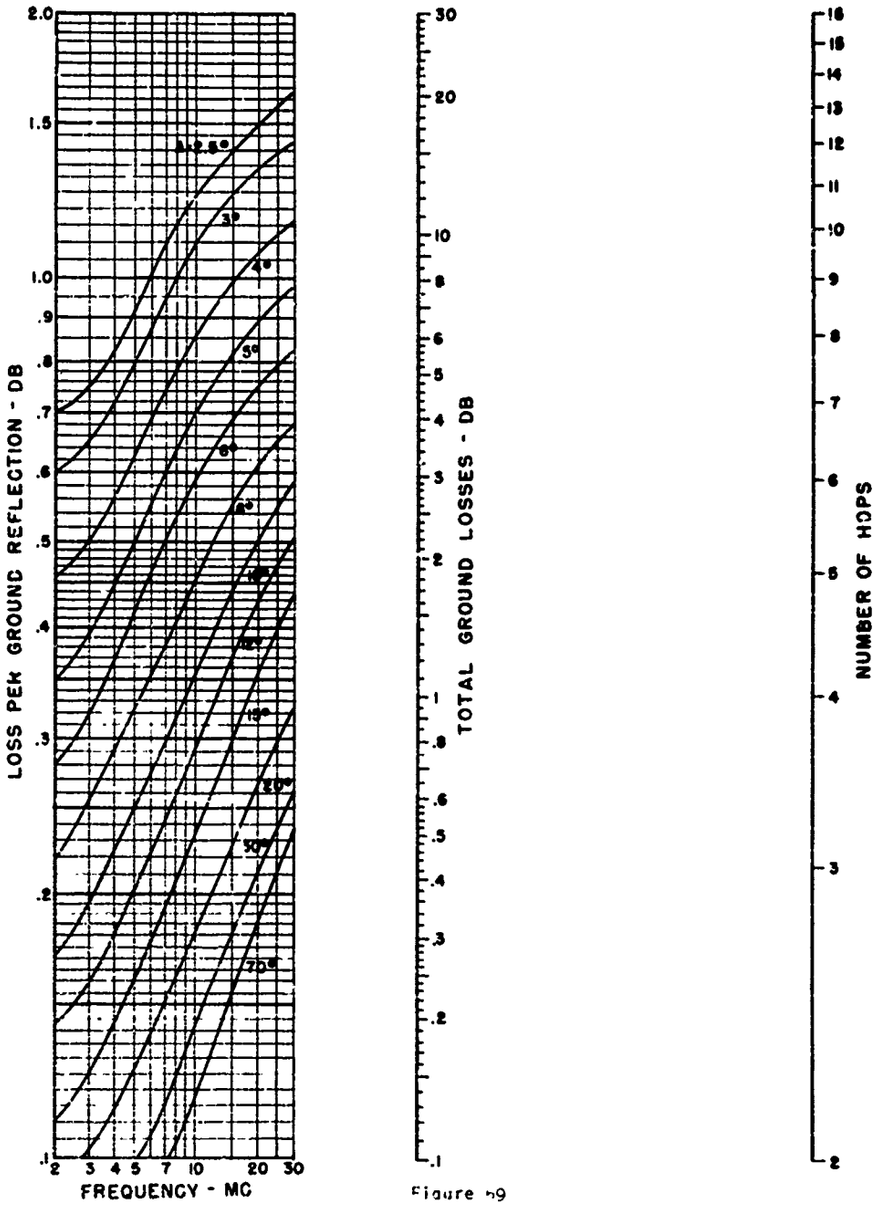

Figure 59

THEORETICAL CONVERGENCE GAIN IN DECIBELS FOR ONE HOP TRANSMISSION

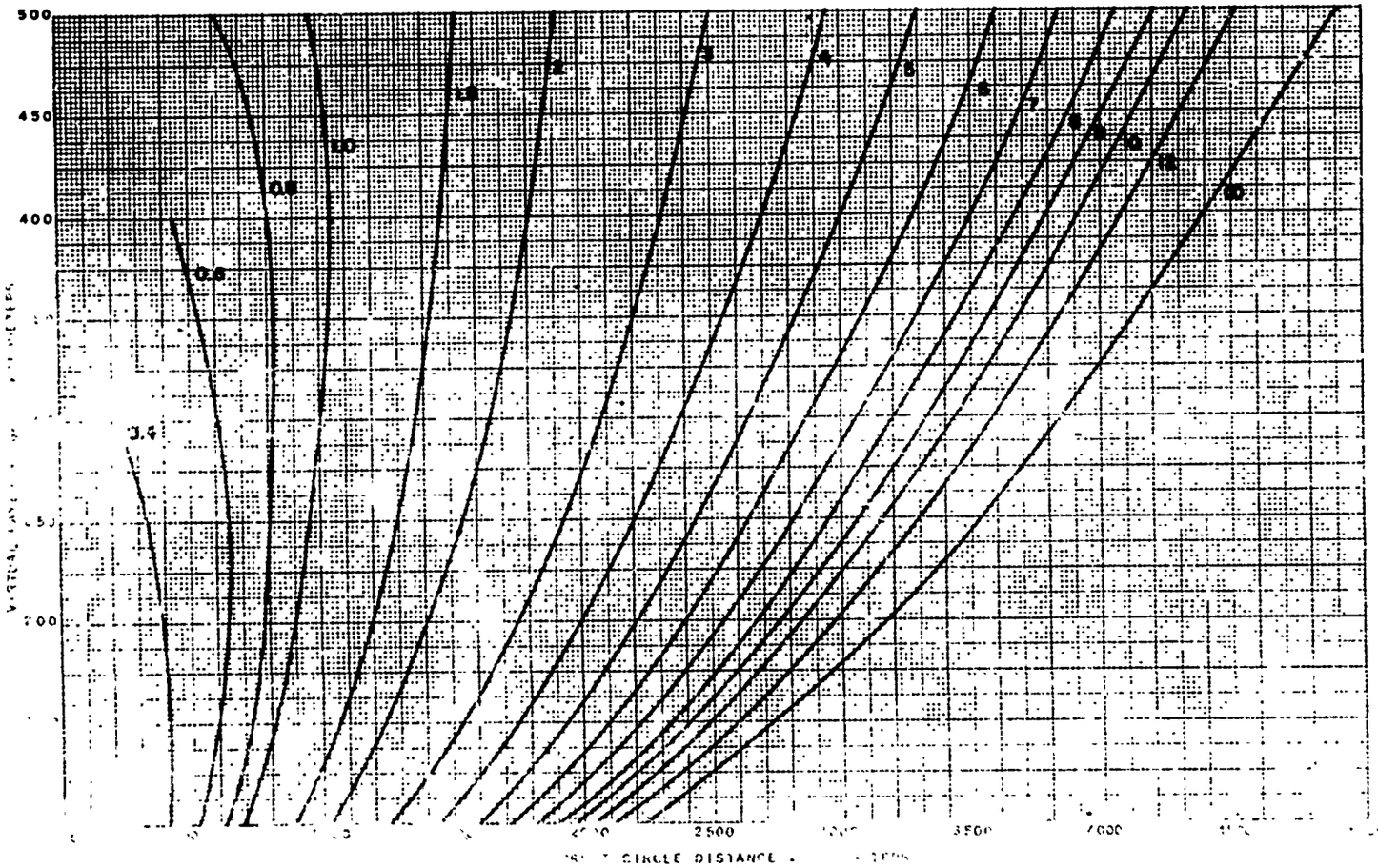

CIRCLE DISTANCE

Figure 60

THEORETICAL CONVERGENCE GAIN IN DECIBELS FOR TWO HOP TRANSMISSION

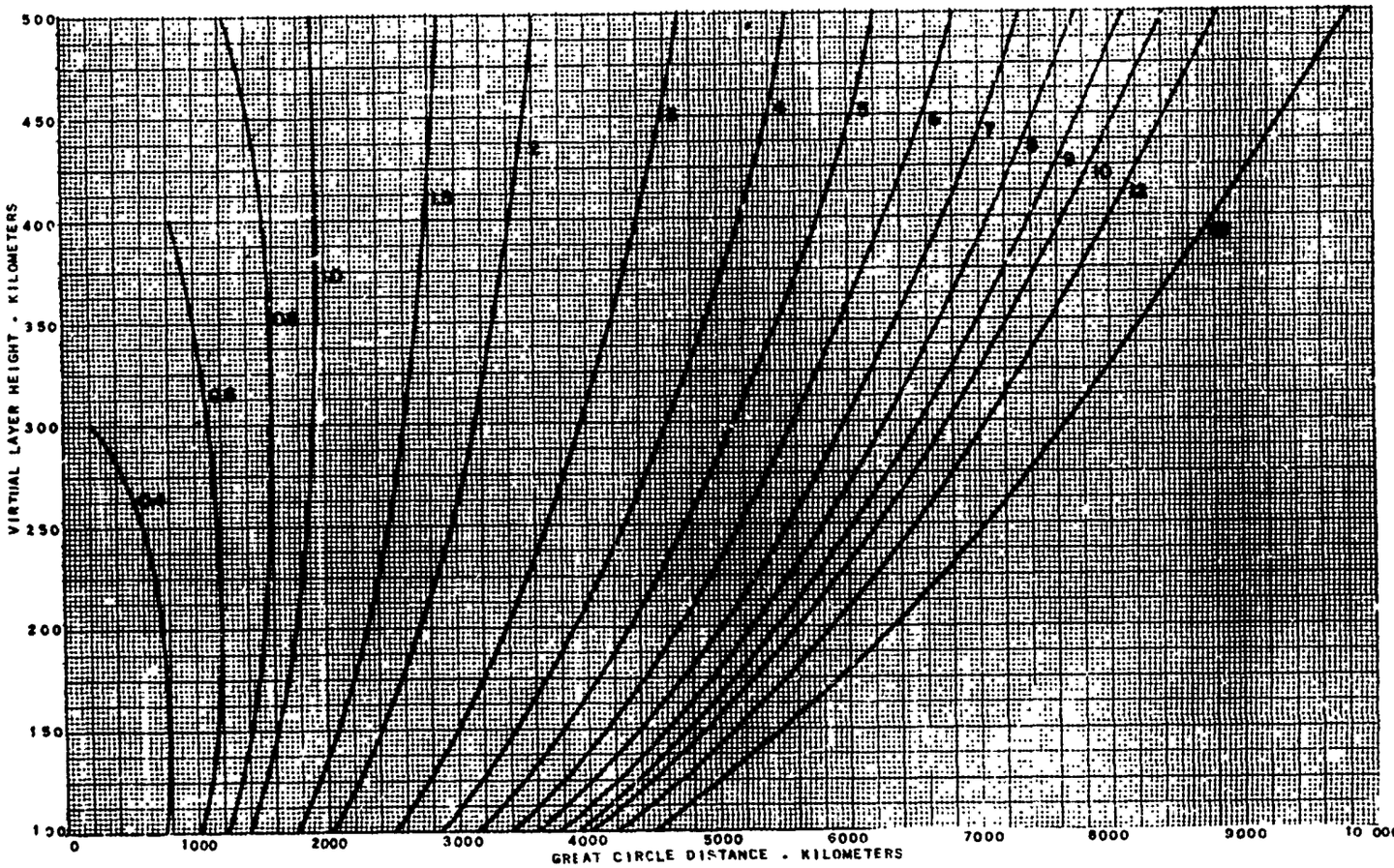

Figure 61

THEORETICAL CONVERGENCE GAIN IN DECIBELS FOR THREE HOP TRANSMISSION

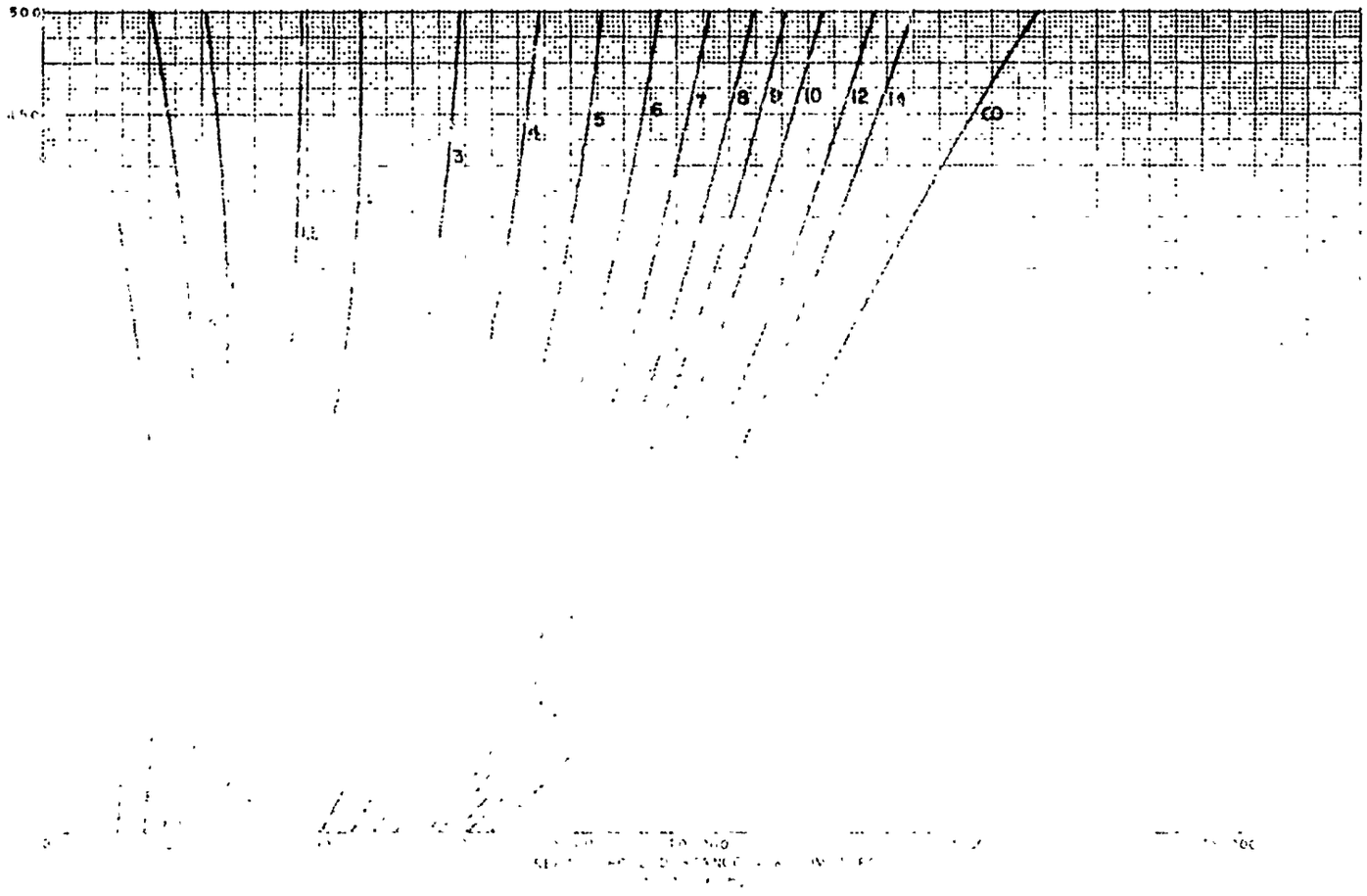

THEORETICAL CONVERGENCE GAIN IN DECIBELS FOR FOUR HOP TRANSMISSION

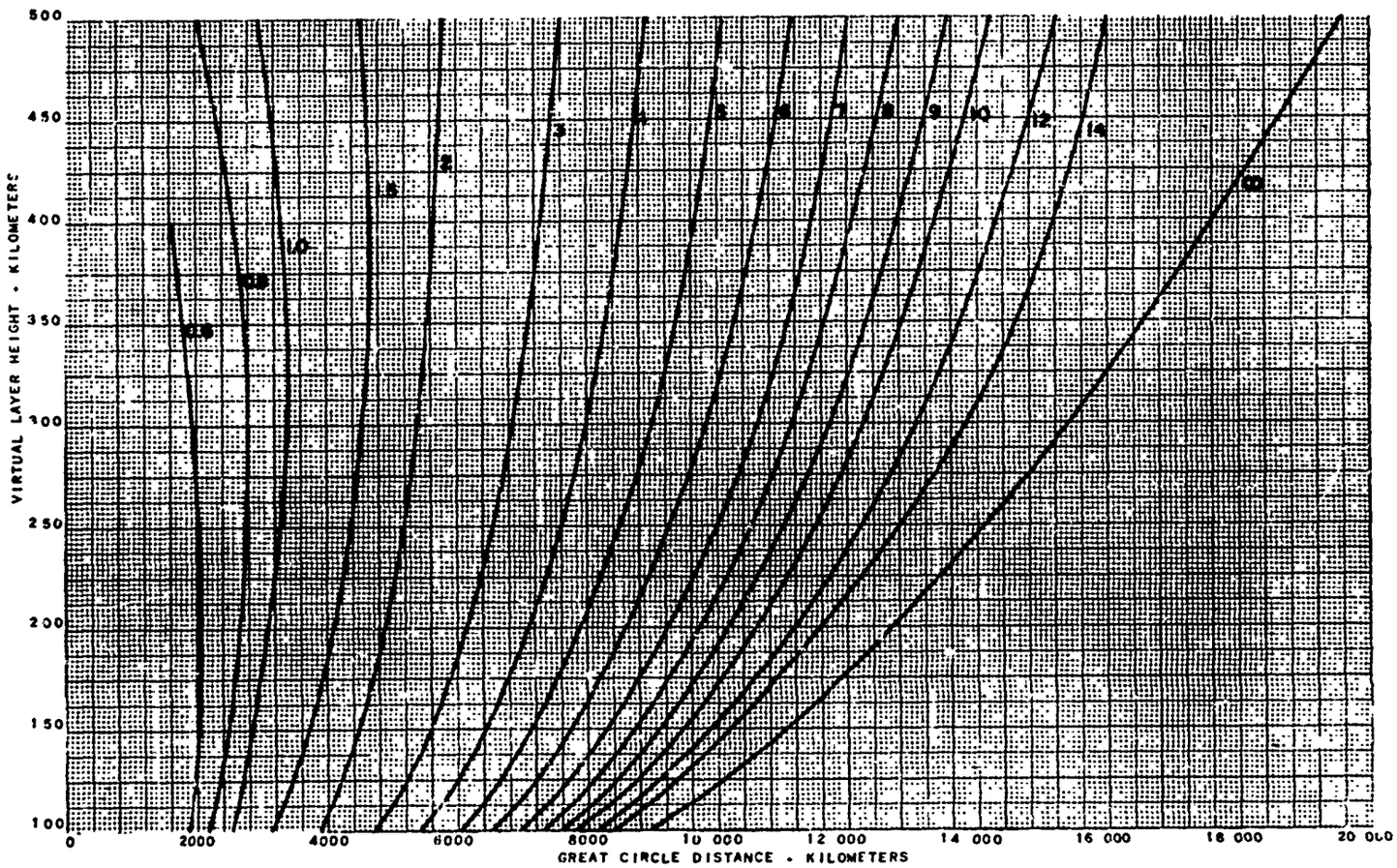

Figure 63

SAMPLE DISTRIBUTION OF HOURLY MEDIAN RECEIVER INPUT VOLTAGES
MAY TO LOUISIANA STATE UNIVERSITY
10 Mc – 16:7 Kv – OCTOBER 1947
MASS PLOT SHOWING DIURNAL DISTIRBUTION

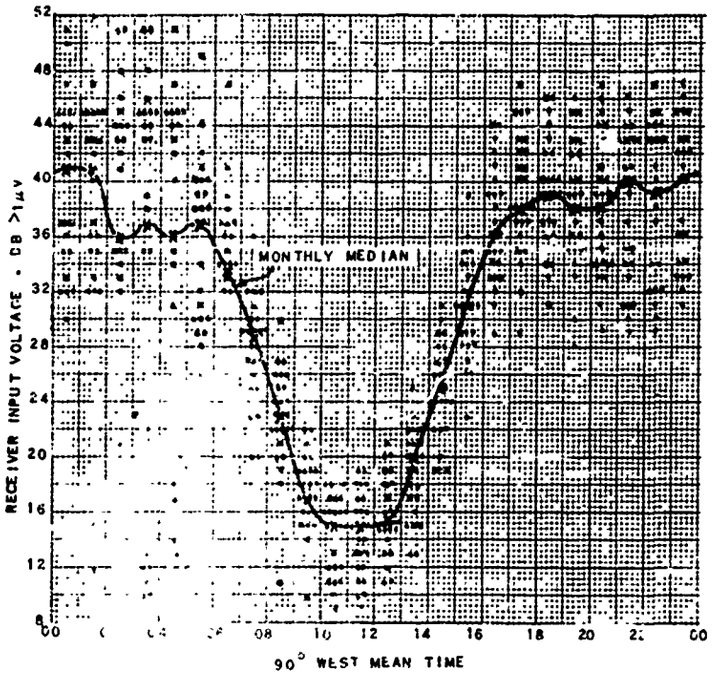

Figure 64

SAMPLE HISTOGRAMS

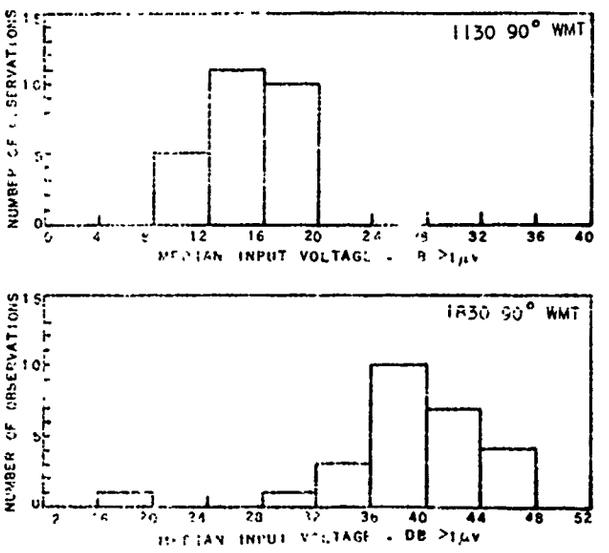

Figure 65

SAMPLE DISTRIBUTIONS OF HOURLY MEDIAN INPUT VOLTAGES AT NIGHT

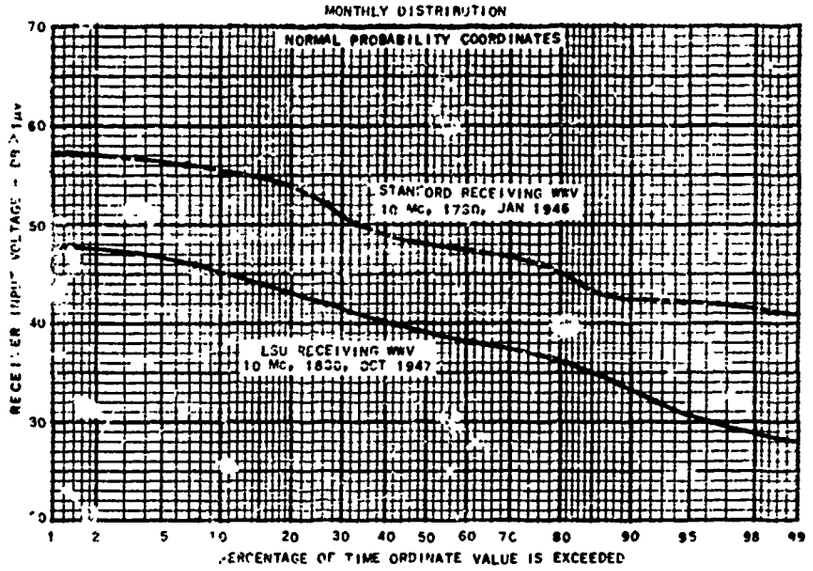

Figure 66

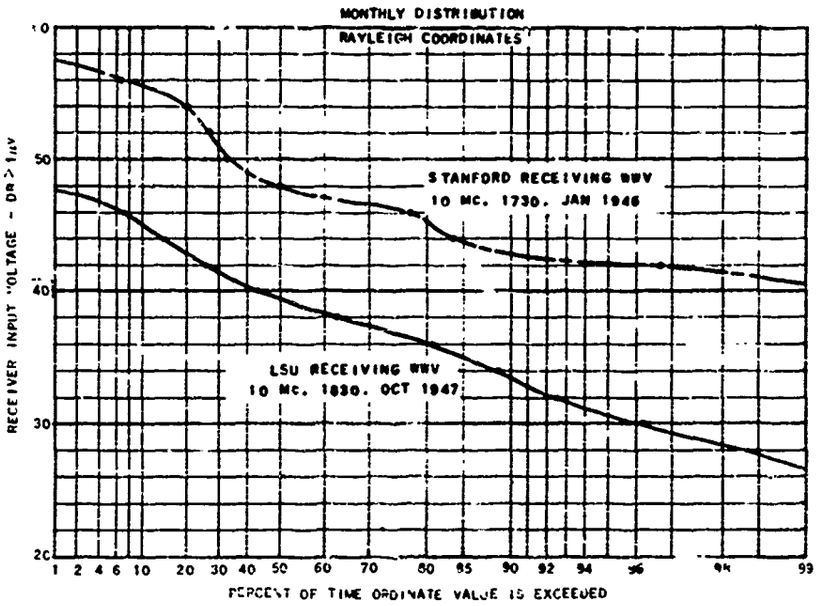

Figure 67

SAMPLE DISTRIBUTION OF HOURLY MEDIAN INPUT VOLTAGES AT NIGHT

WAY TO STANFORD - 10 MC

ANNUAL DISTRIBUTION

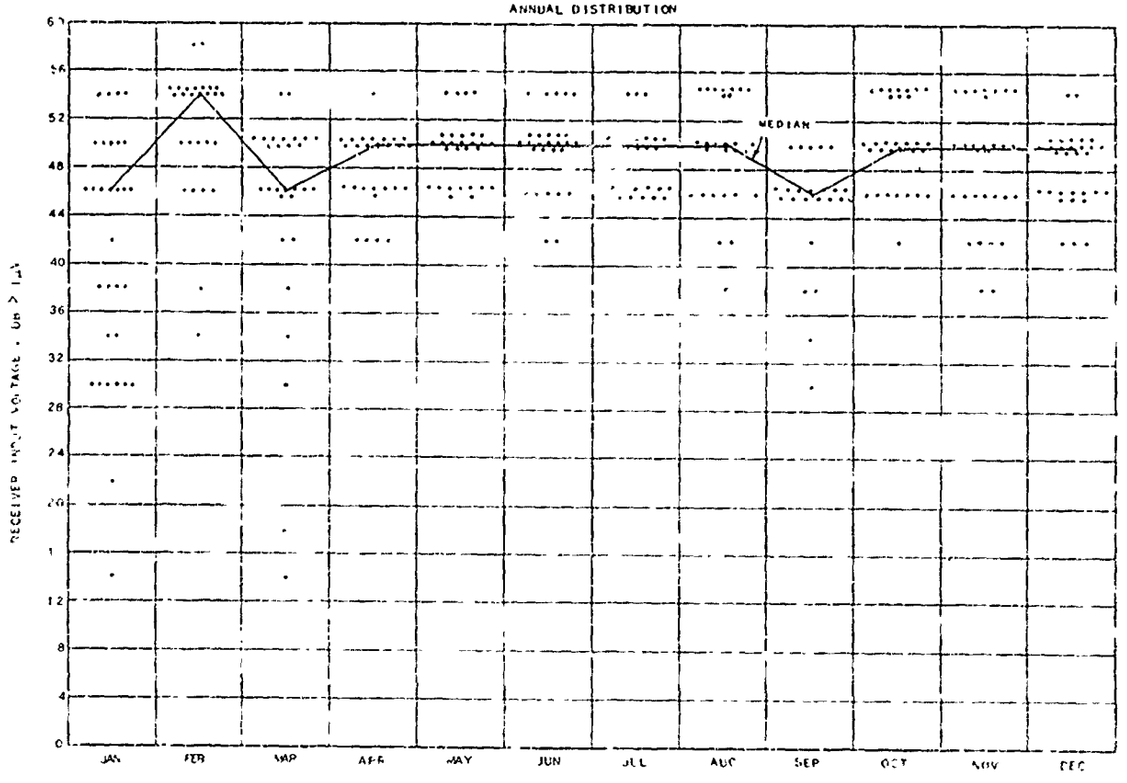

1940

FIGURE 58

CUMULATIVE DISTRIBUTION OF NIGHTTIME HOURLY MEDIAN RECEIVER INPUT VOLTAGES
ON A YEARLY BASIS

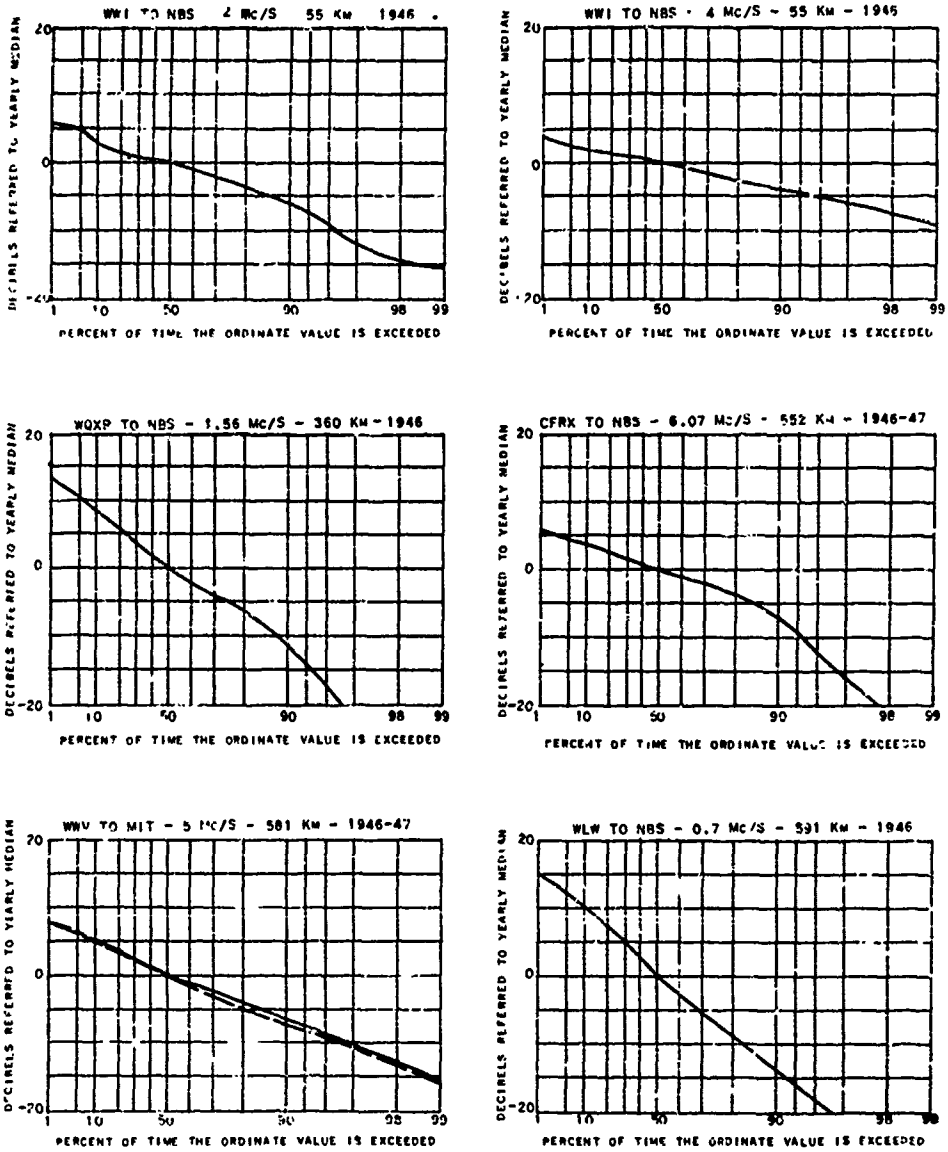

Figure 69

CUMULATIVE DISTRIBUTION OF NIGHTTIME HOURLY MEDIAN RECEIVER INPUT VOLTAGES
ON A YEARLY BASIS

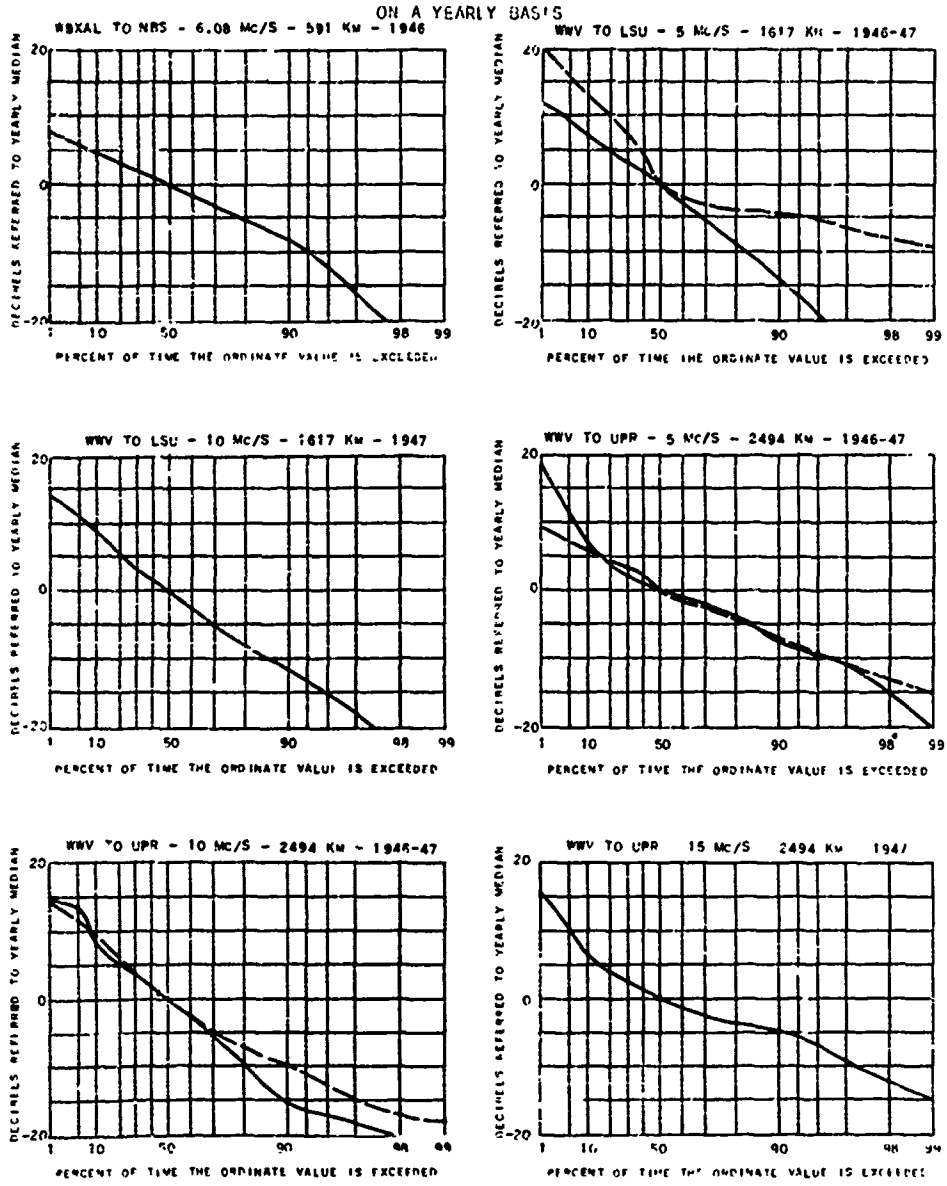

Figure 70

CUMULATIVE DISTRIBUTION OF NIGHTTIME HOURLY MEDIAN RECEIVER INPUT VOLTAGES
ON A YEARLY BASIS

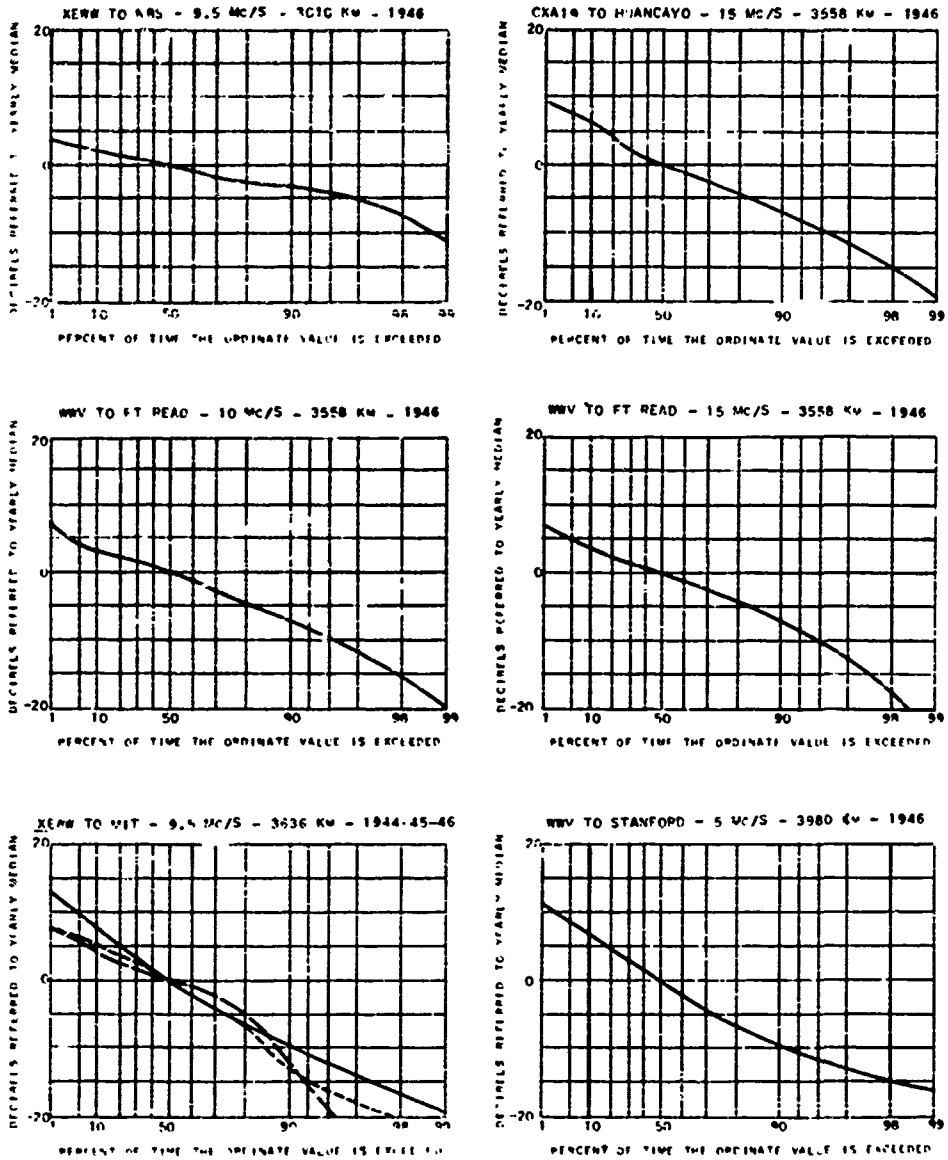

Figure 71

CUMULATIVE DISTRIBUTION OF NIGHTTIME HOURLY MEDIAN RECEIVER INPUT VOLTAGES
ON A YEARLY BASIS

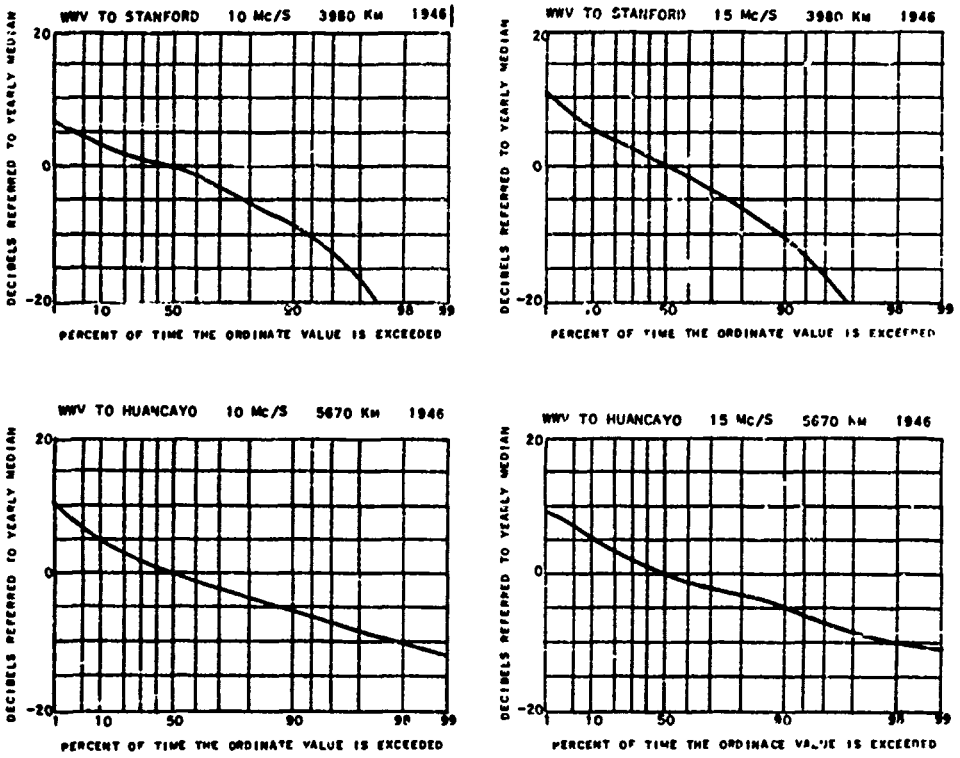

Figure 72

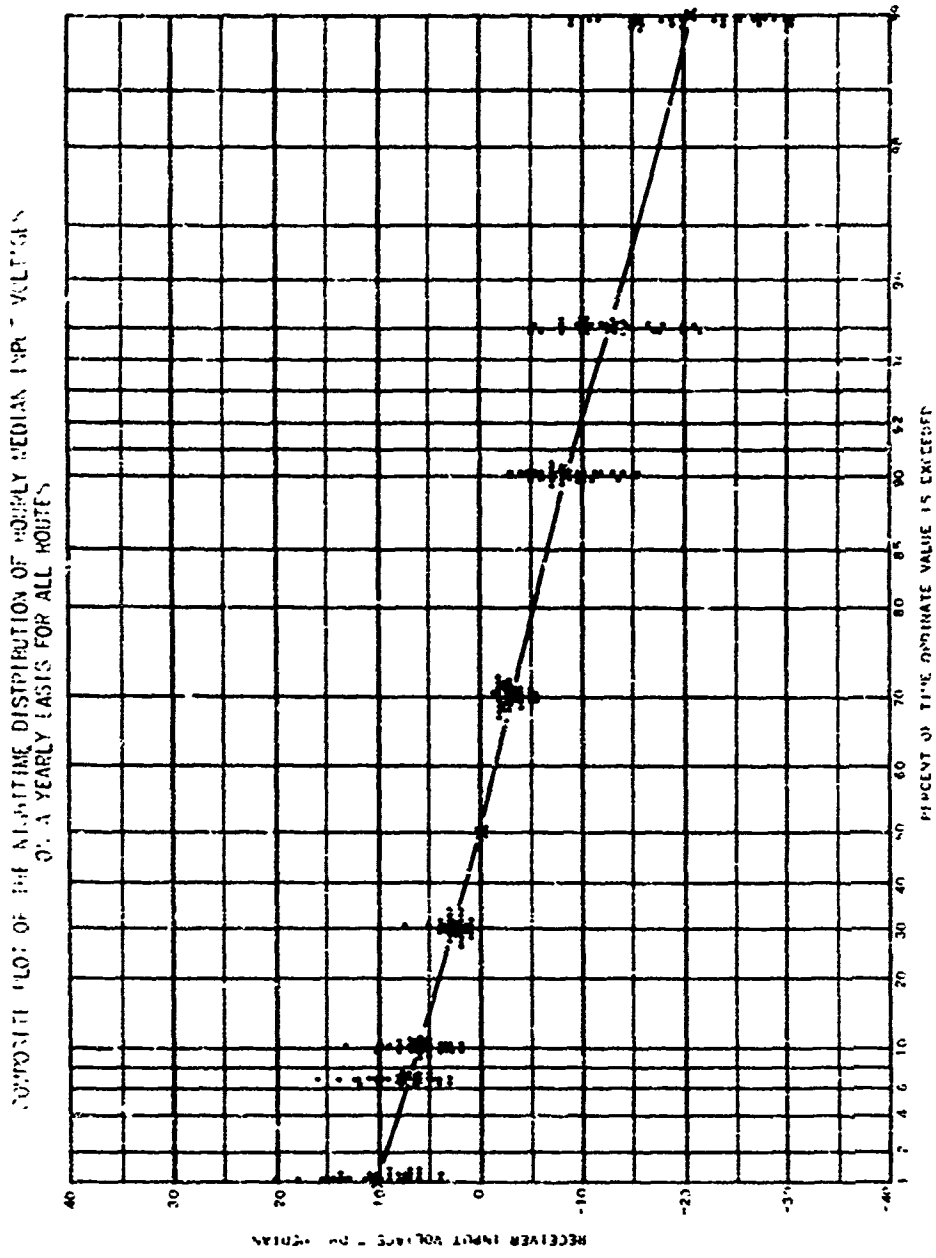

Figure 13

CUMULATIVE CIRCUIT DISTRIBUTION OF THE DIFFERENCE BETWEEN THE NIGHT VALUES EXCEEDED 10 AND 90 PERCENT OF THE TIME

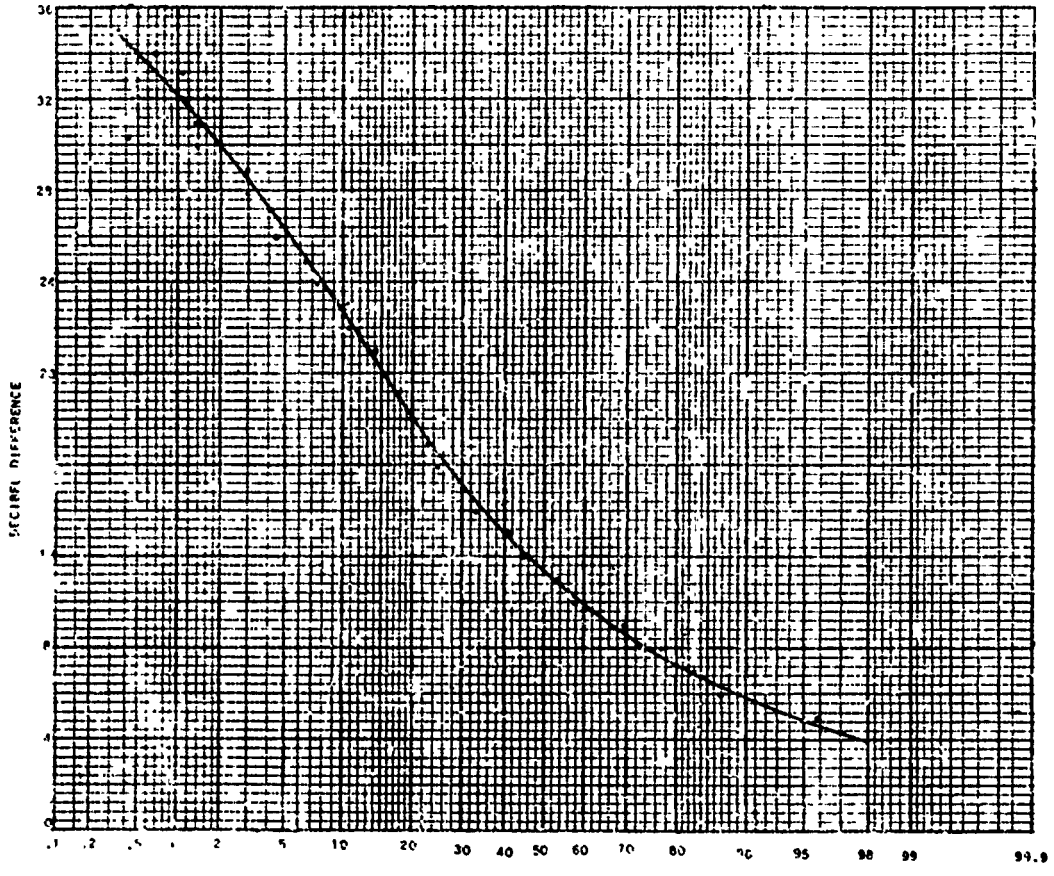

Figure 74

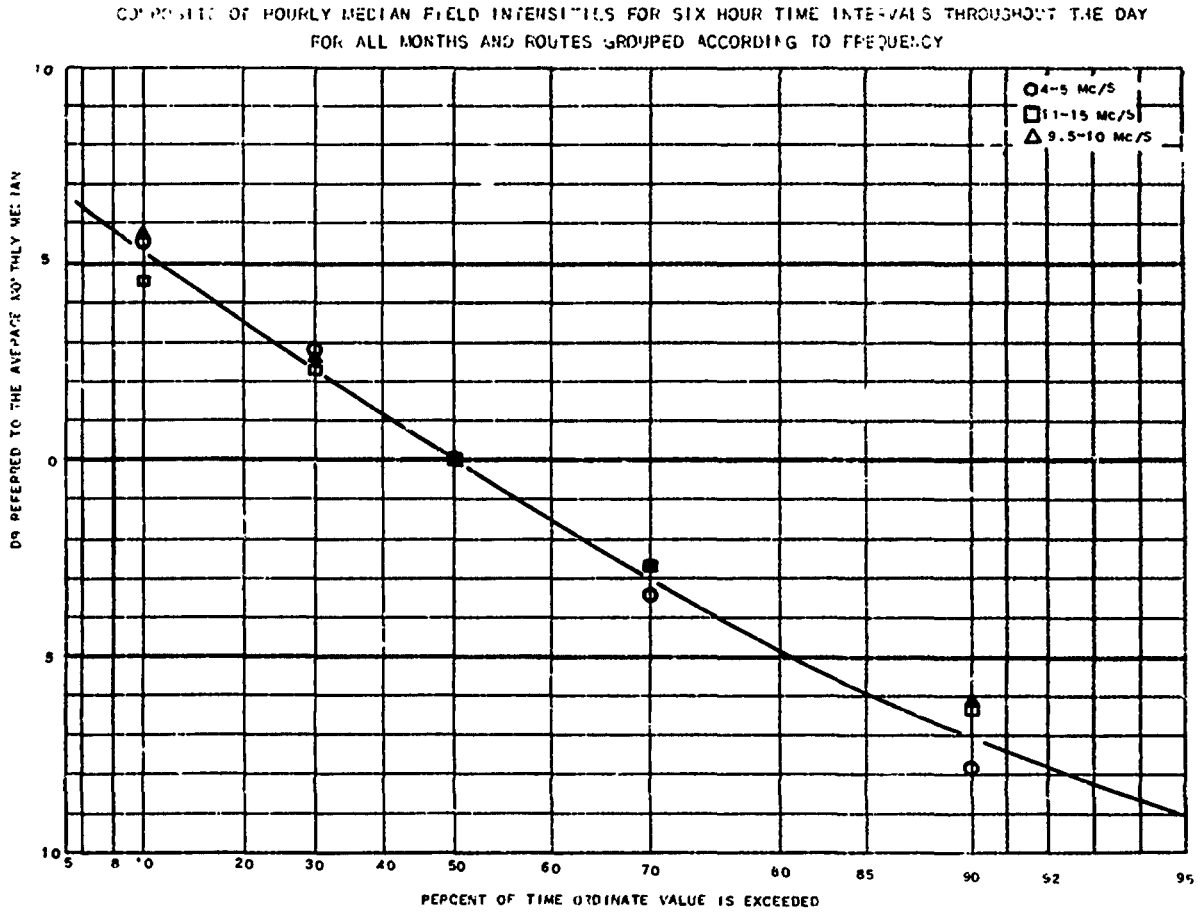
COMPOSITE OF HOURLY MEDIAN FIELD INTENSITIES FOR SIX HOUR TIME INTERVALS THROUGHOUT THE DAY
FOR ALL MONTHS AND ROUTES GROUPED ACCORDING TO FREQUENCY
4-5 Mc/S
11-15 Mc/S
9.5-10 Mc/S
DB REFERRED TO THE AVERAGE MONTHLY MEDIAN
10
5
0
5
10
5
8
10
20
30
40
50
60
70
80
85
90
92
95
PERCENT OF TIME ORDINATE VALUE IS EXCEEDED

Figure 75

HISTOGRAM SHOWING DISTRIBUTION OF HOURLY MEDIAN RECEIVED INPUT VOLTAGES
SOLAR ZENITH ANGLE = 60°

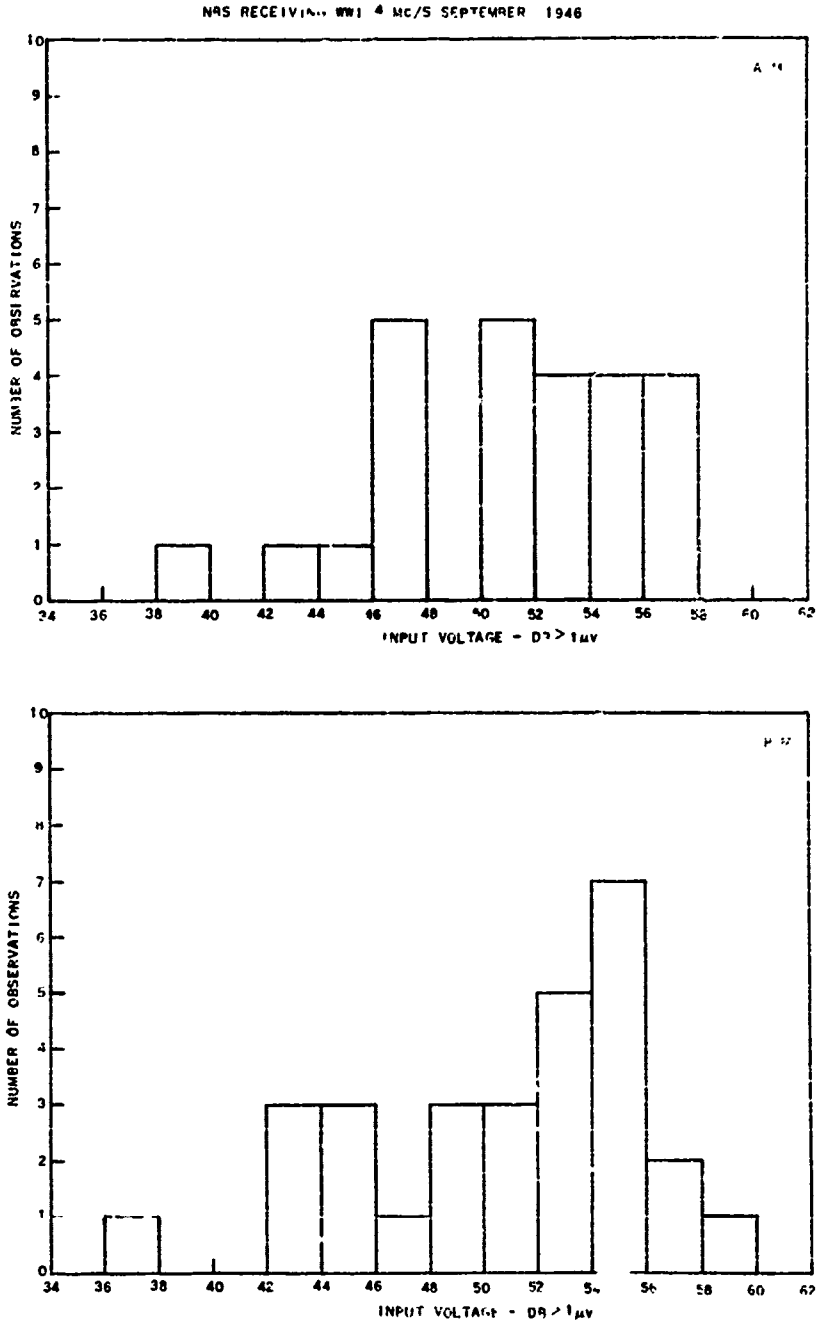

Figure 76

CUMULATIVE DISTRIBUTION OF DAYTIME HOURLY MEDIAN RECEIVER INPUT VOLTAGES
ON A YEARLY BASIS. SOLAR ZENITH ANGLE = 60°

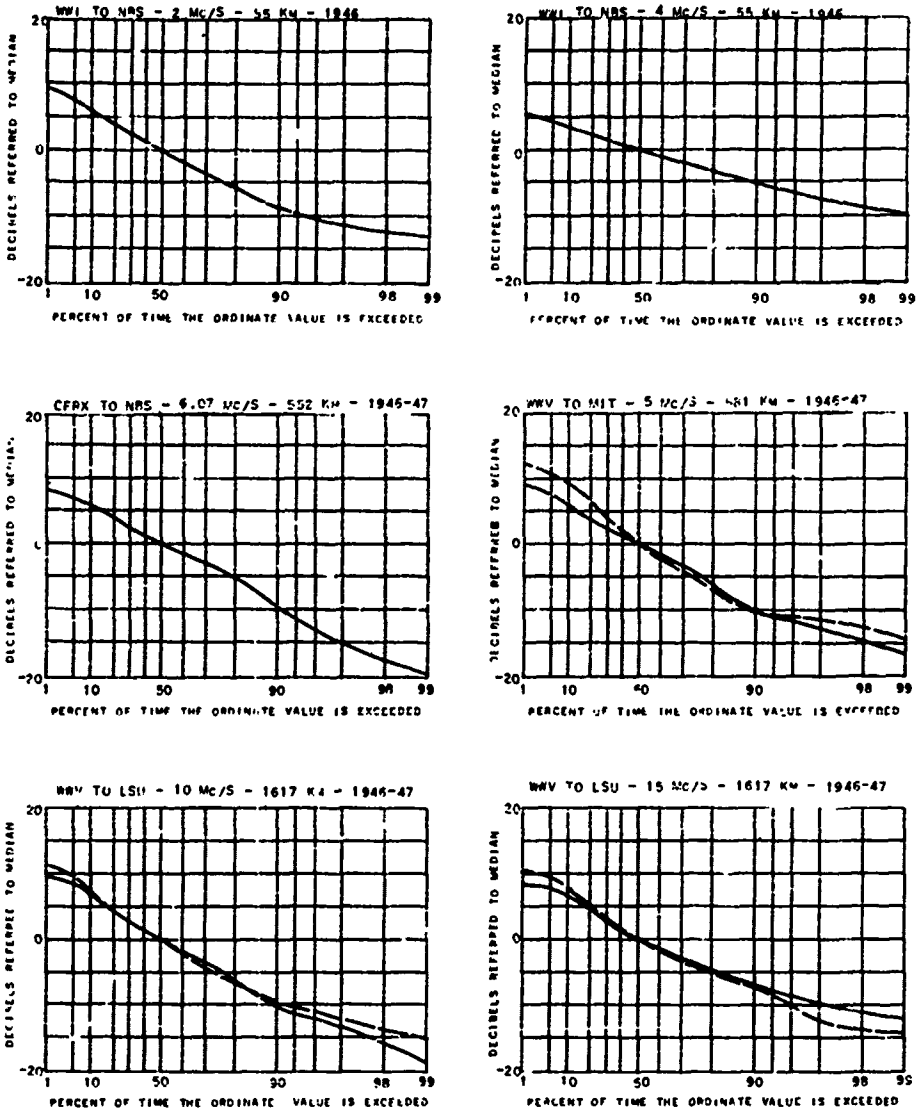

Figure 77

CUMULATIVE DISTRIBUTION OF DAYTIME HOUPLY MEDIAN RECEIVER INPUT VOLTAGES
ON A YEARLY BASIS. SOLAR ZENITH ANGLE = 60°

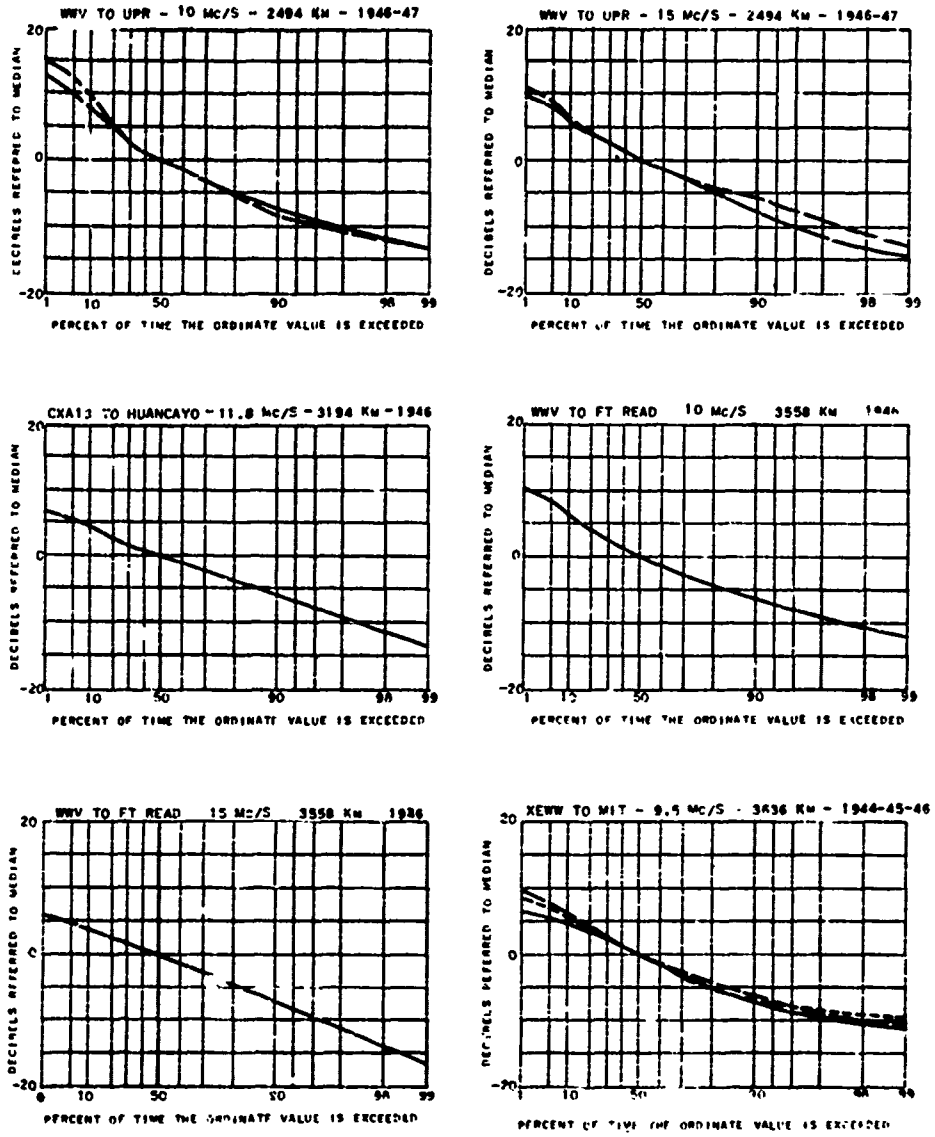

Figure 78

COMPOSITE PLOT OF THE DAYTIME DISTRIBUTION OF HOURLY MEDIAN INPUT VOLTAGES
ON A YEARLY BASIS FOR ALL ROUTES
ZENITH ANGLE OF THE SUN = 60 DEGREES

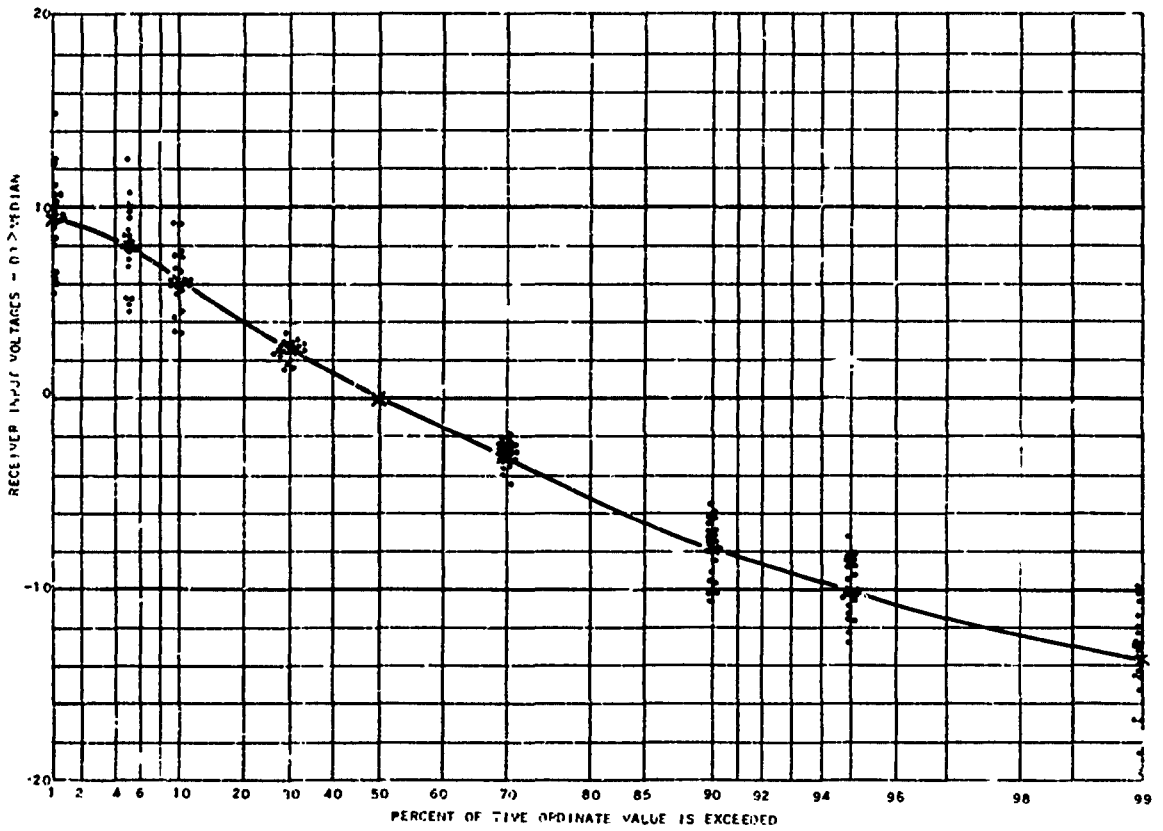

Figure 79

CUMULATIVE DISTRIBUTION OF THE DIFFERENCE BETWEEN THE DAYTIME VALUES EXCEEDED 10 AND 90 PERCENT OF THE TIME

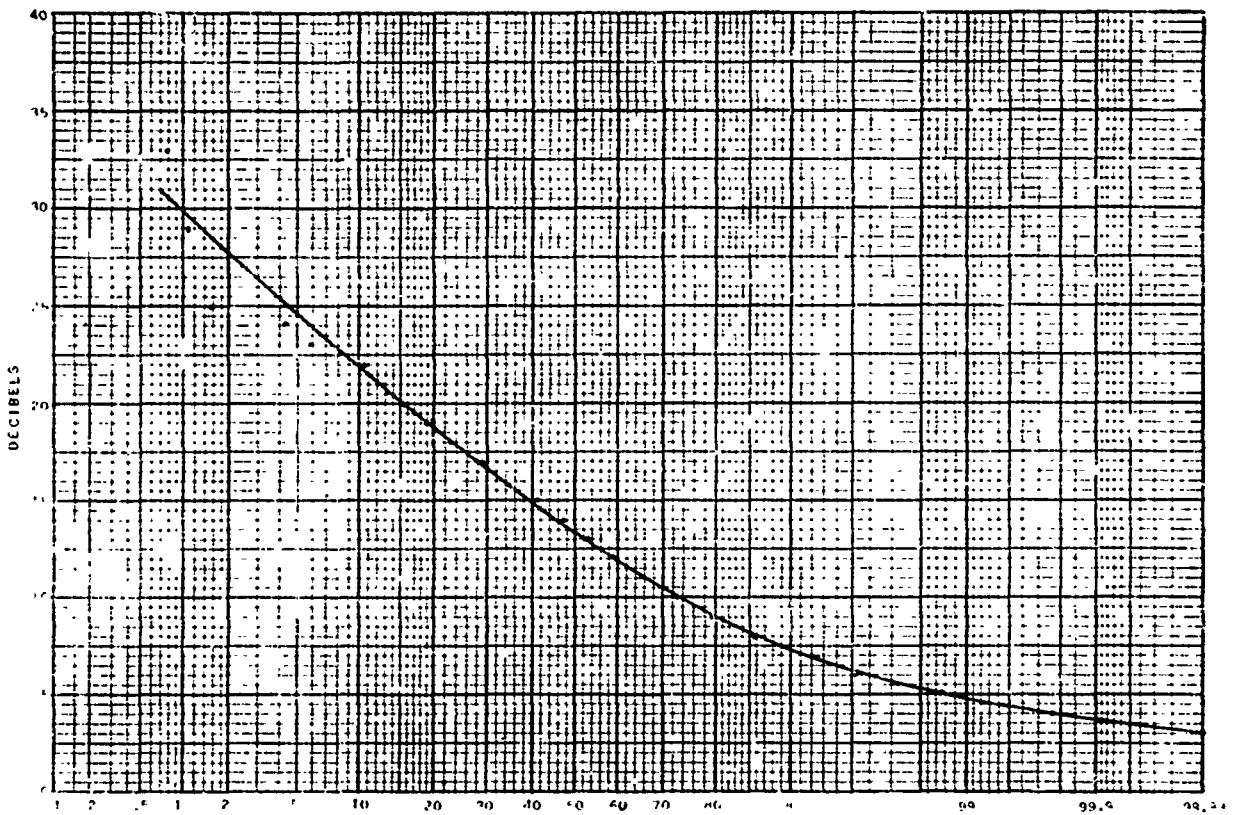

Figure 80

THEORETICAL DISTRIBUTIONS SHOWN ON RAYLEIGH COORDINATES

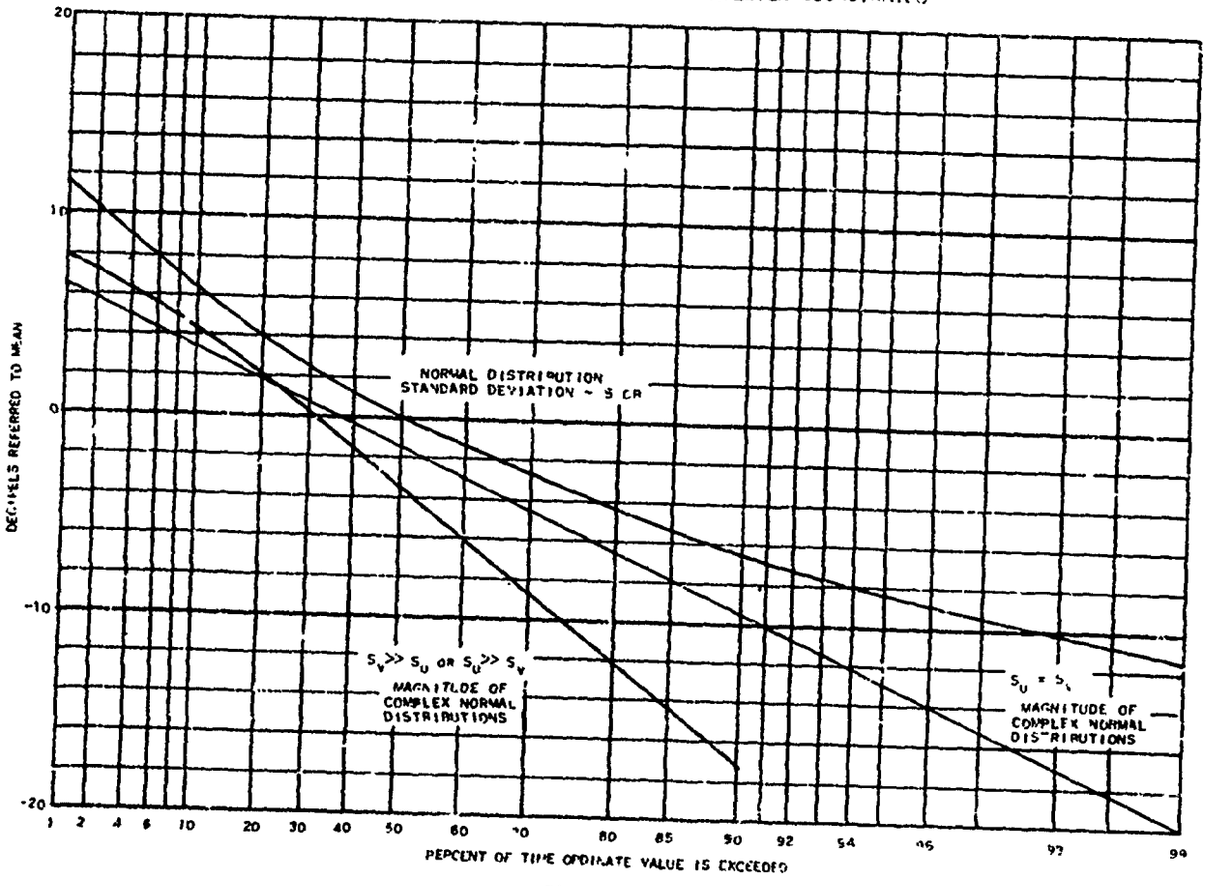

Figure B1

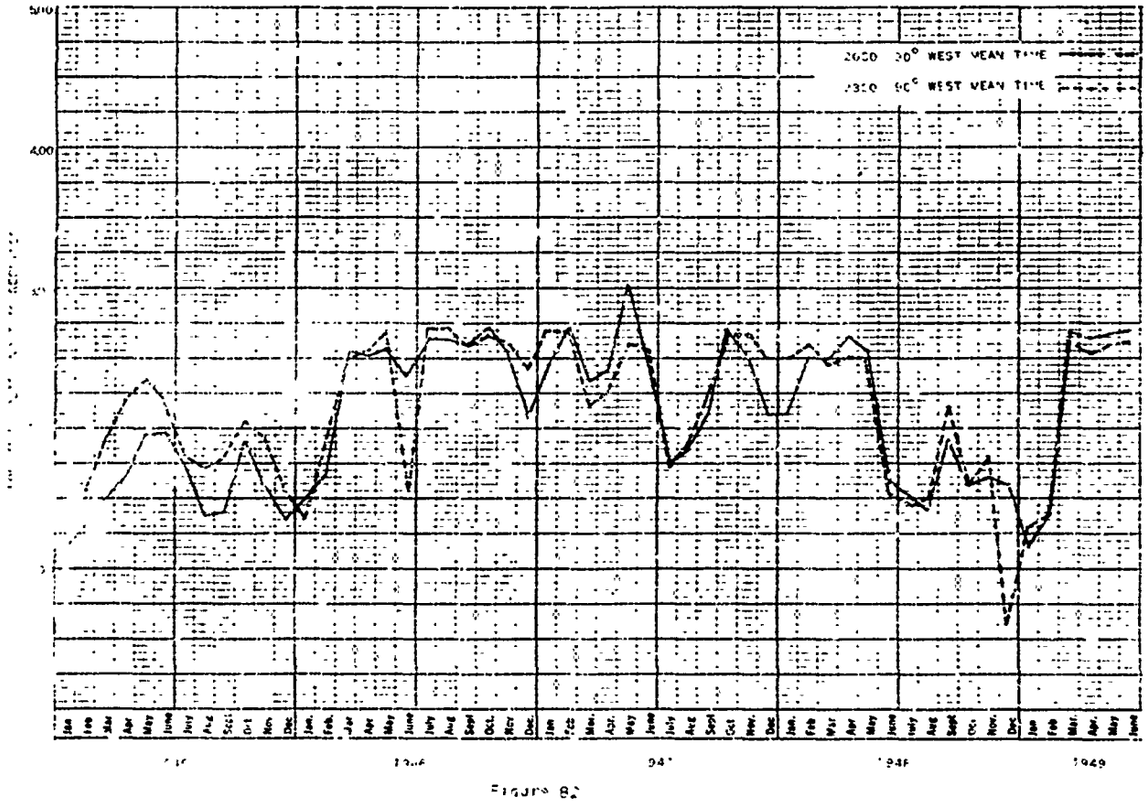
2030 30° WEST MEAN TIME
2330 90° WEST MEAN TIME
500
400
1946
1947
1948
1949

Figure 82

WORLD MAP

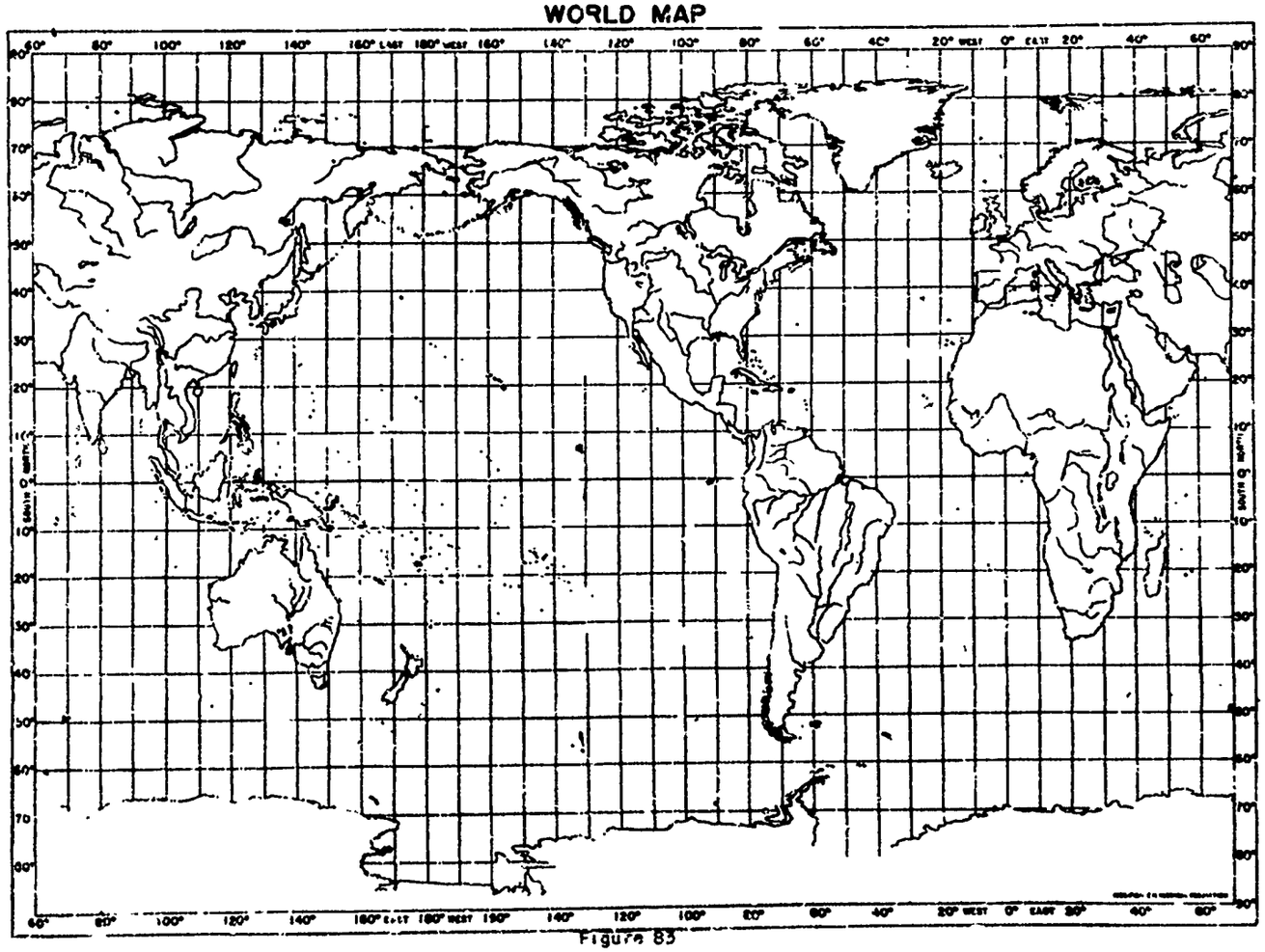

Figure 83

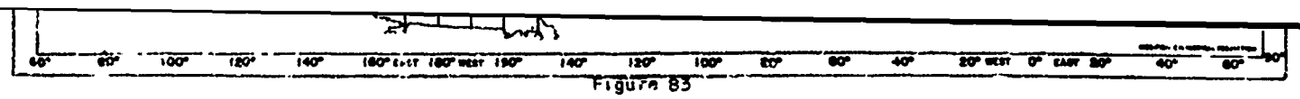

Figure 83

GREAT CIRCLE CHART

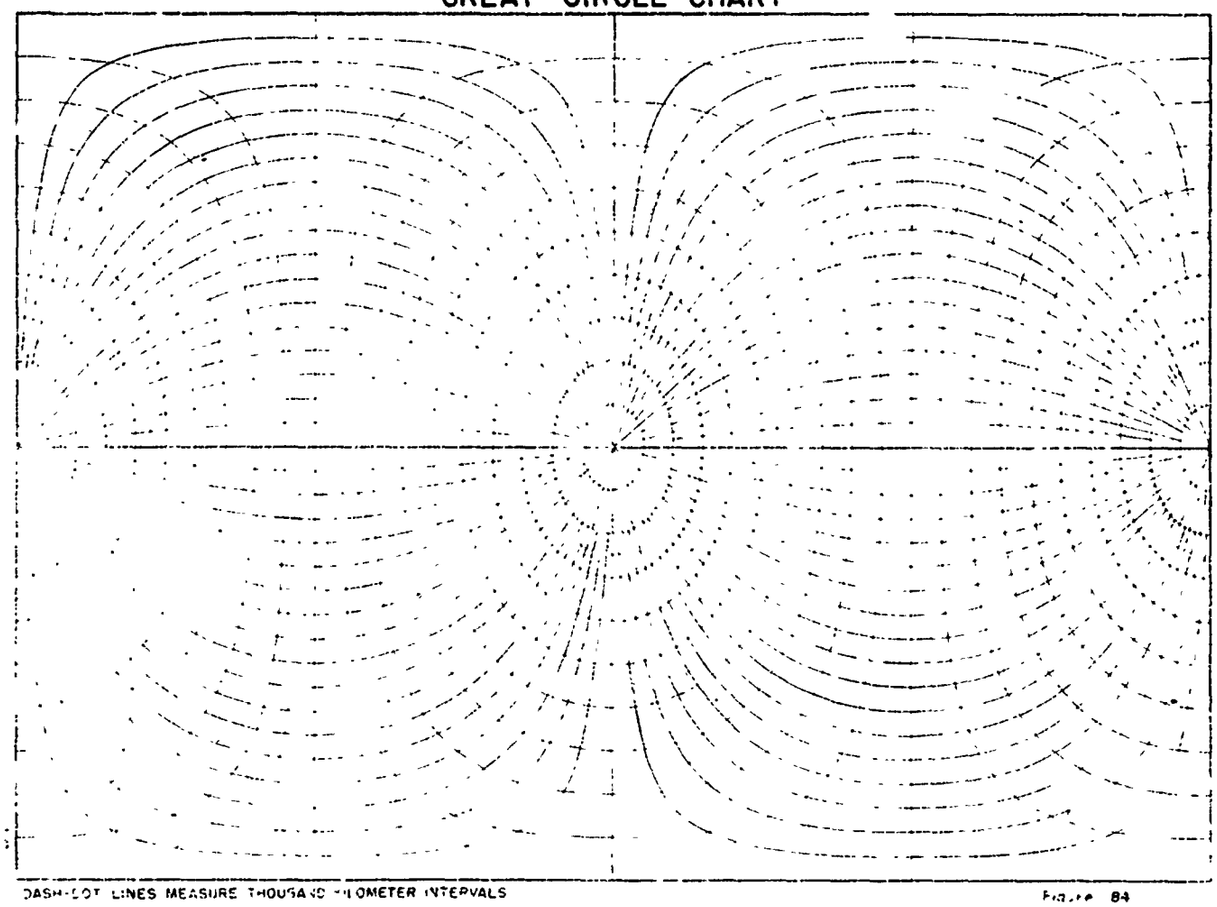

DASH-DOT LINES MEASURE THOUSAND KILOMETER INTERVALS

Figure 84

RADIATION ANGLE NOMOGRAM

TO DETERMINE RADIATION ANGLE FOR EACH POSSIBLE TRANSMISSION MODE WHEN THE GREAT CIRCLE DISTANCE AND THE AVERAGE HEIGHT OF THE REFLECTING LAYER ARE KNOWN

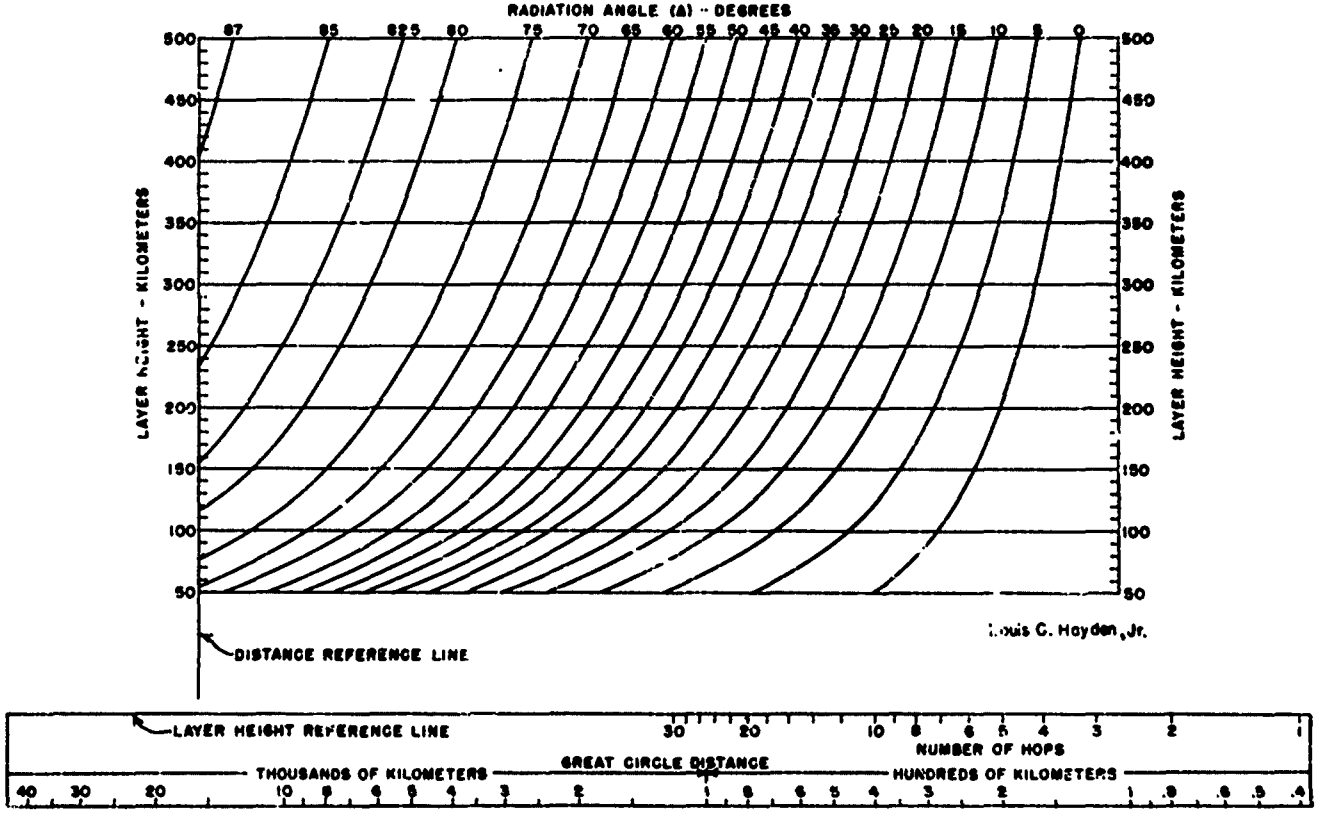

Figure 85

NOMOGRAM

SHOWING RELATION BETWEEN GREAT CIRCLE DISTANCE RADIATION ANGLE AND LAYER HEIGHT

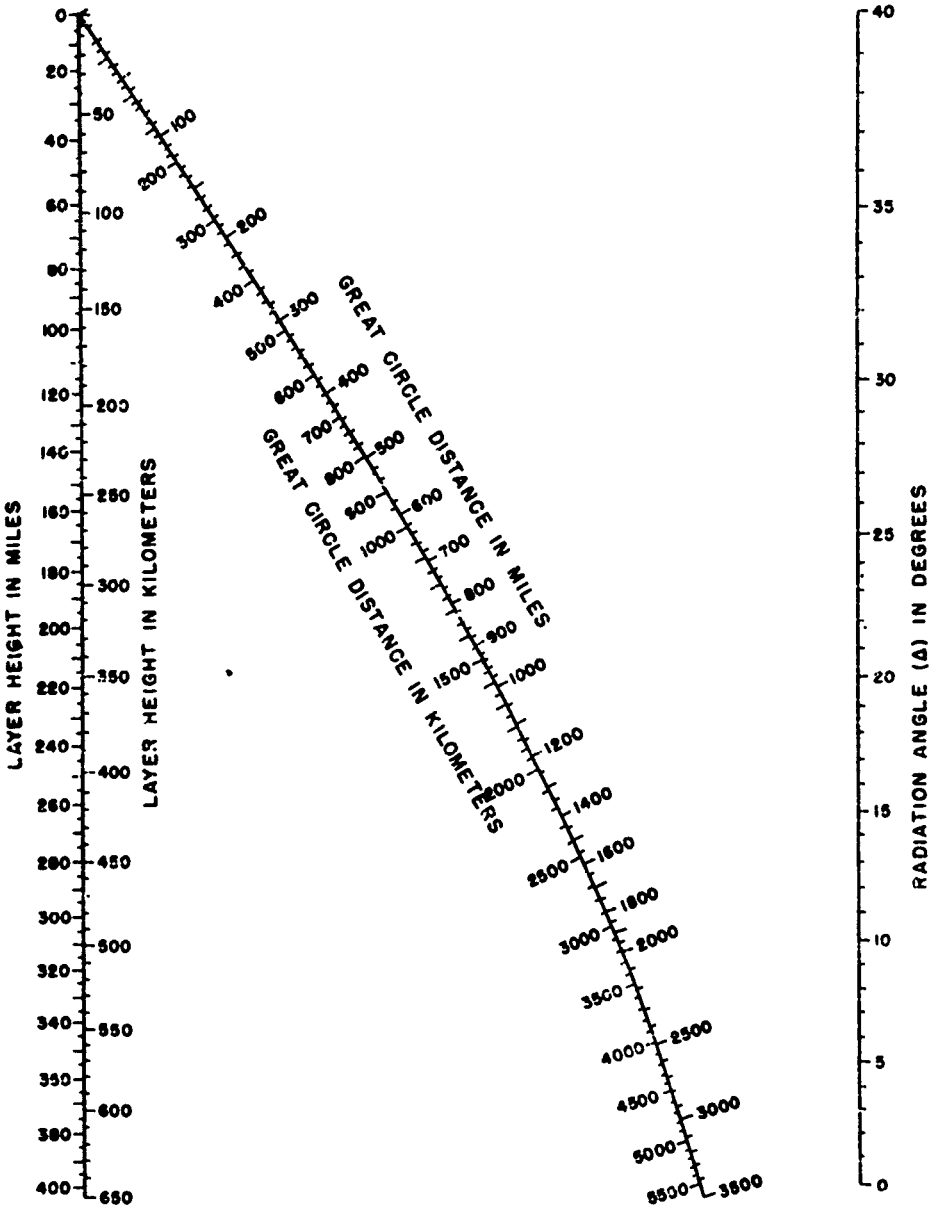

Figure 86

SKY-WAVE ABSORPTION INDEX (I)

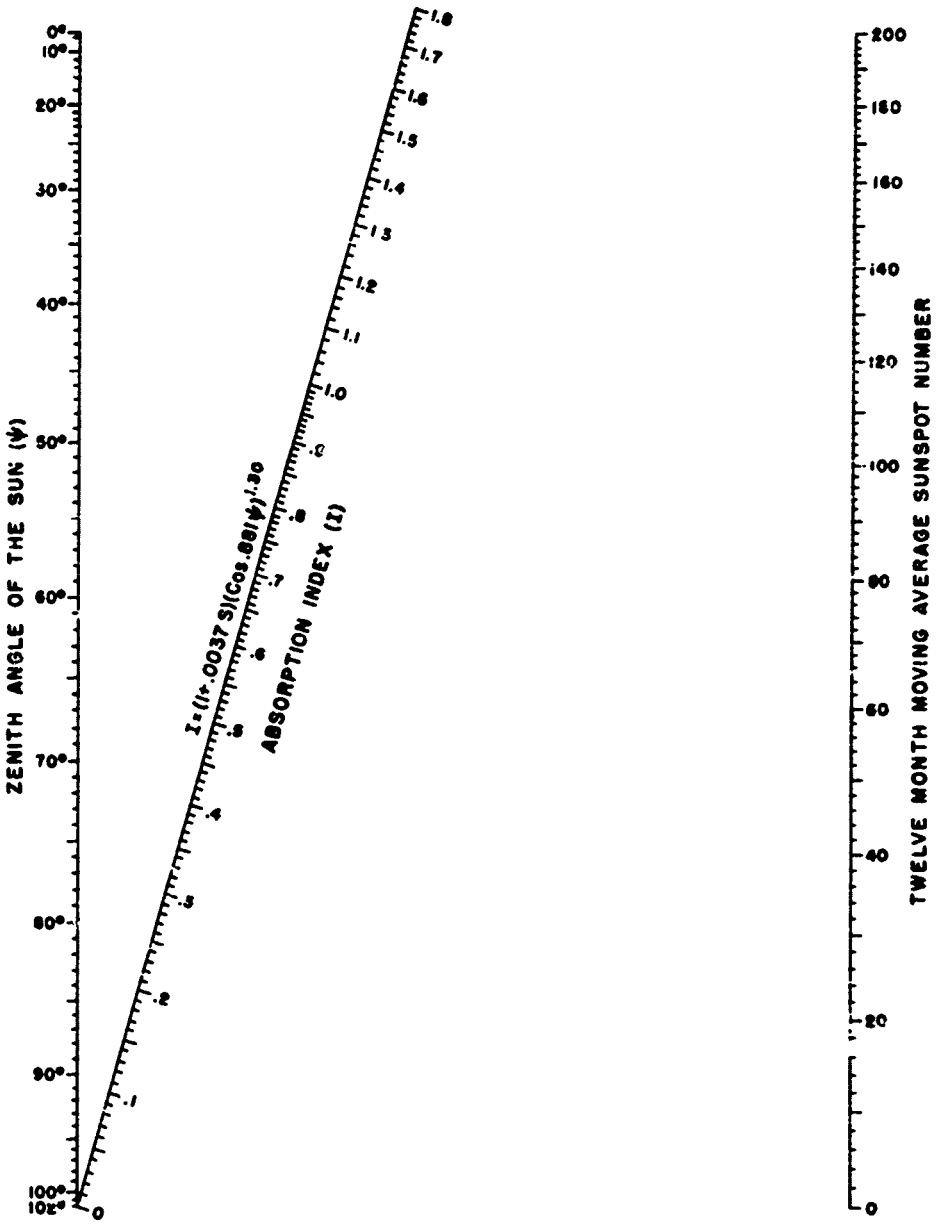

Figure 87

SKY-WAVE ABSORPTION NOMOGRAM

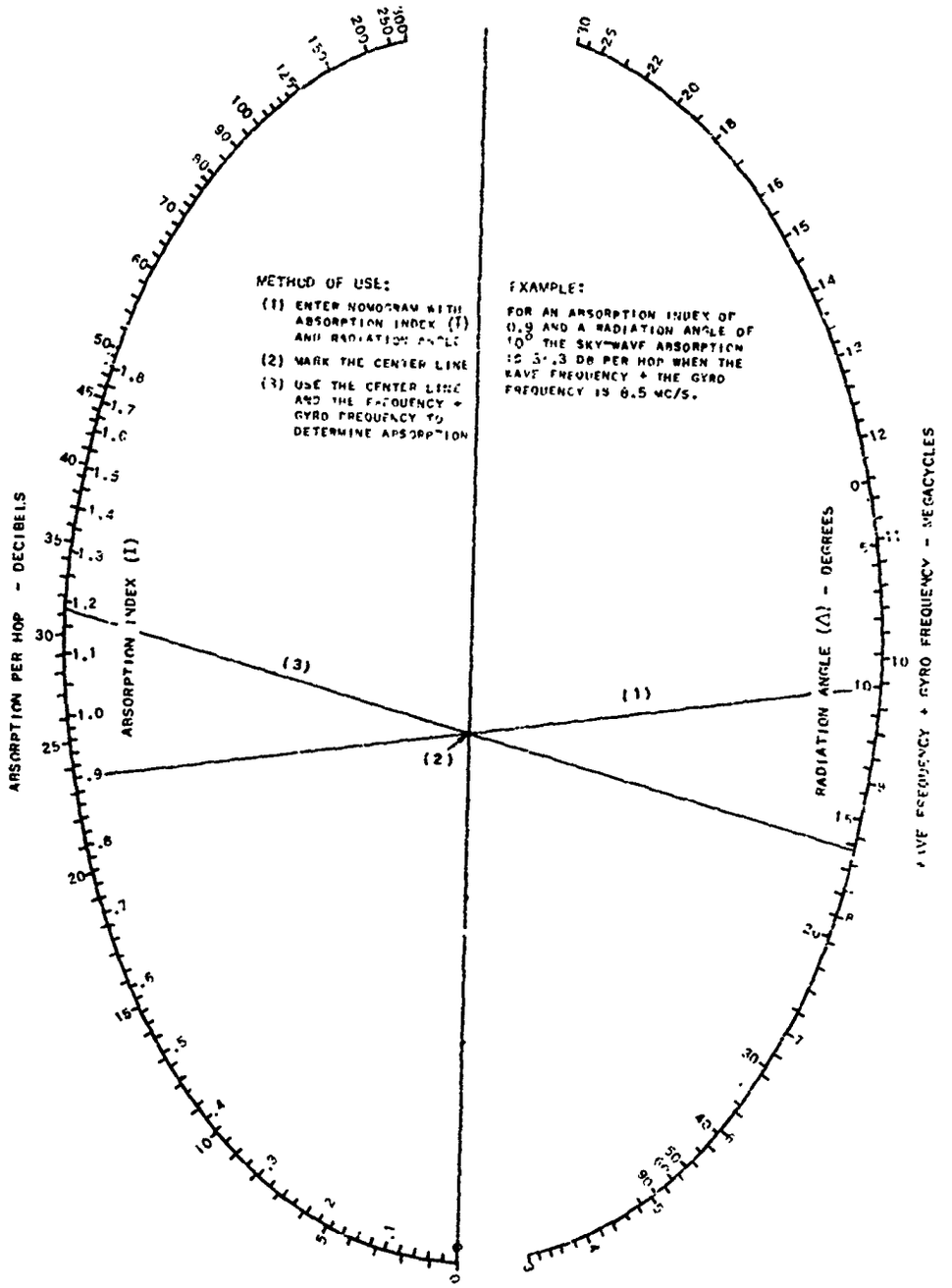

Figure 88

NOMOGRAM SHOWING THE RELATIONSHIP BETWEEN LAYER HEIGHTS, RADIATION ANGLES, WAVE FREQUENCIES, AND THE MUF'S AT STANDARD DISTANCES

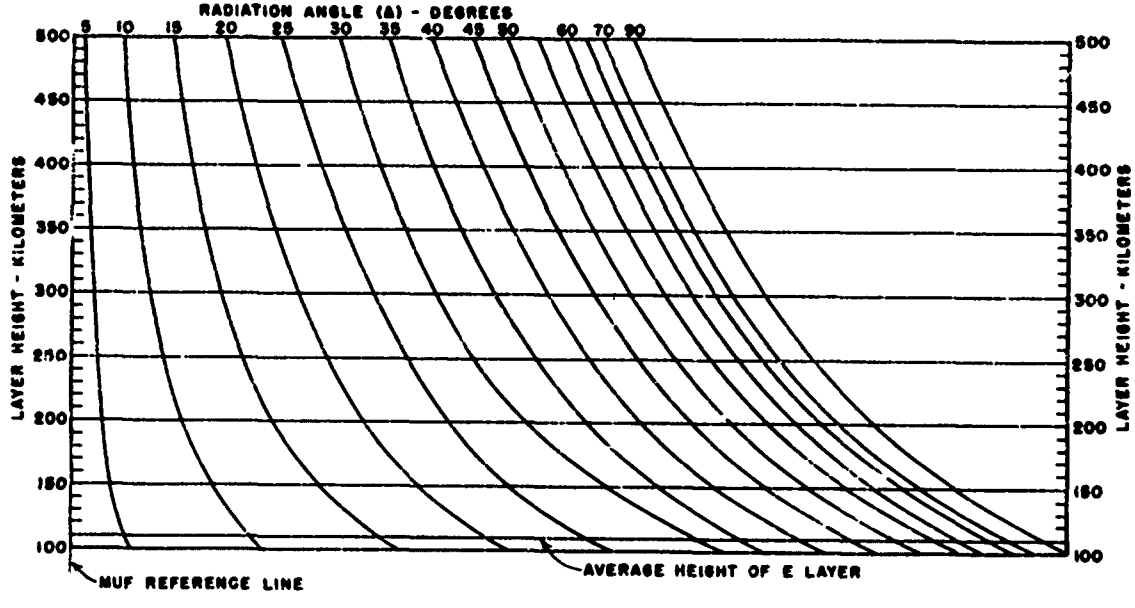

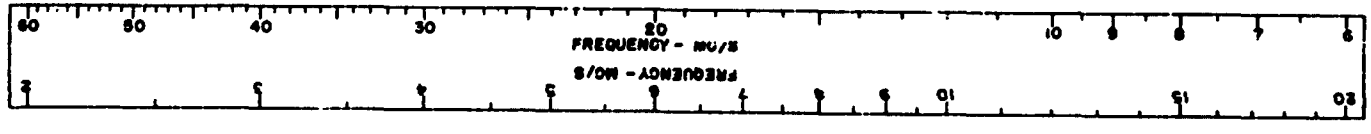

Figure 89

WWV, Washington, D. C., to LSU, Baton Rouge, La.
1617 Kilometers - 10.0 Mc/s

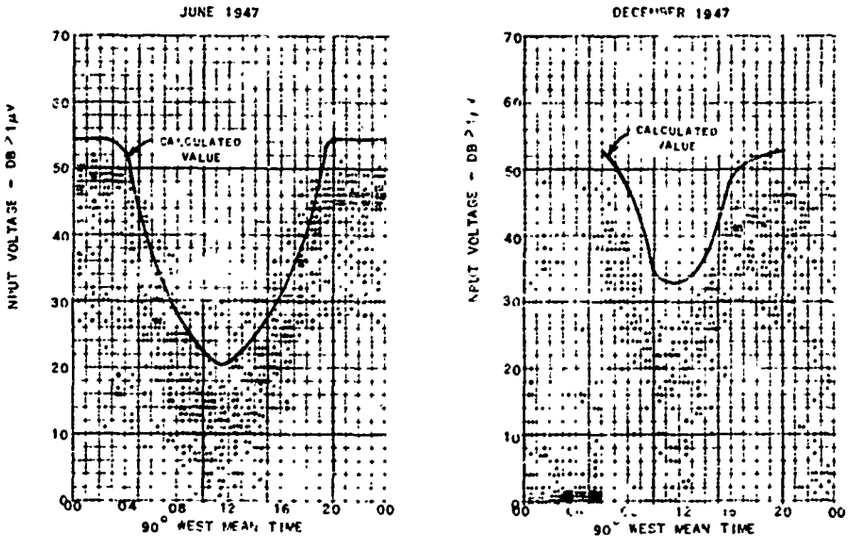

XEWW, Mexico City to National Bureau of Standards
3010 Kilometers - 9.5 Mc/S

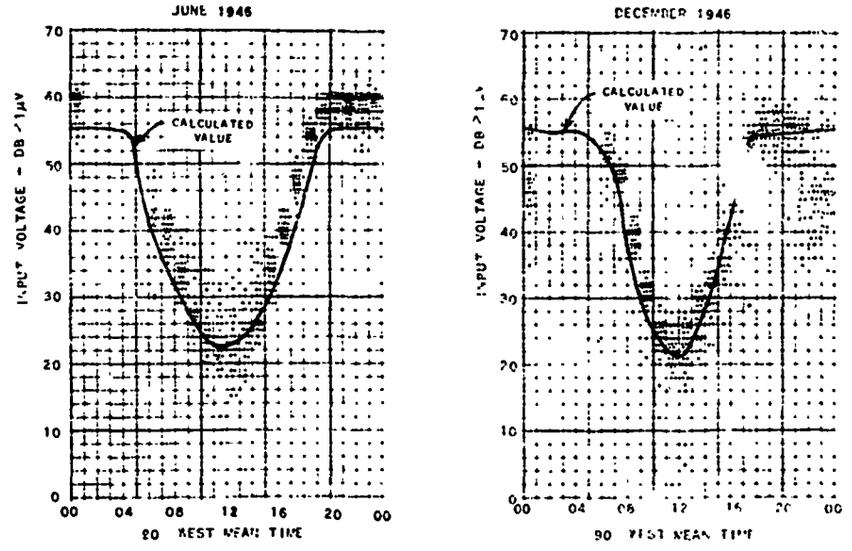

Figure 90

COMPARISON OF CALCULATED AND OBSERVED INPUT VOLTAGES

WWI, Beltsville, Maryland to National Bureau of Standards
55 Kilometers – 4.272 Mc/s

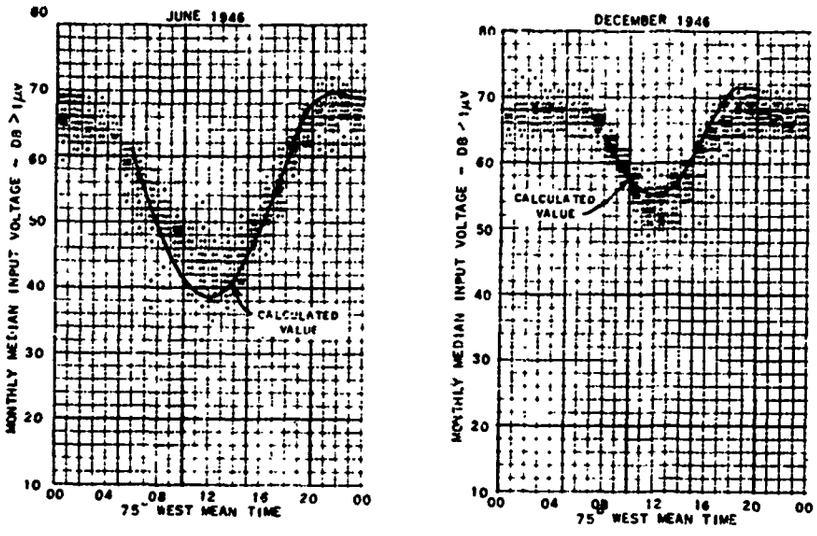

WWV, Washington, D. C., to MIT, Boston, Mass.
581 Kilometers – 5.0 Mc/s

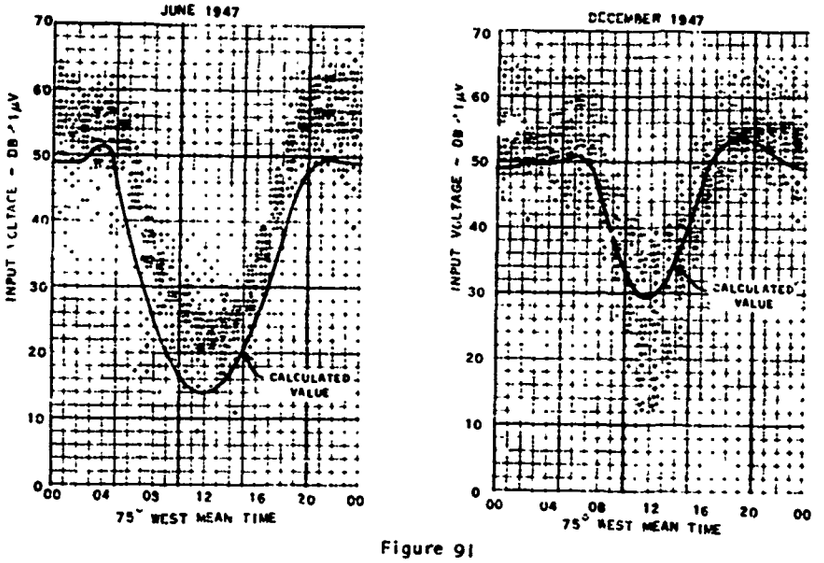

Figure 91

COMPARISON OF CALCULATED AND OBSERVED INPUT VOLTAGES

XEWW, Mexico City to MIT, Boston, Mass.
3636 Kilometers – 9.6 Mc/S

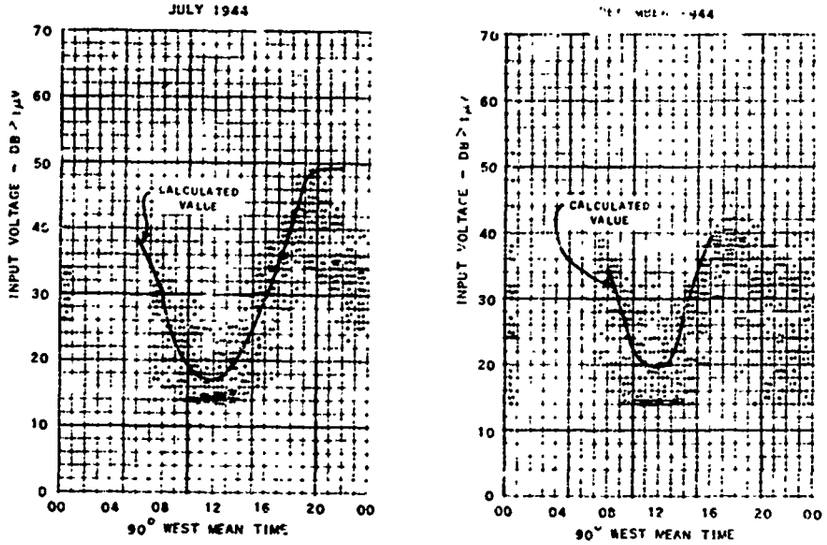

XEWW, Mexico City to MIT, Boston, Mass.
3636 Kilometers – 9.6 Mc/S

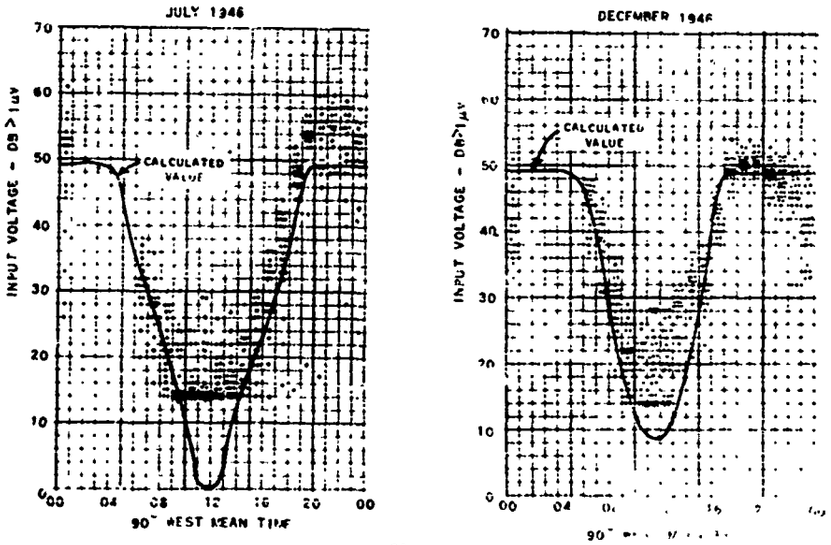

Figure 92

COMPARISON OF CALCULATED AND OBSERVED INPUT VOLTAGES

WwV, Washington, D. C., to Stanford, California
3980 Kilometers – 5.0 Mc/s

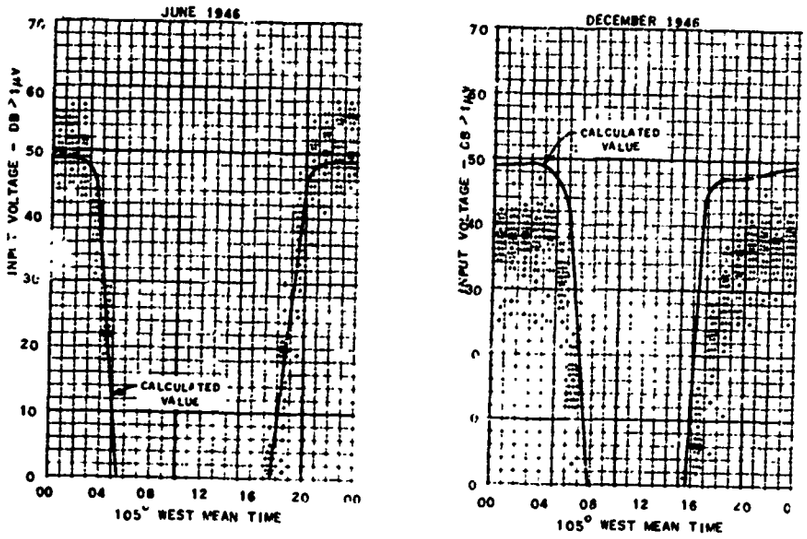

WwV, Washington, D. C., Stanford, California
3980 Kilometers – 10.0 Mc/s

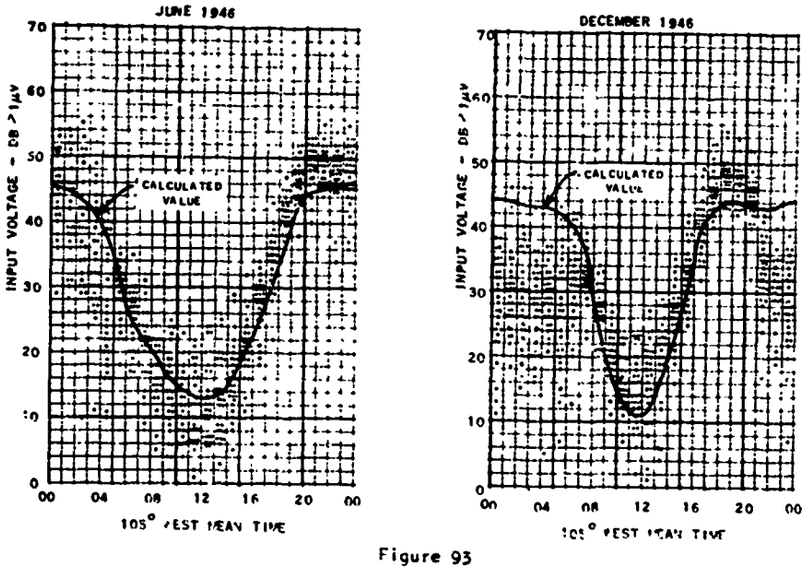

Figure 93

FLOW CHART FOR SKY-WAVE RECEIVER INPUT VOLTAGE CALCULATIONS

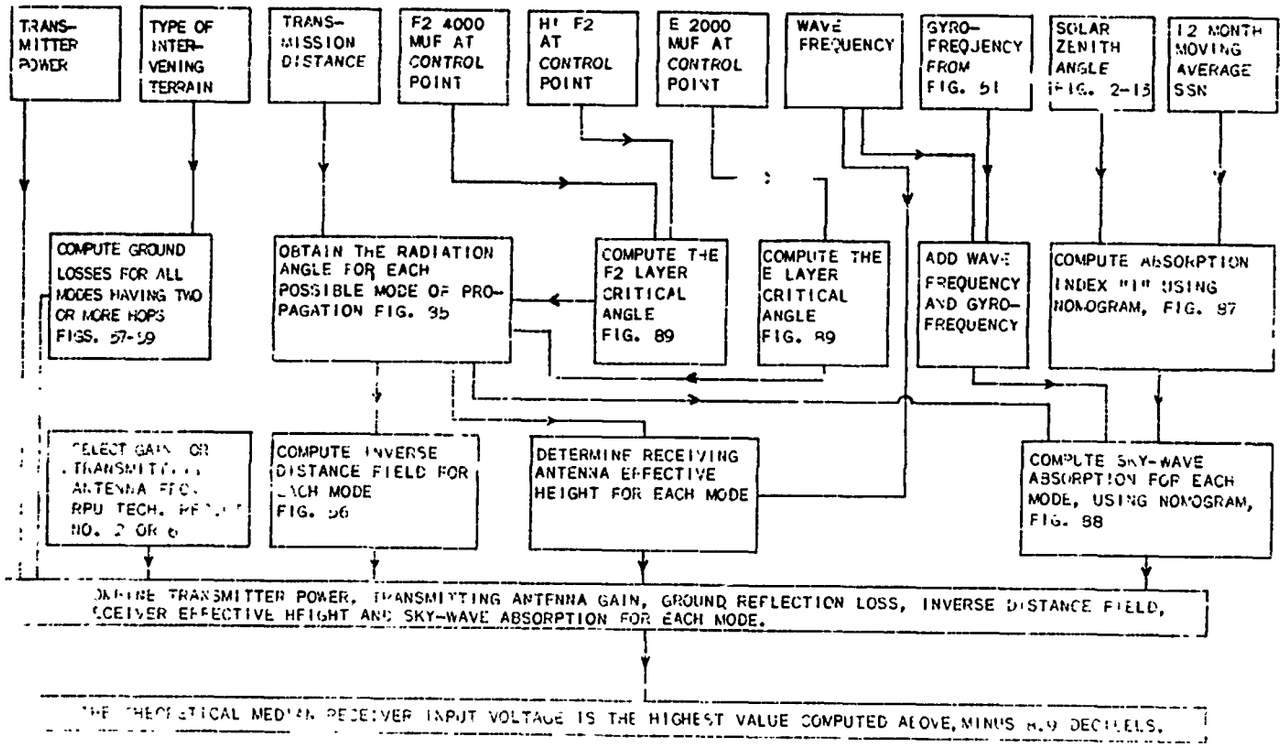

Figure 94